"MAGNETIC RESONANCE SPECTROSCOPY AND DIFFUSION WEIGHTED IMAGING CHARACTERIZATION OF SUPRATENTORIAL BRAIN TUMORS: A ONE YEAR HOSPITAL BASED CROSS SECTIONAL STUDY"

BY

REG. NO. BS0121003

Dissertation

Submitted to the

KLE Academy of Higher Education and Research, Belagavi, Karnataka

In partial fulfillment

of the requirements for the degree of

M.D.

IN

RADIO-DIAGNOSIS

DEPARTMENT OF RADIO-DIAGNOSIS,

J. N. MEDICAL COLLEGE,

BELAGAVI -590010. KARNATAKA

DEC – 2024/JAN – 2025

KLE ACADEMY OF HIGHER EDUCATION AND RESEARCH,

BELAGAVI, KARNATAKA

Endorsement by the HOD/Principal/ Head of the Institution

This is to certify that the dissertation entitled **"MAGNETIC RESONANCE SPECTROSCOPY AND DIFFUSION WEIGHTED IMAGING CHARACTERIZATION OF SUPRATENTORIAL BRAIN TUMORS: A ONE YEAR HOSPITAL BASED CROSS SECTIONAL STUDY"** is a bonafide research work done by **REGISTRATION NO. BS0121003.**

Dr. SANTOSH D. PATIL
M.D.(Radio-Diagnosis)
Professor & HOD
Dept. of Radio-diagnasis
J.N. Medical College, BELAGAVI-10.
KMC Reg No. 58458

Dr. SANTOSH D. PATIL
M.D. RADIO-DIAGNOSIS
Professor and Head,
Department of Radio Diagnosis,
J. N. Medical College,
Nehru Nagar, Belagavi – 590010

Date: 26/06/2024
Place: Belagavi

KAHER BELAGAVI J.N. MEDICAL COLLEGE

Dr. N.S. MAHANTASHETTI
M. D. PEDIATRICS
Principal,
J. N. Medical College,
Nehru Nagar, Belagavi – 590010

PRINCIPAL
J.N. Medical College,
BELAGAVI- 590 010

Date: 26/06/2024
Place: Belagavi

UNDERTAKING

I, **Reg. No. BS0120003,** hereby declare that the information and the data mentioned in my dissertation entitled **"MAGNETIC RESONANCE SPECTROSCOPY AND DIFFUSION WEIGHTED IMAGING CHARACTERIZATION OF SUPRATENTORIAL BRAIN TUMORS: A ONE YEAR HOSPITAL BASED CROSS SECTIONAL STUDY"** belongs to me and is original. I am aware of the definition of plagiarism as detailed below:

- An act or instance of using or closely imitating the language and thoughts of another author without authorization and the representation of that author's work as one's own, as by not crediting the original author.
- A piece of writing or other work reflecting such unauthorized use or imitation.
- The deliberate or reckless representation of another's words, thoughts or ideas as one's own without attribution in connection with submission of academic work, whether graded or otherwise.

I hereby declare that the dissertation prepared by me is original one and does not involve plagiarism anywhere. In case at a later stage, it is found that I have indulged in plagiarism, then I am solely responsible for the same and the institution is at liberty to take any disciplinary action against me including cancellation of dissertation or any other penalties imposed by the University.

Date: 26/06/2024

Place: Belagavi **(REG. NO. BS0121003)**

PLAGIARISM ACCEPTANCE LETTER

KLE ACADEMY OF HIGHER EDUCATION AND RESEARCH

JAWAHARLAL NEHRU MEDICAL COLLEGE

(A constituent unit of KLE Academy of Higher Education & Research Deemed-to-be-University)

(Recognized by National Medical Commission, New Delhi)

Accredited 'A+' Grade by NAAC (3rd Cycle) **Placed in Category 'A' by MoE (GoI)**

Nehru Nagar, Belagavi- 590 010, Karnataka, INDIA

0831 - 2471350 0831 - 2470759 www.jnmc.edu rincipal@jnmc.edu

Ref No: MDC/PG/ Date: 25-06-2024

"ACCEPTANCE LETTER"

The softcopy of thesis entitled: **"MAGNETIC RESONANCE SPECTROSCOPY AND DIFFUSION WEIGHTED IMAGING CHARACTERIZATION OF SUPRATENTORIAL BRAIN TUMORS: A ONE YEAR HOSPITAL BASED CROSS SECTIONAL STUDY"** has been submitted for anti-plagiarism check through Turnitin software. The scan has been carried out and the scanned output reveals a match percentage of **06%** which is within the acceptable limits of **10%** as per the guidelines given by UGC.

Guide.

KAHER BELAGAVI J.N. MEDICAL COLLEGE

Dr. (Mrs.) N.S. Mahantashetti.
Chairperson-Antiplagiarism Committee &
Principal,
J. N. Medical College, Belagavi.

To,
Reg. No. BS0121003
Postgraduate Student,
2021-22 Batch,
Department of Radio-Diagnosis
J. N. Medical College, Belagavi.

ETHICAL CLEARANCE

K.L.E. ACADEMY OF HIGHER EDUCATION AND RESEARCH
(Deemed – to- be- University)
Accredited 'A+' Grade by NAAC in (3rd Cycle) Placed in Category 'A' by MHRD (GoI)
JNMC INSTITUTIONAL ETHICS COMMITTEE
JAWAHARLAL NEHRU MEDICAL COLLEGE,
NEHRU NAGAR, BELAGAVI-590010 (KARNATAKA-INDIA)
Website: http//www.jnmc.edu
E-Mail : dome@jnmc.edu
Phone: (+ 91-(0)831 Office : 2472550
Principal: 2471701
Fax No. +91 (0)831 – 2470759

Ref No.MDC/JNMCIEC/ 244 **Date: 7/10/2022**

To,

REG. NO. BS0121003
PG Student in Radio-diagnosis,
J. N. Medical College,
BELAGAVI.

Sub: Institutional Ethical Clearance for the study.

With reference to the above, we wish to inform you that your proposed research project titled **"MAGNETIC RESONANCE SPECTROSCOPY AND DIFFUSION WEIGHTED IMAGING CHARACTERIZATION OF SUPRATENTORIAL BRAIN TUMORS: A ONE YEAR HOSPITAL BASED CROSS SECTIONAL STUDY"** is ethical and justifiable. The proposed research project has been cleared by the JNMC Institutional Ethics Committee.

(Dr. Smita Sonoli)
Member Secretary
JNMC Institutional Ethics Committee
J.N.Medical College, Belagavi.

(Dr. Harsha Hegde)
Chairman,
JNMC Institutional Ethics Committee
J.N.Medical College, Belagavi

LIST OF ABBREVIATIONS

Abbreviation	Meaning
(-N(CH3)3)	Trimethylamine
1D CSI	1 dimensional chemical shift imaging
'H-MRS	Proton magnetic resonance spectroscopy
2D CSI	2 dimensional chemical shift imaging
3D CSI	3 dimensional chemical shift imaging
ATP	Adenosine triphosphate
CH2	Methyl group
CHESS	Chemical shift selective
Cho	Choline
Cm	Centimeter
CNS	Central nervous system
Cr.	Creatine
CSF	Cerebrospinal fluid
CSI	Chemical shift imaging
CT	Computed tomography
DNA	De-oxy ribonucleic acid
DTPA	Diethylenetriaminepentaacetic acid
DWI	Diffusion weighted imaging
EPI	Echo-planar imaging
EPSI	Echo-planar spectroscopic imaging
FDG PET	Fluorodeoxyglucose positron emission tomography

Abbreviation	Meaning
FLAIR	Fluid attenuation inversion recovery images
FSE	Fast spin echo
GABA	Gamma amino butyric acid
Gd	Gadolinium
GPC	Glycerophosphocholine
HGG	High grade glioma
i.e.	That is
ICP	Intracranial pressure
ICSOL	Intracranial space occupying lesion
IR	Inversion recovery
LGG	Low Grade Glioma
M	Metastatic spread
MGMT	O-6 Methylguanine-DNA Methyltransferase
ml	Mililiter
MPNST	Malignant peripheral nerve sheath tumors
MRI	Magnetic Resonance Imaging
MRS	Magnetic resonance spectroscopy
MRSI	Magnetic resonance spectroscopic imaging
MS	Multiple sclerosis
N	Nodal status
NAA	N-acetyl aspartate
NAAG	N-acetylaspartyl glutamate

Abbreviation	Meaning
NCC	Neurocysticercosis
NMRS	Nuclear magnetic resonance spectroscopy
P	Probability
PC	Phosphocholine
PNET	Primitive neuroectodermal tumor
Ppm	Parts per million
PRESS	Point-resolved spectroscopy
RF	Radiofrequency
SEER	Surveillance, Epidemiology, and End Results
SNR	Signal to noise ratio
STEAM	Stimulated-echo acquisition mode
STIR	Short tau inversion recovery
SV	Single-voxel
SVS	Single-voxel spectroscopy
T	Tumor size
TIWI	T1-weighted images
T2WI	T2-weighted images
TE	Echo time
VOI	Volume of interest
WBC	White blood cell
WHO	World Health Organization

TABLE OF CONTENTS

LIST OF FIGURES

LIST OF TABLES

LIST OF GRAPHS

LIST OF IMAGES

ABSTRACT

Background and objectives:

Tumors within the brain represent a serious health concern. Subtypes of brain cancers include infra- and supra-tentorial brain tumors. It is frequently challenging to distinguish low-grade from high-grade gliomas and neoplastic from non-neoplastic brain masses with conventional MRI, and many patients necessitate biopsy or further imaging. Modern methods of magnetic resonance imaging, such magnetic resonance spectroscopy, can increase the diagnostic precision of magnetic resonance imaging when identifying these types of cancers.

Magnetic resonance spectroscopy can be used to study brain metabolites and tumors, which also enables follow-up and therapy response assessment. These metabolites can provide insight into the type of lesions and brain malignancies. Identifying molecules and learning about their biophysical properties are two analytical uses for magnetic resonance spectroscopy.

As a result, this method is a multi-parametric molecular imaging methodology that can successfully complement a magnetic resonance imaging research and identify biochemical patterns of many characteristics and facets of brain tumors.

Diffusion-weighted imaging (DWI) uses the minute movement of water molecules to reveal more information about the brain. Diffusion-weighted imaging (DWI) has been used to distinguish between brain tumors with high and low cell numbers, as well as to identify the type of brain tumor based on the density of cells.

The study was undertaken to characterize supra-tentorial tumors using magnetic resonance spectroscopy & diffusion weighted imaging in addition to other magnetic resonance imaging (conventional)

Methodology:

The present study was conducted in the Department of (Radiology) Radio-diagnosis, KLES Dr. Prabhakar Kore Hospital and Medical Research Centre, Belgaum (Belagavi) from January, 2023 to December, 2023. It was a one year observational study where in 49 number of patients (cases) with supratentorial brain tumors detected by magnetic resonance (MRI) was studied.

Results:

The average age of the subjects is 53.31 years with a standard deviation of 13.66 years. The median age is 55 years, ranging from 28 to 78 years. In terms of gender, there were 21 (42.80%) female subjects and 28 (57.14%) male subjects. This distribution suggests a slight male predominance in the sample population.

Headache emerges as the most prevalent chief complaint, reported by 42 (85.71%) subjects. Following closely, vomiting was noted in 29 (59.18%) subjects. Other frequently reported complaints include seizures, reported by 23 (46.93%) subjects, and dizziness, noted by 18 (36.73%) subjects.

As far as intracranial neoplasms go, choline (ch) is the most specific marker.

A rise in the levels of the metabolite choline (ch) and the ratio of metabolites choline to NAA is highly suggestive of the malignant character of the tumor, which could be graded

Metabolite specificity for meningiomas was demonstrated by alanine (al), which helped distinguish meningiomas from similar (looking) appearing lesions.

When trying to distinguish between high grade gliomas and metastatic tumors without significant alterations, intralesional ADC levels are inadequate.

It was feasible to distinguish between primary and metastatic brain cancers using perilesional ADC levels.

CONCLUSION:

It can be concluded that MR spectroscopy in combination with DWI & ADC values calculation helps in better characterization of different supratentorial tumors and might enhance MR imaging's ability to diagnose patients.

KEYWORDS:

Brain tumors, supratentorial, magnetic resonance imaging (MRI), magnetic resonance spectroscopy (MRS), diffusion weighted imaging (DWI), apparent diffusion coeffient (ADC), gliomas, neoplasms, metabolites, choline, NAA, tumor grading.

INTRODUCTION

Term supratentorial region of the brain in anatomy, is the area located above the tentorium cerebelli. The area of the brain situated beneath the tentorium cerebelli is referred to as the infratentorial region. In contrast, the supratentorial region encompasses the cerebrum, while the infratentorial region encompasses the cerebellum and in addition to other structures

"Intra-cranial space occupying lesion" refers to any type of neoplasm, whether primary or secondary, malignant or benign, or along with any infectious / inflammatory mass present intracranially i.e. present within the cavity formed by cranial bones.[1] It encompasses various other pathological causes like various kinds of cystic lesions[2], hemorrhages[3,4] and malformations of vascular etiologies[5.6]

To represent any neoplasm, benign or malignant, primary (1^0) or secondary (2^0) lesions the term a tumor is used which means a solid aggregation of tissue formed when abnormal cells attach each other cohesively.

Approximately 9% of all primary neoplasms in humans are primary tumors of the central nervous system and its covering layers.

Neoplastic lesions occurring intracranially can arise from either neuronal tissue or glial tissue. Among them, those arising from central neurogenic origin have more complexity. These tumors account for approximately 50% of all intracranial space-occupying tumors and are derived from neuroepithelial elements of the brain, excluding microglialcells.[7,8]

When Bailly and Cushings began their research in the decade of 1920 , field of the central nervous system malignancies was systematically studied. In the last thirty years, numerous studies have indicated that both the frequency and characteristics of intracranial neoplasms exhibit significant variations in race and geography.[9]

Correct clinical management of patients with supratentorial tumors depends on an specific diagnosis. It becomes extremely tricky to distinguish between non-neoplastic and neoplastic CNS lesions when a patient presents for management of multifocal or focal brain lesion as they can present showing common clinical profile and findings. Which poses an obvious diagnostic uncertainty for doctors and surgeons regarding further treatment & future plan of action.[10]

Therefore, it becomes very crucial to differentiate between non-neoplastic etiologies and malignant conditions since approach for the therapy varies significantly for each. Initial imaging techniques for assessment of these lesions are routine magnetic resonance (MRI) scanning and (CT) computed tomography scanning.

Abnormalities can be located and detected with great sensitivity using magnetic resonance imaging (MRI). Despite of the importance of magnetic resonance imaging in the diagnosis of intracranial diseases, intracranial space occupying lesions (ICSOL's) may not always show up on conventional MRI with specificity, even after administration of intravenous contrast agents. That constraint hampers the precision and capacity of Magnetic Resonance images (MR) in discerning between tumors and non-neoplastic conditions, as well as between benign and malignant diseases.

Conventional imaging techniques also fail to adequately reveal information regarding the blood supply, cellular composition, and metabolic information of the tumors lesions.[10,11]

Morphological classification of these intracranial mass lesions using conventional MRI alone even after contrast imaging may be difficult without the histopathological examination of the suspected tissue. Additional diagnostic tools are necessary if the results are not clearly demonstrable or satisfactory. If there is high clinical suspicion index for aggressive nature of the lesion the histopathological examination can be undertaken.[10-13]

But, a 1.7% mortality rate has been reported with biopsy procedures along with high rate of other serious complications. After undergoing the histopathological examination sometimes it is not possible to comment clearly with respect to the nature of the lesion due to lesion complexities and cases of such lesions undergo these invasive examinations in order to negate the possibilities.

In order to avoid delaying the start of treatment and avoiding needless biopsy, a non-invasive imaging technique that can increase diagnostic accuracy would be highly helpful, particularly in unclear or unusual cases.

One method for figuring out a compound's molecular structure or identifying its presence is magnetic resonance spectroscopy, or MR Spectroscopy.[13] The living brain's metabolic information is obtained through MR spectroscopy.

N-acetyl aspartate (NAA), lipids, lactate, myo-inositol, glutamine, glutamate, and choline are the main brain metabolites that have been identified.[14–15]

These metabolites exhibit aberrant levels in pathological processes when compared to normal brain tissue.

As a method for differentiating between cancerous and non-neoplastic brain lesions, MR spectroscopy is intriguing[16] The use of magnetic resonance spectroscopy (MR Spectroscopy) in describing, classification, and distinguishing neoplastic lesions from focal non-neoplastic lesions such as bleeds, stroke, and infective pathologies has been the subject of numerous studies conducted globally.

Innovations in magnetic resonance spectroscopy (MRS) hold significant potential for furnishing supplementary functional and metabolism related data in the examination of intracranial tumors. These techniques can yield biomarkers pertaining to neural integrity, the growth of cells or cell breakdown, how energy is used, and changes in the dead tissue.

To investigate tumors, grade gliomas, plan therapy, and assess treatment response, a variety of spectroscopic techniques have been employed, such as single (S) and multivoxel (M) MRI spectroscopy It has also been reported that the typical MRS appearances of non-neoplastic intracranial pathologies like cerebral infarction, TB, and abscess are distinct from the spectroscopic characteristics of tumors.[17]

Consequently, MRS may be able to differentiate between neoplastic and non-neoplastic disease conditions. Although there have been few reports [(15–20)] indicating a need of more extensive research studies and larger clinical trials to address this important clinical issue.

But since MR spectroscopy has not been readily available at many centers, only a small number of investigations have looked at its use in the identification of intracranial tumors in India yet. The current research investigation assessed the potential benefit of MR spectroscopy when combined with diffusion weighted imaging for the analysis and diagnosis of intracranial space-occupying lesions when employed in addition to traditional magnetic resonance imaging (MRI) with the goal

to better understand neoplastic lesions. This will help in integrating MR spectroscopy & diffusion weighted imaging along with regular MRI examination for better diagnosis of intracranial space occupying lesions.

AIM & OBJECTIVES:

To characterize supra-tentorial tumors into benign and malignant using magnetic resonance spectroscopy & (DWI) diffusion weighted imaging sequences of magnetic resonance (MRI) imaging in addition to conventional magnetic resonance sequences.

REVIEW OF LITERATURE

"Intra-cranial space occupying lesion" refers to any type of neoplasm, whether primary or secondary, malignant or benign, or along with any infectious / inflammatory mass present intracranially i.e. present within the cavity formed by cranial bones.[1]

Intracranial space occupying lesions are mass lesions occurring within the cranial cavity, either intra or extra-axial, which can expand in volume causing displacement of normal intracranial structures and increase in intracranial pressure. These lesions can be classified as:

1. Congenital: Dermoids, Epidermoids.
2. Traumatic: Subdural & Extradural haematomas.
3. Inflammatory: Abscess, Tuberculoma, Syphilitic gumma, fungal granulomas.
4. Parasitic: Cysticercosis, Hydratid cyst, Amoebic abscess, Schistosoma japonicum infection.
5. Neoplasms: Intra-axial, extra-axial, primary or secondary masses.

A study conducted in 1995 at Jinnah Postgraduate Medical Centre, Karachi, using CT scan and MRI revealed that 32.1% of the 386 cases of (SOL) Intracranial Lesions included neoplastic etiologies with inflammatory masses. Research undertaken also revealed that 13.7% of the cases were meningiomas, 13.2% were abscesses, and 13.2% were pituitary tumors. Authors also reported that, ICSOLs had lower occurrence in females as compared to males as per the study and the peak age group was 11-20 years.[21]

ANATOMY [22]

The brain, an enormous collection of nerve tissue, is split into the cerebrum, cerebellum, midbrain, pons, and medulla oblongata, the five regions that make up the brain architecturally and functionally.

EMBRYOLOGY

During fetal development the ectoderm overlying the notochord becomes thickened to form the neural plate which is then converted into neural groove and neural tube. The brain is formed by the bigger cranial portion of the neural tube, whereas the spinal cord is developed from the narrower caudal end.

The cranial part of the neural tube consists of three dilatations.

The first one is prosencephalon which divides into diencephalon and telencephalon. The thalamus is developed from the diencephalon, and the cerebral hemispheres through the telencephalon.

Second dilatation is of the mesencephalon which forms the midbrain. Finally there is rhombencephalon which gives rise to metencephalon forming the pons & cerebellum and myelencephalon which forms the medulla.

Gross anatomy

A dura matter layer recognized as the tentorium cerebelli splits the cranial compartments into supra and infra tentorial spaces.

The supra-tentorial compartment is the larger compartment of the two and is occupied by cerebral hemispheres.

The cerebrum, which makes up the majority of the brain's structure, is split into the left and right hemispheres. Its numerous twisted ridges (called gyri), multiple depressions (called sulci), and its fissural areas combine to give it a surface area of about 2.2 m^2.

Fissures further divide each half of the cerebrum into various lobes, every single of which performs a different role.

The four lobes that make up the brain are the occipital, parietal, temporal, and frontal.

Lateral surface of each of the hemisphere is convex in shape and has two prominent sulci - the central sulcus (Rolando's fissure) and lateral sulcus (fissure of Sylvius). The central sulcus separates the frontal lobes and parietal lobes. Frontal lobe and temporal lobes are separated with fissure of Sylvius. Temporo-parieto-occipital junction is an ill-defined area rather than a clear anatomical demarcation.

The hemispheres have a flat medial surface. In a sagittal section, the obvious landmark on the medial surface is the cut surface of the corpus callosum, whose components being the rostrum & genu anteriorly, the body in the middle, and splenium posteriorly. The corpus callosum is well demarcated by callosal sulcus which is continuous with the hippocampal sulcus.

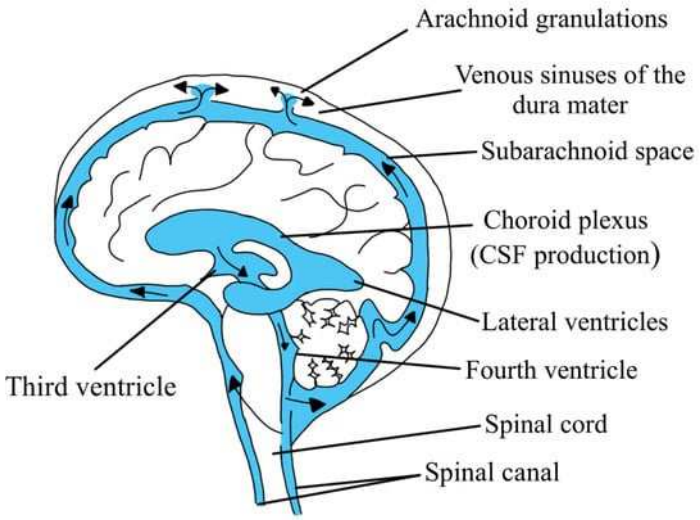

Figure 1 – Ventricular System of Brain

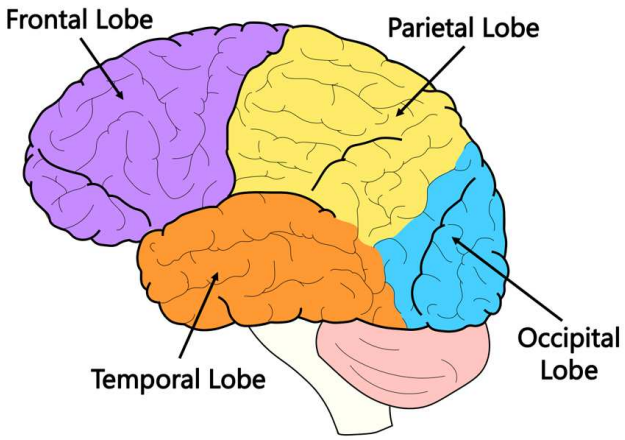

Figure 2 – Lobar Anatomy of Brain

With a thickness of 2-5 mm and a population of over 40 billion neurons and 240 billion neuroglia, the cortex of the brain is the external most part of the cerebrum. The thicker innermost layer is called the white matter, and it is here that interconnecting groups of axons extend from the diencephalon's thalamus to the cerebral cortex and from the cortex to other areas. Right-sided motor and sensory function is regulated by the left side of the cortex, while left-sided function is regulated by the right side of the cortex. Cortex's sensory and motor regions are linked to association areas that process incoming information and plan a motor response.

The brain's second largest region is the cerebellum. Coordination, equilibrium, body postures, and the accuracy and timing of actions are all processed by the neurological center.

The medulla oblongata and pons are located anterior to the cerebellum. Tentorium cerebelli, which divides it from the cerebrum, covers its upper surface. The cerebellar surface has many foliae that differ in depth at different locations, but it is not as convoluted as the cerebrum. The cerebral cortex is composed of two types of matter: white matter makes up its interior and gray matter makes up the outermost layer.

There is also grey matter in the midbrain, which connects the cerebral hemispheres above the pons. The third and fourth ventricles of the brain are linked by a small canal called the cerebral aqueduct of Sylvius.

The pons is located superior to the medulla oblongata, anterior to the cerebellum, and inferior to the midbrain. It is made up of white matter fibers that join the cerebral hemispheres. Linking the pons above with the spinal cord below, the medulla oblongata is situated at the base of the brainstem.

The brain's ventricular system is made up of a continuing network of cavities that are filled with cerebrospinal fluid. There is a lateral ventricle with frontal, temporal, and occipital horns in each cerebral hemisphere. The interventricular foramina of Monro serve as a conduit between the two lateral ventricles and the third ventricle. The Sylvius aqueduct connects the third ventricle, which is situated midway among the two thalami, to the fourth ventricle. The choroid plexuses in the lateral ventricles produce CSF. The third and fourth ventricles also contain portions of the choroid plexuses.

The foramen of Magendie and Luschka, which are continuous with the spinal subarachnoid space caudally as well as the subarachnoid space over the exteriors of the cerebral hemispheres upwards, are where the CSF departs into the basal cisterns after flowing from the lateral ventricles to the third ventricle and then to the fourth ventricle.

Brain Tumors

As mentioned previously brain tumors are the most important cause of ICSOLs and constitute the majority of cases of this study so they will be discussed briefly in the following paragraphs.

A brain tumor, one of the most frequent intracranial space-occupying lesions, is a neoplasm, or abnormal growth of cells, within the brain. Usually in the brain parenchyma, but also in lymphatic tissue, blood vessels, cranial nerves, meninges, the skull, the pituitary, or the pineal gland, they are created by an aberrant and unregulated division of cells. The cells that are involved in the brain can be either glial (ependymal, oligodendrocyte, or neuronal). Additionally, brain tumors may have metastasized, especially in older individuals.

Because they are invasive and infiltrative within the restricted volume of the cranial space, brain tumors are inherently hazardous and may even be potentially fatal. Nonetheless, certain brain tumors, such as lipomas, do not always result in death. Brain tumors may be benign or malignant. The location, type, stage of development, and size of the tumor are just a few of the numerous factors that influence its level of danger.

Since the skull protects the brain, early brain tumor detection is only possible with the use of diagnostic tools, especially imaging tools. Typically, a tumor is only detected when it has progressed to the point where it is causing inexplicable symptoms.

Of all primary CNS tumors, 85% to 90% are brain tumors. The average annual occurrence of primary aggressive CNS tumors in the USA is 6.36 per 100,000 persons annually, with an estimated mortality of 4.22 per 100,000 persons annually, according to information accessible in the Surveillance, Epidemiology, and End Results (SEER) database for the year 2007. In the year 2008, there was an estimated 238,000 fresh cases of malignant brain tumors along with various CNS tumors discovered across the globe, and 175,000 fatalities had been reported.[23]

In the year 2012, there were 22,910 cases reported and 13,700 fatalities in the USA due to brain and other nervous system tumors.[23]Anaplastic astrocytoma, glioblastoma and the glial cell tumors make up about 38% of primary brain tumors. On the contrary hand, about 27% of primary brain tumors are mesenchymal tumors and meningiomas.[23]

Additionally fewer cases of primary brain tumors are contributed by schwannomas, oligodendrogliomas, ependymal tumors, pituitary tumors, medullo-blastomas, central nervous system (CNS) lymphomas and astrocytomas (low grade).

Variations with respect to race

Variations exist across various ethnic populations living in a single nation, and reports of a three-fold variation in occurrence among nations have been made. The greatest numbers seem to be found in industrialized nations, yet this could just be the result of improved identification procedures.[24]

Variations with respect to gender

Men are diagnosed with brain tumors at a rate of 1.5:1, indicating that men are more likely than females to have one. In comparison to men, females are slightly more probable to develop meningiomas and pituitary adenomas.[24]

Variations with respect to age group

Preadolescent children are more likely to have posterior fossa tumors, while supratentorial tumors are more common in adolescents and adults. Younger adults are more likely than older adults to develop low-grade gliomas, such as astrocytomas. High-grade gliomas typically appear in the 4th or 5th decade of life or later. Examples of these include glioblastoma multiforme and anaplastic astrocytoma. When it comes to childhood cancers, brain tumors are the most common solid tumor

in children second only to leukaemia. Primary CNS neoplasms affect 3.6 out of every 100,000 children in a single year.[24]

Among all CNS malignancies, gliomas make up over 70%. The most prevalent and aggressive histopathological subgroup among these is glioblastoma multiforme (WHO - World Health Organization, Grade IV).

Regarding those suffering from gliomas, the likelihood of survival remains poor besides in instances of the World Health Organization Class I pilocytic astrocytomas. Individuals with glioblastoma, in particularly, not often live greater than five years following discovery (no more than 3 percent do so), and the adverse outcomes tend to be related to elderly status. In addition, although these kinds of cases are extremely uncommon, it could be that gliomas are closely associated with several types of inherited disease conditions.[25]

During the span of the previous 20 years, patterns of tumors of the central nervous system in men and women were assessed in five cancer databases based on the population in India: the city of Mumbai, Delhi, Chennai, Bangalore & Bhopal. Among CNS malignancies, the mean age-adjusted rate of incidence ranged between 2.53 (the city of Chennai registry) from 4.14 (Delhi registry) per 100,000/year for men and 1.46 (Bhopal registry) to 2.66 (Delhi registry) for females. All databases, with one notable exception of New Delhi, indicate a rising pattern in the occurrence percentages of malignancies related to the nervous system in men and women. There was no statistically significant difference in the incidence between the Delhi and Bhopal registry.

In overall Bangaluru , Chennai and Mumbai registries, there was a statistically noteworthy rise among the age-adjusted incidence rates of CNS malignancies

reaching in excess of 3% for men and women. This approach unveiled a rising pattern in nervous system cancers among both genders across almost all registries throughout the entire observation period.[26]

There exist multiple studies linking various factors related to lifestyle and the environment, such as work-related hazards, nutrition, and carcinogens in the environment, with an increased risk of glioma. However, medical irradiation used for therapy is the sole variable that has been demonstrated to be directly associated with an increased risk of glioma.[25]

In particular, kids who received radiotherapy for treating the diagnosis of (ALL) leukemia had a significantly greater likelihood of brain tumors and neuroectodermal malignancies, often ten years after radiation.

Multiple investigations have found an important connection between the TP53 gene's G:C -> A:T shifts and the promoter methylation of the 06-methylguanine-DNA methyltransferase (MGMT) gene in gliomas. This suggests that O6-methylguanine DNA adducts, that can be generated by either endogenous or exogenous alkylating agents, might play a role in the formation of gliomas.[25]

CLASSIFICATION

The WHO classification of CNS tumors constitutes as the basis for this categorization. The WHO methodology aims to provide a cellular categorization that is both prognostically and globally relevant by integrating and relating structure, cellular genetics, molecular biology, and immunological indicators.

A number of factors led to the abandonment of earlier attempts to create a TNM-based categorization system: the size of the tumor (T) is not as significant as tumor histopathology and the location; lymph nodal involvement (N) is meaningless because there do not exist lymphatics in the brain or spinal cord; and metastatic

dissemination (M) is scarce because the majority of individuals with central nervous system neoplasms fail to survive for lengthy periods to grow metastatic cancer.[27]

Rather, grade is established by the World Health Organization's classification system for CNS cancers, which relies upon the tumor's histopathological features.[28]

Following represents the histology classes:

Grade I WHO

Distinct tumors, limited proliferative capacity tumors, with the chance of recovery after surgery to remove them are all considered part of this.

Grade Il WHO

Compared to class I cancers, tumors in this group reoccur with greater frequency after local treatment, and but exhibit less proliferation and invasion.

A few tumor forms have the potential to advance to more advanced stages of cancer.

Grade III WHO

This group comprises tumors that exhibit elevated levels of mitotic activity and nucleus atypia, two histopathological indicators of aggressiveness. These lesions exhibit anaplastic histopathology with the ability to infiltrate. Typically, aggressive adjuvant therapy is employed in their treatment.

Grade IV WHO

This category encompasses lesions with high mitotic activity, a propensity for necrosis, and a history of rapid advancement before to and during surgery, which frequently results in grave consequences. Aggressive adjuvant therapy is frequently used to treat these lesions.

The WHO's listing of CNS tumors is shown in below. Tumor categories and categories that are specific to the peripheral nervous systems are excluded.[29]

WHO grades for CNS tumors [30]

TUMOR TYPES	WHO GRADES
ASTROCYTIC TUMORS	
SUBEPENDYMAL GIANT CELL ASTROCYTOMA	I
PILOCTIC ASTROCYTOMA	I
PILOMYXOID ASTROCYTOMA	II
DIFFUSE ASTROCYTOMA	II
PLEOMORPHIC XANTHOASTROCYTOMA	II
ANAPLASTIC ASTROCYTOMA	III
GLIOBLASTOMA	IV
GIANT CELL GLIOBLASTOMA	IV
GLIOSARCOMA	IV
OLIGODENDROGLIAL TUMORS	
OLIGODENDROGLIOMA	II
ANAPLASTIC OLIGODENDROGLIOMA	III
OLIGOASTROCYTIC TUMORS'	
OLIGOASTROCYTOMA	II
ANAPLASTIC OLIGOASTROCYTOMA	III
EPENDYMAL TUMORS	
SUBEPENDYMOMA	I
MYXOPAPILLARY EPENDYMOMA	I
EPENDYMOMA	II
ANAPLASTIC EPENDYMOMA	III
CHOROID PLEXUS TUMORS	
CHOROID PLEXUS PAPILLOMMA	I
CHOROID PLEXUS ATYPICAL PAPILLOMA	II

CHOROID PLEXUS CARCINOMA	III
OTHER NEROEPITHELIAL TUMORS	
ANGIOCENTRIC GLIOMA	I
CHOROID GLIOMA OF THIRD VENTRICLE	II
NEURONAL AND MIXED NEURONAL GLIAL TUMORS	
GANGLIOCYTOMA	I
GANGLIOGLIOMA	I
ANAPLASTIC GANGLIOMA	III
DESMOPLASTIC INFANTILE ASTROCYTOMA AND GANGLIOGLIOMA	I
DNET	I
CENTRAL NEUROCYTOMA	II
EXTRAVENTRICULAR NEUROCYTOMA'	II
CEREBELLAR LIPONEUROCYTOMA	II
PARAGANGLIOMA OF SPINAL CORD	I
PAPPILARY GLIONEURONAL TUMOR	I
ROSETTE FORMING GLIONEURONAL TUMOIR OF FORTH VENTRCLE	I
PINEAL TUMORS	
PINEOCYTOMA	I
PINEAL PARENCHYMAL TUMOR OF INTERMEDIATE DIFFERENTIATION	II & III
PINEOBLASTOMA	IV
PAPILLARY TUMOR OF PINEAL REGION	II & III
EMBRONAL TUMORS	
MEDULLOBLASTOMA	IV
CNS PNET	IV

ATYPICAL TERATOMA / RHABDOID TUMOR	IV
TUMORS OF CRANIAL AND PARASPINAL NERVES	
SCHWANNOMA	I
NEUROFIBROMA	I
ANAPLASTIC/MALIGNANT MENINGIOMA	I, II & III
MALIGNANT PERIPHERAL NERVEW SHEATH TUMOR	II, III & IV
MENINGEAL TUMORS	
MENINGIOMA	I
ATYPICAL MENINGIOMA	II
MALIGNANT / ANAPLASDTIC MENINGOMA	III
HEMANGIOPERICYTOMA	II
ANAPLASTIC HEMANGIOPERICYTOMA	III
HEMANGIOBLASTOMA	I
TUMORS OF SELLAR REGION	
CRANIOPHARYNGIOMA	
GRANULAR CELL TUMOR OF NEUROHYPOPHYSIS	I
PITUICYTOMA	I
SPINDLE CELL ONCOCYTOMA OF THE ADENOHYPOPHYSIS	I I

The WHO classification of brain tumors has been widely accepted for more than 25 years since the first edition was published in 1979. The fourth version of the WHO classification was released in 2007 after revisions to the previous one. Pathophysiology[24]

Brain malignancies can present neurological symptoms in a variety of ways. Certain neuronal circuits that traverse the cerebral cortex may sustain damage from tiny tumors in strategic sites. Normal operation may be disrupted by tumors that infiltrate, permeate, or alter healthy parenchymal mater. High intracranial tension can result from the emergence of cerebral tumors and associated swelling since the brain

can only occupy a certain volume within the skull. The presence of tumors close to the third and fourth ventricles might block the circulation of CSF and cause hydrocephalus with obstruction. Moreover, tumors cause the development of new blood vessels, which compromises the regular blood-brain barrier.

The combined impacts of hydrocephalus, swelling, and tumor growth may increase tension inside the skull and decrease cortical blood flow. An increase in compartmental pressure (ICP) can result in tissues displacement or prolapse across the magnum foramen, via the tentorium (transtentorial) or beneath the falx cerebri (subfalcine). More subtle medical history may be linked to slow-growing tumors. When these tumors are found, they are typically enormous. The majority of initial brain tumors do not spread, but when they do, local extension of the primary tumor usually happens before metastasis

Beyond the nervous system, brain tumors that have grown and progressed from primary tumors may be the first sign of cancer or suggest a possible relapse. On the other hand, symptoms and indicators of neurological metastases are analogous to those of the primary brain tumors. Several cranial nerve impairments may be the initial symptom of leptomeningeal invasion.

History

The best way to comprehend the medical manifestations of various brain tumors is to look at how complaints and signs connect to the structure of the brain[31]

Headache, changed psychological state, nausea, movement disorder, deficits, vomiting, and disturbances in posture are among nonspecific signs that may be experienced. Additional symptoms of CNS tumors include difficulties with speech, localized sensory defects, vision alterations, and focal convulsions. Though most

symptoms appear over time, there are times that they appear unexpectedly, such as an intraventricular tumor abruptly blocks a third ventricle or whenever hemorrhage starts within the tumor.

Brain tumors need to be distinguished from other space-occupying lesions such infections, vascular malformations, and stroke, which may appear with an identical medical picture, regardless of whether they are 1^0, metastatic, cancerous, or noncancerous.[32]

1^0 brain tumors and cerebral metastases can appear similarly in terms of individual appearance in cases of cerebral neoplasms. The origin of the symptoms—a rise in intracranial tension, compression of vital gray or white matter, movement of intracranial contents, or subsequent cerebral ischemia—determines how it appears.

Intracranial tumors may cause a focal or generalized impairment depending on where they are located, although there may not be any specific symptoms or they may even erroneously localize.

A deviation or mass effect of sixth cranial nerve near the base may cause diplopia. Pineal tumors may cause Parinaud syndrome, or impaired upward sight. Tumors of the frontal lobes can cause anosmia.

Tumors located in the occipital lobe can specifically lead to the development of homonymous hemianopia or partial visual field deficits.

Imaging in the diagnosis of ISOL

There are several conditions that can cause focal cerebral disease, such as primary neoplasms, metastatic tumors, abscesses, subacute infarcts. Differentiating between malignancies and non-malignant imitators is crucial since everyone has a distinct course of therapy.[17]

When evaluating individuals who have brain tumors, radiological investigations are essential two of the main & most often used ways of imaging in healthcare are CT scan and MRI scan.

The diagnosis and assessment of intracranial malignancies have greatly improved because of technological advancements in these modalities, the utilization of contrast media, and the advent of additional methods for imaging.[33]

When a brain tumor is medically anticipated an imaging study is necessary to identify the tumor's position, dimensions, and connection to nearby structures. When choosing the best course of treatment, which may include procedures like treatment with chemoradiation, surgery, this knowledge is very important.[33]

Magnetic resonance imaging

When assessing individuals who have a brain tumor that is medically suspected, a magnetic resonance imaging scan (MRI) is the preferred method. Due to the multi-planar technique , superior contrast image quality, and adaptable standards, it can be used to guide biopsy procedures, plan suitable treatment, evaluate treatment response, and determine the precise position and size of tumors.

Spin-echo T1-weighted sequence (TI WI), T2-weighted sequence (T2WI), fluid attenuation inversion recovery sequence (FLAIR), and T1 weighted sequence (in all planes) following the injection of para-magnetic substance (Gd chelates) are the conventional protocols that are used most frequently across organizations.[33]

Most brain tumors have longer T1 and T2 relaxation durations, which causes them to appear low signal on T1-weighted sequence (T1WI) and high signal on T2-weighted sequence (T2WI) in comparison to normal tissue in the brain. The majority of tumors exhibit mixed signal strength on PD Weighted sequence. Some tumors have a mixed morphology due to an abundance of lipids, bleeding, tissue necrosis, and

calcium deposits. As with CT, the addition of contrast agent to a conventional MRI can help identify many tumors in the brain and help differentiate specific tumors from adjacent neural tissue. Gd chelates is among the more often utilized MRI contrast media for visualizing tumors in the nervous system (CNS).[33]

A variety of new MR approaches are being investigated to improve the accuracy of diagnosis in cancer imaging, including before and following treatment, even though conventional spin-echo MR sequencing in conjunction with post-contrast MR Images are unquestionably effective in identifying and delineating brain tumors. The goal of these methods is to provide enhanced contrast intensities and enhance the quality of images as well as information gathering over traditional MR spin-echo imaging. These include gradient echo pulse imaging, fast spin echo (FSE) imaging, inversion recovery (IR) imaging, short tau inversion recovery (STIR) imaging, and echo-planar (EPI) imaging. But without a histopathological investigation of the suspicious tissue, a diagnosis made only on the basis of morphologic and anatomic observations is frequently deemed questionable. Easy, noninvasive methods which can offer greater detection accuracy than radiologic imagery are obviously needed.[33]

MR Spectroscopy

An intriguing non-invasive method of using magnetic resonance imaging to access numerous chemicals from bodily tissues is called MR spectroscopy. The disorders are then diagnosed, observed, and their response to therapy is seen using the metabolite data. While nucleus of 1H, 19F, 31P, 13C, and 23Na can also be used for MRS, the majority of nuclei used in clinical practice today are 1H and 31P. While MR spectro and MRI use similar basic principles for signal gathering, they differ in

processing, displaying, and interpreting the data. Rather than visuals, a graph is produced that compares maximum amplitudes to corresponding frequencies.

Source of signal

Fat & water proton signals predominate in the tissue's proton signal, which is used to create MRI imagery. The weak signal of proton derived from additional metabolites makes them unhelpful for imaging.

Similar to MRI the goal of MRS is to identify minute molecules. The majority of clinically significant compounds resonate within the fat and H_2O frequencies.

Suppressing the significant signal of fat and H_2O is necessary in order to recognize these tiny compounds.

In what way are the tissue's minute metabolites identified? [34]

Chemical shift forms the basis of MRS while it is the cause of artifacts in MRI. Protons' accompanying chemical atmosphere / electron cloud affects their precessional frequency. Protons in H_2O undergo an entirely distinct precession rate as compared to protons in lipids, and similarly positioned protons within various substrates have which also have a different precession rate. Chemical shift is the term used to describe such type of variation in precessional frequencies caused by a changed chemical microenvironment. Therefore, we may identify the metabolites at which they're precessing by calculating the frequency of those protons.

Proton frequency for a particular metabolite equals a chemical shift - location of peak in a uniform background.

The chemical shift expressed in hertz will vary according to various magnetic field intensities because the precessional frequency for each proton is exactly related to the magnitude of the magnetic field surrounding it (Larmors frequency). To avoid

disarray, chemical shift is expressed as (ppm) parts per million; this ppm value will remain constant for a given metabolite at all field strengths.

Since chemical shift is related to the outside magnetic fields, minor chemical shifts won't be noticed at lower field strengths. MRS can be used with 0.5 T or higher, however for better spectral discrimination and a higher ratio between signal and noise, 1.5 T or higher field magnitude is needed. Compared to MRI, this requires a substantially more homogeneous environment since it must detect smaller amounts of metabolites having small chemical shifts.[34]

Spins with small difference in precessional frequency within the same molecule interact with each other this is known as J coupling. The presence of electrons surrounding the nuclei facilitates this process. An involved spin's resonance frequency is altered by this spin-spin interaction. A lactate doublet near 1.3 ppm is one example of how the J-coupling splits spikes on a spectroscopic map[34]

There are two broad categories into which spatial localisation methods can be categorized:

1. Single-voxel approaches, that gather the entire spectrum representing one part of the brain
2. Multi-voxel methods (sometimes referred to as chemical shift imaging (CSI) or MR spectroscopic imaging (MRSI)) wherein several areas are recorded concurrently.

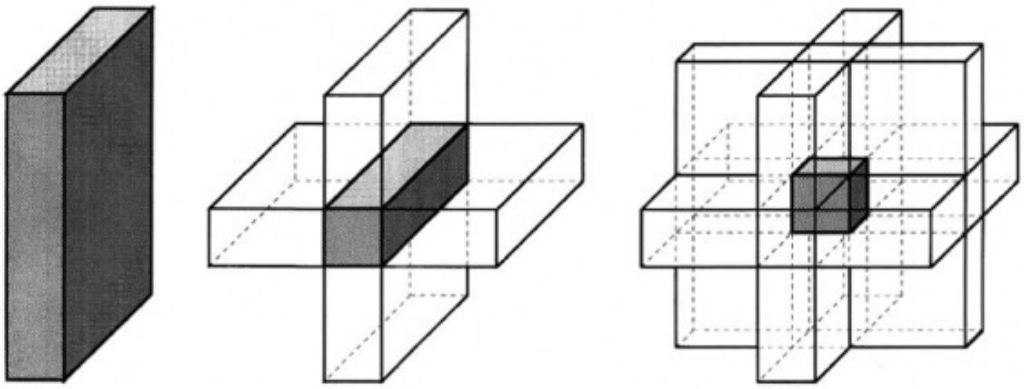

Figure 3 – Localization with single voxel spectroscopy

Single-Voxel Proton MR Spectroscopy:

Medical MRS investigations employ two single-volume protons localisation approaches.[35]

1. STEAM [S-Stimulated E-echo A-acquisition M-mode]

2. PRESS [P-Point RE- resolved SS- spectroscopy]

Magnetic field inhomogeneity's are necessary for 'H MRS spatial localization, just like in MRI localization. Three orthogonal gradients are applied sequentially in STEAM and PRESS to choose three slices that characterize the spatially localized volume to be investigated. Three in total 90° pulses are utilized during STEAM sequencing & the "stimulated echo" is recorded.

In PRESS, first pulse is a 90° pulse, refocusing (180°) pulses are what the second and third pulses are. In the slice-selective event, specific Radiofrequency pulses are administered for stimulating the spins within every slices.[35]

Thus, only spins that are excited and observable are within the defined three-slice sequence.

Advantages of STEAM

- The fact that echo times (TE) smaller than 20 msec are practiced in this method, STEAM provides benefits for the monitoring of proton metabolites with short T2 relaxation, such as glutamine, glutamate & (Myo) myoinositol.
- STEAM can be used to dampen the water resonance signal more effectively.
- STEAM typically yields a superior slice profile due to the relative ease of generating a sharp slice profile with a 90° pulse compared to pulse of180°.
- Accessibility to large bandwidths 90° excitation pulse is easier and consume less power compared to their high bandwidth 180° counterparts.

The primary benefit of the PRESS sequence lies in its theoretical doubling of signal intensity compared to the STEAM sequence, resulting in twice the signal recovery relative to STEAM.

PRESS is notably has low susceptibility for eddy current effects human motion, effect of coupling (homonuclear).

The distinctions outlined above are relatively subtle, resulting in similar outcomes between STEAM and PRESS in clinical brain spectroscopy. However, PRESS is predominantly favored due to its higher signal/ noise ratios (SN Ratio).[35]

Size of the voxels:

Spectroscopy via single-voxel typically involves a standard voxel size of 2.0 x 2.0 x 2.0 cm, with resulting voxel volume approximately 8 cm^3.

Minimum voxel size: approximately 1.5 × 1.5 x 1.5 cm (~3.38 cm^3).

Multi-voxel MRSI, standard voxel size ~ 1-2cm^3, minimum ~ 0.5 cm3[35]

Multi-Voxel Proton MR Spectroscopy

Chemical shift imaging (CSD), also known as magnetic resonance spectroscopic imaging (MRSI), is a technique that gathers spectral data from a volume made up of several voxels. Magnetic resonance spectroscopic imaging (MR SI) and chemical shift imaging (CSI) are two common names for multivoxel MRS. This is due to the fact that it entails the conversion of metabolite signal intensities, fractions of peak regions, or max resonance areas into imagery. After that, these representations are superimposed on anatomic magnetic resonance imaging (MR) images to reveal information about the dispersion of metabolites, either quantitatively or qualitatively, within the targeted brain region.

A useful method for mapping the spatial distribution of metabolites in a particular (VOI) volume of interest is two- / three-dimensional MRSI.

Volume determined pulse sequencing for the CSI multivolume method, which specifies a bigger slice, are either STEAM or PRESS pulse sequences. Phase encoded in one, two, or even three dimensions is employed to create spatial localization.[35]

Newer Techniques

The methods used to "speed up" MRI scans are often the same ones employed in fast MRSI procedures; for example, methods based on the utilization of multiple spin echoes ("turbo"-MRSI, equivalent to fast-spin-echo MRI)

• Echo-planar methods (also known as EPSI, or echo-planar spectroscopic imaging)

• Parallel imaging methods, such as sensitivity-encoded (SENSE)-MRSI or SPIRAL-MRSI

Which kind of protocol—multi or single -voxel?

Whether it is worthwhile to investigate the spatial distribution of metabolites, for example, will determine this. The spectrum acquired will differ based on the position within the tumor from which the voxel is collected, as many brain tumors show heterogeneity.

Furthermore, it's possible that the precise position of the metabolic anomaly was unknown prior to the scan, which would support the multi-voxel method. When considering spatial coverage, multi-voxel will consistently seem to be preferable.[36] Wide coverage MRSI is ineffective at shorter TE, hence certain brain regions—such as the posterior fossa, frontal lobes, anterior temporal regions, and when a patient exhibits metallic artefacts—are not suitable candidates for multi-voxel spectroscopy.

Because MRSI requires a longer scan time, it might not be an option for patients who are unstable or have less time. While neither method performs well when head motion is noticeable, MRSI is likewise marginally more sensitive to head motion than SV-MRS.

Steps to obtain a spectra[34]

1. Positioning of the patient

2. The receiver coil's whole observed volume is tailored for magnetic field uniformity. The initial value for localized shimming is provided by global shimming.
3. Obtaining MRI images for the localizing: To insert voxels, images are acquired in the coronal, saggital and axial planes. If the patient has not moved, MR imagery that have been taken during regular imaging can be useful for identifying the location.
4. Choosing the necessary variables and measurements for MRS

Two crucial parameters are TE and TR. Longer TR results in an improved signal to noise ratio. TEs of 20–30 ms, 135–145 ms, and 270 ms are often utilized.

The only significant metabolites that show peaks at longer TEs of greater than 135 ms are choline, lactate, NAA and creatine. At greater TEs, glutamate, lipid, glutamine, inositol, GABA and peak expression is inhibited. At higher TEs, there is significantly less noise. Shorter T2 metabolites, like glutamate, glutamine, and inositol, are treated with shorter TEs.

5. Selection of VOI

SVS or CSI is used depending upon the clinical scenario.

6. Shimming locally

Here, the magnetic field homogeneity over the chosen volume of interest is optimized. More spectral resolution, narrower metabolite peaks, and high signal-to-noise ratio are all indicators of good local shim.

7. The Suppression of Water

Metabolite peaks become visible when the water peak is suppressed. Chemical shift selective spectroscopy, or CHESS, is the method used to suppress water peaks.

8. Data gathering from MRS

Single-voxel spectroscopy typically takes three to six minutes, whereas data collection for CSI can take up to twelve minutes. The quality of the spectral "quality" is largely dependent on how well prescan operations work, which adjust various aspects of scanner functionality prior to data collection. These steps involve optimizing flip angles for water suppression pulses, modifying scanner center frequency to coincide with water resonance, fine-tuning transmitter and receiver gains, and adjusting field homogeneity (also known as "shimming"). A spectrum that is hard to understand can result from any one of these processes failing.

Many of these tasks were previously completed by the operator manually; however, these days, the scanner typically completes these tasks automatically.

9. Processing of the data and displaying it

After processing, the data is converted into spectra and spectral maps. The software sets the zero point of the spectrum in relation to the trimethylsilane frequency.

10.Interpriting

The number of spins that contribute to a metabolite's peak directly relates to the area under its peak. Age and location affect each metabolite's absolute values.

Lack of a vertical scale [35]

There is no Y-axis (vertical) scale shown in the MRS spectra display. Little control over the vertical scale is provided by many software programs, which often automatically scale the data so that the greatest peak occupies the visible region. This may cause ambiguity when comparing various voxels from the same patient, particularly if there are concurrent increases or decreases in all metabolites.

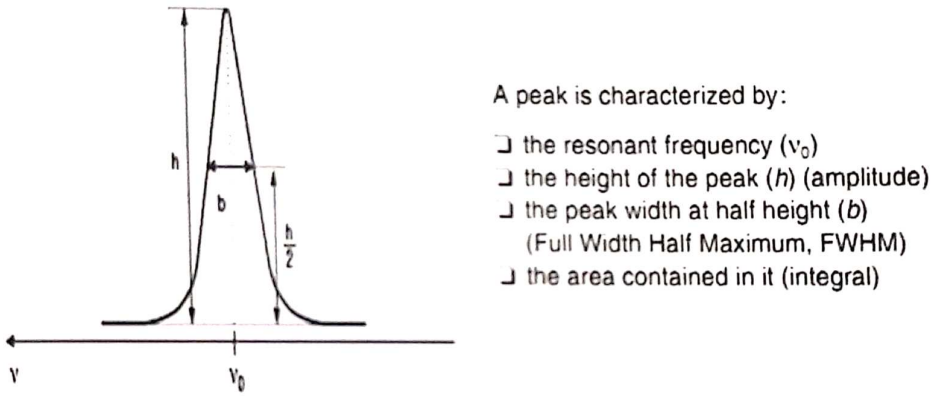

Figure 4 – Characteristics of spectroscopy peak

The metabolites are detected in the spectra because of the following properties:

• They consist of protons (H)

• They exist at concentrations > 0.5 mmol/L

• They oscillate at different frequencies along the horizontal chemical shift axis.

• The hydrogen signal from water is nulled

Common Metabolites Which Are Studied By Using MR Spectroscopy [35, 36, 37]

NAA

Within the typical adult brain spectrum, it is the largest signal. At 2.01 pm, the acetyl group of N-acetyl aspartate resonates, and at 2.04 pm, N-acetyl aspartyl glutamate (NAAG) contributes. Aspartate and acetyl-CoA are transformed into NAA in brain mitochondria. NAA is widely accepted as a neuronal marker and is backed by several lines of research. Research on conditions that are known to cause loss of neurons and/or axons (such as brain tumors, multiple sclerosis plaques, or infarcts) has consistently shown lower levels of NAA. NAA measurements could be helpful in evaluating the CNS's neuronal integrity.

Choline

The phosphocholine (PC), glycerophosphocholine (GPC), and a trace amount of free choline comprise the trimethylamine (-N(CH3)3) groups that contribute to the choline signal (Cho, 3.20 pm). These substances have a role in both the formation and breakdown of cellular membranes, and their levels are higher in disease conditions where there is a higher turnover of membranes, such as tumors. Other circumstances that lead to a rise in Choline encompassing active demyelination, which is mostly caused by breakdown of myelin phospholipids to GPC or inflammation.

Creatine

A composite peak made up of creatine and phosphocreatine, which are involved in energy metabolism through the creatine kinase reaction and produce ATP, is known as the creatine methyl resonance (Cr, 3.03 ppm). A second resonance from creatine's CH2 is also visible at 3.91 ppm in a number of spectra. The equilibrium between PCr and Cr maintains the stability of size of Cr peak in the face of bioenergetic irregularities observed in many pathologies. This stability holds true for all ages. Consequently, the Cr resonance functions as a stable internal reference. Alterations in the numerator metabolite are commonly interpreted as changes in metabolite ratios with creatine as the denominator.

As an example, decline in the NAA to Creatine ratio is commonly understood to indicate a drop in NAA levels.

Lactate :

Due to the relatively small amount of lactate in the brain in normal conditions, the lactate methyl resonance seen at 1.31 ppm in the human cerebral cortex is below identification in the majority of studies. Occasionally, a slight lactate signal can be seen in the ventricles' cerebrospinal fluid (CSF). In pathological circumstances, lactate is frequently elevated. When the Krebs cycle is unable to continue the utilization of glucose, a lack of blood oxygen (from hypoxia or ischemia) will result in a rise in lactate. When the lactate resonance is properly shimming, it appears as a pair of frequencies with peaks separated by 7 Hz. It could be challenging to discern lactate from spatial contamination resulting from lipid signals in the scalp or from overlapping lipid resonances coming from the brain by itself.

The myo-inositol

Myo-inositol (ml) at 3.5–3.6 ppm is one of the stronger signals in the short echo time spectrum. A pentose sugar, ml is a component of the intracellular second messenger system that is triggered by inositol triphosphate. Decreases in hepatic encephalopathy and increases in demyelinating disorders and Alzheimer's dementia have been noted. A leading theory is that heightened mi represents greater numbers of glial cells, which are known to express higher amounts of mi than neurons. The precise pathological implications of changes in ml is unknown.

Glutamate And Glutamine

While the multiplets for 3CH2 and 4CH2 are usually detected between 2.1 and 2.4 ppm, the 2CH protons of both Glu and Gln resonate at about 3.7 ppm. Important functions in brain metabolism are played by glutamine (Gln) and glutamate (Glu). The most commonly found amino acid in the brain and its main neurotransmitter is glutamate. Since GIn and Glu nearly entirely overlap at a field strength of 1.5 T, they are typically referred to as a composite peak Glx and are exceedingly challenging to distinguish.

Lipids[37]

Resonance is observed in lipids around 0.8 and 1.5 ppm, which could conceal lactate. Mobile lipids are markers of high-grade tumors, including primary brain tumors and their metastases, and are typically observed in necrosis. Due to contaminants from fat under the skin and fat derived from the skull's marrow, lipids may also be detected in the spectra.

Gamma aminobutyrate GABA is a neurotransmitter that inhibits function and is a type of amino acid. GABA resonances share a great deal of overlap with signals from other, more prevalent metabolites, particularly creatine. Reduced or aberrant GABA concentrations have been discovered via H MRS research in a number of neuropsychiatric conditions, such as drug addiction, significant depression, anxiety disorders, and epilepsy. Reduced or aberrant GABA concentrations have been discovered via H MRS research in a number of neuropsychiatric conditions, such as drug addiction, significant depression, anxiety disorders, and epilepsy.

Glycine

Widely dispersed across the nervous system's , glycine is an amino acid that serves as an antioxidant and an inhibitory neurotransmitter. Patients with hyperglycinemia and tumors have elevated glycine levels. Since the glycine resonance for in vivo MRS studies overlaps with that of myo-inositol (at 3.55 ppm), it is not possible to definitively observe glycine during shorter echo lengths. However, because of the reduction of inositol, its existence may be confirmed at longer echo times.

Valine

Valine, an indispensable amino acid crucial for protein synthesis, manifests in spectra as two doublets from its methyl protons. These resonances overlap with leucine and isoleucine in the 0.95–1.05 ppm range. Conditions like branched-chain ketonuria and hypervalinemia can lead to heightened valine levels, which have also been linked to occurrences of abscesses of brain parenchyma.

Alanine

During MRS analysis of intracranial tumors, alanine emerges as a significant metabolite to examine. Positioned at 1.47 ppm, it's considered a non-essential amino acid, potentially overshadowed by fats and lactate in readings. Elevated alanine levels have been specifically observed in meningiomas.

Macromolecules

Lipids are examples of macromolecules that are only visible at brief echo times. In a number of diseases, including multiple sclerosis (MS) and brain tumors, the presence of pathologically changed macromolecules or mobile lipids may offer helpful extra diagnostic data.

Regional Variations In The Metabolites[36]

NAA: In comparison to the cortical subcortical junction, the hippocampus contains less NAA. Compared to other brain regions, the cerebellum has a lower concentration of NAA.

Cr: As opposed to white matter, gray matter has greater amounts of creatine.

Cho: As opposed to gray matter, white matter has a slightly greater amount of choline. Generally speaking, the pons contains greater choline than the other regions of the brain.

Differences in brain spectra with years of age

Early Development of the Brain in Children: Cho and ml are high at birth, while NAA is low. During the first few years of life, there is a gradual shift towards adult values. The first year of life is when the biggest changes happen, with subsequent changes happening more slowly. Additionally, certain areas—like the

white matter of the frontal lobe—may develop more slowly than others. According to a study, the gray matter's NAA/Cho ratio peaked between the ages of 10 and 12 years old, after which it began to gradually decline. The elderly Brain: Only in the parietal region does NAA slightly decline with age, while Cho and Cr show little rise in frontal regions.

MRS at different field strengths[36]

Higher magnetic field strengths result in superior in vivo MRS because SNR and chemical shift dispersion increase roughly linearly with increasing field strength. The optimal time for high field MRS to be conducted is during short echo times, like 35 msec or less, as the apparent T2 relaxation times of metabolites decrease as the magnetic field increases. MRS at 1.5 T can be completed fairly successfully at TE 280 msec; at 3.0 T, 140 msec is the suggested echo time to take into account for lengthy TE scans.

After receiving gadolinium contrast, is it possible to perform MRS? It is reasonably possible to perform MRS post-Gd because Gd-chelates have not much or any discernible impact on the MRS signal. At regular, steady-state concentrations of substances, Gd only slightly broadens the line when it comes to metabolites because it remains within the vasculature in the normal brain. Gd most likely resides in the extravascular, extracellular space even in enhancing brain lesions, and since most metabolites are located in the intracellular space, it does not appear to significantly alter metabolite T1 or T2 relaxation.[36]

Common artifacts (and other problems) in MRS[36]

- Inadequate field homogeniety
- Inadequate water suppression
- Inadequate lipid suppression
- Effects of head motion
- Absence of vertical scale
- Incorrect voxel placement
- Incorrect choice of protocol
- Lesion too small / unfavourable location
- Out of voxel magnetization
- Chemical shift displacement effects

MRI spectroscopy is a powerful technique to identify early changes compared to standard MRI morphologic methods because, in numerous health processes, biochemical modifications occur before morphologic variations in tissues. Generally speaking, when compared to normal brain tissue, brain gliomas tend to show higher Cho and lower NAA peaks. The relative Cho/Cr and Cho/NAA ratios also show a significant increase from low- to high-grade gliomas, in accordance with tumor grading.

The distinction between (a) infections and tumors low, (b) radiation-related necrosis and recurrence of tumor, (c) secondary and primary malignant tumors, and (d) and high grade gliomas are some of the most significant clinical applications of magnetic resonance spectroscopy. These applications can be made either alone or in conjunction with diffusion and perfusion weighted imaging techniques.

Assessing the therapeutic impact through preliminary assessments and follow-up investigations to find changes caused by treatments and direct treatment is yet another significant practical application of MRI spectroscopy.[33]

Clinical Applications Of MR Spectroscopy

Early investigations on brain were done using 31P MRS, and even though 31P MRS is very useful in the study of muscle and mitochondrial diseases, most of the diagnostic and research work nowadays is done using 'H- MRS. This is because of three reasons. First, the hardware required for 'H MRS is the same as that for conventional MRI and 'H MRS can be used on most commercial 1.5T scanners, without the need of any modifications or special equipments.

Second, as the sensitivity of MR is greater for protons than phosphorous, 'H MRS has a higher spatial resolution and smaller volumes can be sampled as compared to phosphorous MR spectroscopy.

Thirdly, the information available from the changes in NAA, which can be easily measured by 'HIMRS, provides specific biochemical evidence of neuronal injury, this information cannot be obtained by using any other MR imaging modality[38,39]

The initial accounts of magnetic resonance spectroscopy of unaltered tissue samples date back to 1973. Moon and Richards[40] used P-31 MRS to study unaltered red blood cells, and Hoult et al.[41] used the same technique to study the removed muscles on the legs of a rodent in 1974. from that time, MRS is currently used on practically each organ in the human body, such as the liver, kidneys, and prostate, heart, brain, and extremity.

Water-suppressed and section-selective proton MRS scans on human brain, leg muscle, liver, and heart were examined by Bárány M. et al.[42] with aid of 1.5-T MR scanner.

A major focus of brain imaging has been detection and characterization of intracranial neoplasms.[17,43-46] Conventional MR imaging has tremendously increased the sensitivity by which tumors can be detected and localized, but the gains in specificity have not been as high as gains in sensitivity.

In their examination of eighteen individuals afflicted with glial brain tumors, Barbarella G, et al.[47] analyzed the in vivo single voxel 'H MRS of these tumors by correlation alongside tissue histology as well as in vitro MRS. Utilizing localized single-voxel "H MRS, "necrosis, blood vessels proliferation, cellularity of the neoplastic lesion, histological nuclear atypia and the proportion of Ki-67 positive cells in the total cell populations were assessed. A limited number of 'H MRS parameters were discovered to be associated with the tumor's histological features. Specifically, there was a correlation between the Ki-67 cell proliferation index and the Cho/Cr metabolite ratio that was extracted from the tumor tissues.[48]

MR spectroscopy is abnormal at presentation in nearly 100% of primary brain tumors.[49-50]

Reduced or absent NAA, elevated Cho, and occasionally elevated Lac and lipid peaks are all seen in the H-MRS of active brain tumors. As neurons are destroyed and replaced by neoplastic cells, decreased NAA is indicative of neuronal loss. Most likely, a changed metabolism is connected to a decrease in creatine. An increase in choline is indicative of a higher cellularity and membrane turnover. Raised Cho:Cr ratios are common in adult brain tumors, while decreased NAA:Choline and NAA:Creatine ratios are frequently observed in normal brain tissue.[51–52]

N-acetyl-aspartate and creatine/phosphocreatine amounts are typically lower than detectable levels in most tumors, but choline-containing compounds are typically more, according to a 1989 study[53] on the noninvasive differentiation of brain tumors with localized in vivo "H-MRS." Every tumor has a distinct spectrum from the normal brain parenchyma. The varying quantities of amino acids, lipids, lactic acid, and carbohydrates were the primary cause of the reproducible variances observed in the spectra acquired from various tumors.

In adult brain tumors and radiation necrosis areas, N-acetyl aspartate levels are lower, and choline concentrations are higher in the majority of solid brain neoplasms.[54] In a related investigation, all first scans using single-voxel "H-MRS" showed elevated Cho and decreased NAA levels in 75 children with brain tumors. One of the most trustworthy indicators of malignancy in pre-treatment "H-MRS" scans is the total Cho peak[55]. Malignant juvenile brain tumors have shown similar outcomes, with an increase in the Cho: NAA ratio and a decrease in the NAA: Cr ratio, as well as a drop in the levels of NAA and Cr and an increase in Cho.[56,57]

A prospective trial[58] with 16 normal volunteers and twenty-three individuals with brain mass lesions used H-MRS. The average peak height ratios of NAA/Cho and NAA/Cr in the tumors were much lower than those of the tissues from normal people, while Cho/Cr was significantly higher.

Every glioma and meningioma had an increased Cho. Numerous malignant primary brain tumors have high lactate levels, which varied depending on the kind of tumor. H-MRS is a potent tool for safe, noninvasive tissue chemical investigation in vivo, and it may one day be used to classify tumor histology and evaluate the effectiveness of tumor therapy, according to the conclusion.

The discovery of metabolic alterations linked to tumor growth, tumor grading, responses to therapy, and therapeutic side effects may be possible with MRI spectroscopy.[59]

Imaging characteristics of high-grade and low-grade astrocytomas are often different. All astrocytomas have low NAA levels, with grade-IV tumors having the lowest values. On the other hand, choline levels in solid astrocytomas are consistently greater, especially in higher grade cases. A greater degree of aggressiveness and necrosis are typically indicated by an elevated level of lactate.

According to a few publications, there may be a correlation between a higher degree of neoplasia and increased choline when lactate is present. Elevated concentrations of lactate are frequently seen in high grade tumors like glioblastoma multiforme.[60] A higher than normal level of lactate could be a sign of tumor hypoxia. Additionally, compared to low-grade gliomas, the Choline concentrations in high-grade gliomas is substantially greater.[61]

The standardized choline value didn't prove useful in differentiating the severity of the tumor as necrotic lesions of high grade had reduced choline values. This was discovered in a study[54] of brain tumor metabolism using 'H-MRS and FDG PET in 50 patients. Solid high-grade gliomas had higher normalized choline values than solid low-grade gliomas. When solid anaplastic tumors were contrasted with chronic radiation necrosis, choline concentrations were also shown to be lower.

It has also been reported that some of the metastatic tumors to the brain could indicate resonances of lipid [62]

Astrocytomas with high grade could indicate lipids most likely due to the presence of necrosis. The measured lipid, lactate, and macromolecule levels increase with grade of tumor, as the tumors progress from hypoxia to necrosis.[63]

Ninety-five percent of the tumors from 33 children with posterior fossa tumors were properly identified by a computer-based method that included MRI, MRS, and clinical data to predict the tumor histology[64,65]. Thus, 'H-MRS has been applied not only to tumor identification but also to noninvasively grade and classify brain tumors.' In contrast to low-grade astrocytomas, anaplastic astrocytomas and glioblastomas have decreased myoinositol levels, according to a study that correlated the two variables.[66]

Preul MC et al[67] discovered an effective patient classification utilizing a multivariate pattern recognition analysis of peaks corresponding to choline, creatine, N-acetylasparate, lactate, lipid, and alanine in another investigation that used two-dimensional 1-H MRSI. Because meningiomas were the only lesions having alanine, they were distinguished from other lesions by their metabolite levels in each class. In most cases, grade 2 gliomas showed low levels of lactate and lipid, some N-acetylaspartate, and some creatine. Grade 3 gliomas showed lower amounts of lactate and lipid, less N-acetylaspartate and creatine, and higher levels of choline.

'H MRS NAA and Cr levels are very low in meningiomas and schwannomas as they are non-neuronal in origin. However, NAA and Cr may be present if there is contamination by adjacent parenchyma. Elevated choline has been reported in meningiomas particularly in recurrent meningioma. Presence of Alanine and Glutamine[68-70] are highly suggestive of meningioma.

Lymphomas have a "H MRS appearance" comparable to metastases and primary high-grade astrocytomas. MR spectroscopy reveals a significant decrease in creatine and NAA and a considerable rise in choline and lipids.[71, 72]

MR spectroscopy is particularly helpful in evaluating how well lymphomas respond to treatment, as these tumors exhibit gradual lipid and choline declines after successful treatment.

Choline, creatine, lactate, and lipid levels vary throughout cerebral parenchymal metastases [73]. Because there is typically no neuronal tissue in metastases, NAA is typically low or non-existent; when it is present, it represents a partial volume average from nearby normal brain tissues. The elevated levels of choline resulting from accelerated membrane turnover and lactate resulting from rapid tumor growth and necrosis are the hallmark findings of "H MR spectroscopy" in metastases. Lipids are present in certain brain metastases as well. Because of necrosis, lipids can also be observed in high-grade astrocytomas.[74]

Using in vivo MR spectroscopy (MRS) to identify lesion-specific metabolite patterns that could aid in improved tissue characterization through imaging. Poptani H, et al[75] assessed 34 individuals with cystic cerebral mass lesions on MR imaging. Grading cystic gliomas according to the NAA/Cho ratio was not feasible.

A small number of low-grade gliomas displayed lactate, although lipid/lactate was present in high-grade gliomas. Renewals from lactate, alanine, and acetate were observed in brain abscess patients. The findings suggested that cerebral cystic mass lesions could be more accurately described by combining MR imaging and in vivo MRS.

Cho YD et al.[76] tried to differentiate schwannomas and meningioma by using 'H MRS, they found that NAA was decreased in both of the tumors due to their non-neuronal origin. Elevated ml was seen in schwannomas.

Investigations have shown that all types of upper aerodigestive tract squamous-cell malignancies have an increased Cho/Cr ratio. H MRS has additionally

been used to describe extracranial head and neck cancers.[77] Although ocular tumors have been studied using HMRS, it is challenging to acquire a sufficient MR spectrum because of the nearby bone tissue. Melanin is represented by a strong peak found in ocular melanotic melanomas at 6.72 ppm. Using MR spectroscopy, thyroid malignancies reveal resonances of amino acids such as valine (at 0.70 parts per million) and glutamate (at 2.19 parts per million).

Areas of maximum spectroscopic abnormalities correlate with areas of maximum histopathologic abnormality, thus making MRS a helpful tool to guide biopsies.[68]

The accuracy of stereotactic biopsy targeting has been shown to be significantly improved by CSI-directed stereotactic biopsy, particularly when metabolite maps were employed during the selection of biopsy targets.[78]

Merely relying on magnetic resonance imaging (MR) to differentiate tumor development from non-neoplastic therapy response, such as radiation necrosis, might be challenging.

High choline levels indicate a recurring tumor, while radiation exposure typically shows low levels of NAA, creatine, and choline on spectroscopy. Raised lipids and lactate can be additionally visible on the spectrum if radiation necrosis is present.

The tumor response to radiation therapy has also been detected spatially targeted with H MRS, and it has been shown that lactate levels dramatically drop 48 hours after radiation therapy[79].

In a study evaluating the use of H-MRS in adult brain tumors and how to distinguish them from similar-looking space-occupying tumors, it was discovered that patients with meningioma and high- and low-grade gliomas had substantially larger

Cho/Cr ratios when compared to the control group, while their NAA/Cr and Cho/NAA ratios were reduced from their usual levels.

On the other hand, the Cho/Cr ratios did not demonstrate statistically significant differences in non-neoplastic tumors. So, it was concluded that in doubtful intracranial space-occupying lesions with similar morphological imaging patterns MR Spectroscopy was useful to arrive at a more definitive diagnosis.

Often with conventional MRI, even with contrast, a complete diagnosis of an intracranial space occupying lesion is not possible. A large intracranial abscess often mimics a necrotic high-grade glioma and vice versa. Hence though sensitive, MRI can prove to be nonspecific. According to an investigation, trends from in vivo "H MR spectroscopy allow for differentiated detection of cerebral abscesses from necrotic or cystic lesions since the former contain merely lactate resonances while the latter only comprise, acetate, amino acid, lactate and unknown resonances.[80]

The H MRS patterns of the cystic component of diverse intracranial tumors were examined by Kim SH, et al.[80] and associates in order to distinguish those lesions. From the cystic components of various cerebral cystic tumors in 39 patients, 40 'H MR spectra were examined. 35 instances (or 88% of the cases) yielded sufficient 'H MR spectroscopic data.

The lactate peak was detected in high-grade gliomas, while merely a lactate resonance was seen in most other gliomas and metastases.

Some neoplasms have both lactate and lipid signals, such as metastases and malignant gliomas. Absesses were found to include varying combinations of lactate, acetate, succinate, valine, alanine, and/or leucine amino acid combinations, as well as unassigned resonances.

Succinate, alanine, Lactate, acetate, and/or unassigned resonances were visible in cases of cysticercosis. Lactate signal was the only significant peak in epidermoid cysts. The arachnoid cysts and porencephalic cyst did not exhibit any detectable resonances.

Another study[81] employed in vivo MR spectroscopy to distinguish between brain abscesses and cystic tumors. Cystic tumors lacked amino acid resonance at 0.9 ppm at in vivo H MR spectroscopy at moderate TE, which was only observed in bacterial abscesses.

241 patients with suspected neoplastic CNS lesions detected on MR images were studied with single voxel proton MR Spectroscopy in a study by Krouwer HG, et al.[82] to evaluate common histologic findings in a diverse group of non-neoplastic diseases in patients with in vivo MR spectroscopic profiles suggestive of a CNS neoplasm.

Six individuals were included, none of whom had a tissue diagnosis, and five of whom had a non-neoplastic diagnosis were detected retrospectively.

The results of MR spectroscopy that were consistent with a tumor included decreased creatine, N-acetylaspartate, elevated choline with or without apparent mobile lipid and lactate peaks.

Significant white blood cell infiltrates were found in the histologic specimens of all five patients with tissue diagnosis. These infiltrates included interstitial and perivascular accumulations of macrophages, histiocytes, lymphocytes and plasma cells in one case.

Reactive astrogliosis was also observed in most tissue samples. It was discovered that nonneoplastic disease processes in the central nervous system may cause a reactive proliferation of immune system and glial tissue cellular elements

using current in vivo MR spectroscopic techniques. This reactive proliferation is associated with MR spectroscopic profiles that are indistinguishable from neoplasms in the central nervous system.

Hydatid cysts and cysticercus cysts can also be differentiated on the basis of their metabolite patterns by using H' MRS. The spectra from hydatid fluid differ from cysticercus cysts as they do not show creatine resonances. In fertile hydatid cysts, malate and/or fumarate is also observed, which is absent in cysticercus cysts.[83] The reason why creatine is exclusively found in cysticercus fluid could be attributed to both the active diffusion of the substance from the surrounding host tissue and the muscle in the cyst's bladder wall.

In addition to diagnosing non-neoplastic lesions, H' MRS may be able to further characterise the etiology of infectious lesions.

A 2003 study found that metabolite patterns—specifically, the ratios of amino acids and lactate—observed at H' MRS can also be used to distinguish anaerobic brain abscesses from aerobic or sterile ones.[83]

Diffusion weighted imaging [82-84]

A particular form of magnetic resonance imaging called diffusion-weighted imaging (DWI) measures the irregular motion of water molecules within a tissue voxel. Put simply, tissues that are highly cellular or swollen cellularly tend to have lower diffusion coefficients. DWI is especially useful for identifying brain ischemia and tumors.

Unlike water, which diffuses almost freely in a container, cell membrane borders are the main obstacle to water diffusion in brain tissue. The total diffusion behaviour of a volume is a reflection of the collective diffusion of water across a number of compartments: intracellular fluid, cytoplasm, organelles, extracellular

fluid, interstitial fluid, intravascular lymph, different biological cavities, such as the brain's ventricles, and diffusion between intra- and extracellular compartments. Each of these will have a different contribution based on the tissue and pathophysiology.

It is believed that a number of factors contribute to the decline in apparent diffusion coefficient (ADC) values in cases of acute cerebral infarction. First, compared to the extracellular space, water prefers to diffuse into the intracellular compartment where organelles obstruct it more. Second, the extracellular space gets narrowed as a result of the cellular enlargement brought on by this movement. The low ADC levels found in high grade gliomas (glioblastoma) and highly cellular tumors (such as tiny round blue cell tumors like lymphoma/PNET) are caused by similar causes.

A single water molecule is more susceptible to shifting gradient strengths and dephases as it diffuses farther along the sequence, which reduces the quantity of signal that is returned. The size at which this phenomenon occurs is far smaller than that of a single voxel. The b number determines the extent of this impact, or how much diffusion dampens the signal.

MRI sequence[82-84]

A number of methods have been developed for producing diffusion maps. Spin-echo echo-planar sequence (SE-EPI) is the basis of the most commonly applied method. Other non-EPI methods, like turbo spin-echo, are accessible though; these are especially helpful in regions close to or inside bone, wherein T2* effects can cause aberration, artifacts, and signal degradation in EPI sequences.

The overall gross idea behind diffusion-weighted images:

The basic principle of diffusion-weighted imaging is the attenuation of T2* signal according to the diffusion coefficient of water molecules in that area. The

amount of initial T2* signal that remains decreases with increasing water diffusion, or the distance that a water molecule can travel throughout the sequence. Diffusion-weighted images of the ventricles appear black because, for example, water in cerebrospinal fluid (CSF) can diffuse very freely, resulting in minimal signal retention. On the other hand, the water in the brain parenchyma is blocked by cell membranes, which results in only a partial reduction of the initial T2* signal. This has the important consequence that no matter the tissue's diffusion properties, a brain region with zero T2* signal cannot display signal on isotropic diffusion-weighted images.

Getting a T2*-weighted image without diffusion attenuation—also referred to as the b=0 image—is the first step in the procedure of extracting diffusion data from the structure of the tissue. After that, the simpleness of water diffusion is assessed across three orthogonal directions (X, Y, and Z), usually in various directions. Strong shifts are applied symmetrically on both sides of the 180-degree pulse to achieve this. The region under the diffusion gradients, that is determined by the gradient's, duration, interval between gradients & amplitude is the primary factor determining the level of diffusion weighting. The b value is determined by the sum of all of these factors; greater values indicate stronger attenuation of signals associated with diffusion. When the initial gradient is applied, fixed molecules of water learn about phase.

The advantages of the preceding 180-degree pulse are, however, eliminated because they have not moved and are therefore exposed to the same gradient following the 180-degree pulse (because they have flipped by 180 degrees). As a result, these immobile water molecules still have signal when the echo is produced. On the other hand, water molecules in motion obtain phase information from the

initial gradient. They are not in the same position as before and, therefore, do not experience precisely the same gradient following the 180-degree pulse because they are moving when exposed to the second gradient. Consequently, they lose part of their signal because they are not completely rephased. The farther they can travel, the less successfully they will be rephased and the less signal they will hold.

Isotropic DWI and ADC map generation

The process outlined produces four sets of images: one T2*-weighted image with no diffusion weighting (b=0) and three diffusion-weighted images corresponding to the directions X, Y, and Z, where the T2* signal is attenuated according to the diffusion of water in each direction. The combination of these images can be used to create apparent diffusion coefficient (ADC) maps and isotropic diffusion-weighted images (DWI), which are directional information-free images by mathematical means.

Isotropic DWI maps are generated by computing the geometric mean of the direction-specific images. Conversely, the ADC map is calculated by dividing the natural logarithm of the isotropic DWI by the initial T2* signal (b=0). The isotropic DWI images can be used to compute ADC values directly, or they can be calculated by averaging the values of each directional diffusion map.

DWI IN BRAIN TUMORS: CLINICAL APPLICATIONS [84–92]

These include noticing lower ADC values in tumors with a high cell content, such as high-grade gliomas, medulloblastomas, and CNS lymphomas. Higher tumor grades and a worse prognosis are frequently linked to lower ADC values. Quantitative ADC measurements are useful in identifying pseudo-progression and pseudo-response, as well as in predicting the therapeutic response.

A condition known as pseudo-response is noticed following anti-angiogenic therapy in which the tumor does not exhibit improvement even though it is still alive or is actually progressing. When contrast enhancement is not present, DWI can be helpful in identifying ongoing or developing tumor activity.

However, instead of actual tumor progression, pseudo-progression happens when Edema linked to an inflammatory response occurs. According to reports, ADC values can differentiate between these two entities with an accuracy of up to 80%.

According to the investigation done by Pavlisa et al. [(93)], Ja Lee et al. [(94)] & Ohba et al. [(95)] and, there was actually no appreciable difference in apparent diffusion coefficient inside the lesion between metastatic and primary brain tumors. As a result, it was not possible to differentiate between primary and metastatic brain tumors using intralesional ADC values. This was explained by the fact that DWI was unable to distinguish between any of the lesions due to their increased cellularity.

Contrary to the results of this study, Chiang et al.[(96)] found that the ADC values in the tumoral regions of metastasis were significantly higher than those in the primary tumors.

Perilesional ADC values have been shown in a study by Faria et al.[(96)] to be a highly sensitive means of differentiating primary brain tumors from metastatic ones. According to the explanation given, metastatic cases lack perilesional infiltration and increase ADC values in perilesional edema, while perilesional infiltration of primary high-grade tumors results in increased cellularity in the perilesional area.

MATERIALS AND METHODS

The present study was carried out from January 1st to December 31st of 2023 at the KLES Dr. Prabhakar Kore Hospital and Medical Research Centre in Belgaum in the Department of Radio-diagnosis.

Study design:

An observational study for an entire year was the study's design.

Source of data:

Patients with supratentorial brain tumors detected by MRI brain (plain/contrast) scans.

Sample size:

A total of 49 patients fulfilling the selection criteria and willing to undergo MR spectroscopy and DWI imaging were studied.

Study period and duration:

The current investigation was carried out from January, 2023 to December, 2023.

Sampling procedure: Convenient sampling

The following criteria must be met for inclusion:

• Follow-up patients with brain tumors

• All patients with incidentally discovered brain tumors by CT.

• Cases with a clinical suspicion.

• Cases involving all age groups, regardless of gender.

The following criteria was used for exclusion:

• Patients having metallic medical implants (intraocular metallic foreign bodies, cardiac pacemakers, and intracranial clips of arterial brain aneurysms that are not compatible with magnetic resonance imaging) are excluded.

• Patients who are clinically unstable or unfit for examination

• Individuals who objected to the examination.

Ethical clearance:

Prior to the study's start, the Institutional Ethics Committee of Jawaharlal Nehru Medical College in Belgaum granted ethical clearance.

Informed Consent:

Patients who met the eligibility requirements were notified of the study's goals and design, and they were only enrolled with their signed informed consent (Annexure I).

Sampling data

Through an interview, the study population's demographic details, including age and sex, were gathered. comprehensive clinical examination and complete history taking. These results were documented using pre-made proforma (Annexure-Il).

Imaging using magnetic resonance:

The 3.0 Tesla MRI (MAGNETOM® Spectra), made by SIEMENS (Erlangen, Germany), was used for each scan.

The next the variables were used to conduct the evaluations.

Thickness of slice : 10, 5, 3 mm

Field of view (FOV) : 14 to 24 cm

Size of the matrix : 256 x 256

In order to properly position and immobilize the head, patients were examined in the supine position using an MRI scanner. The head coil that was used to acquire the images was standard.

Axial DWI, T1, T2, and PD images, as well as coronal and sagittal T1 images, were used for pre-contrast scanning, with a 5 mm slice thickness.

After taking plain images in the beginning, 0.1 mmol/kg of the body's weight of contrast agent, gadolinium DTPA, was injected. After contrast was injected, images were taken and evaluated.

As a contrast agent, Magnilek (Dimeglumine Gadopentetate) was administered intravenously at a dose of 0.1 mol/kg body weight. Coronal, sagittal, and axial post-contrast TWI were acquired.

Thinner sections were taken in the interest region whenever needed. In the event that an MRI lesion suggestive of a tumor was found, patients underwent a MR Spectroscopy

1H Spectroscopy by magnetic resonance:

Prior to performing spectroscopic measurements, both global and local shimming were performed to account for static and dynamic magnetic field inhomogeneities. With an FWHM (Full width at half maximum) of 5-7 Hz, the global shimming was optimized at 15–17 Hz. Water suppression was achieved with a gaussian pulse.

To avoid signal contamination, edematous areas, the nearby calvarium, ventricles, and paranasal sinuses were avoided. In certain cases, optimal shimming and water suppression were attained. Using the STEAM (stimulated echo acquisition method) sequence, single (SV) and multivoxel (MV) techniques were used to perform 1H MR spectroscopy at short TE (30 ms), long TE (270 ms), and intermediate TE (135 ms) as appropriate. The acquisition times for each technique were roughly 3-6 minutes.

According to the size of the tumor lesion and if single- or multi-voxel MRS is being employed, the voxel size had been chosen. Highly Experienced radiologists who had access to all offered histopathological, the clinical, as well as imaging data, who was working in consultation validated and established the standard of reports.

STATISTICAL ANALYSIS & RESULTS

METHODS

Data is analysed using statistical software R version 4.4.0. and Microsoft Excel. Categorical variables given in the form of frequency tables. Continuous variables given in Mean ± SD / Median (Min, Max) form. Chi square test is used to check the association of categorical variables with groups. Normality of variable is checked by Shapiro Wilk test and QQ plot. If data follows normal distribution, parametric tests will be used. Otherwise, non-parametric tests will be used. One way ANOVA is used to compare the means of variables over final diagnosis. Kruskal Wallis test is used to compare the distribution of variables over final diagnosis. P-value less than or equal to 0.05 indicates statistical significance.

RESULTS:

1) Data contains measurements on 49 subjects. The following table gives the distribution of subjects according to demographic details.

Table 1: Distribution of subjects according to demographic details.

Variables	Sub Category	Number of subjects (%)
Age (years)	Mean ± SD	53.31 ± 13.66
	Median (Min, Max)	55 (28, 78)
Gender	Female	21 (42.80%)
	Male	28 (57.14%)

The average age of the subjects is 53.31 years with a standard deviation of 13.66 years. The median age is 55 years, ranging from 28 to 78 years. In terms of gender, there were 21 (42.80%) female subjects and 28 (57.14%) male subjects. This distribution suggests a slight male predominance in the sample population.

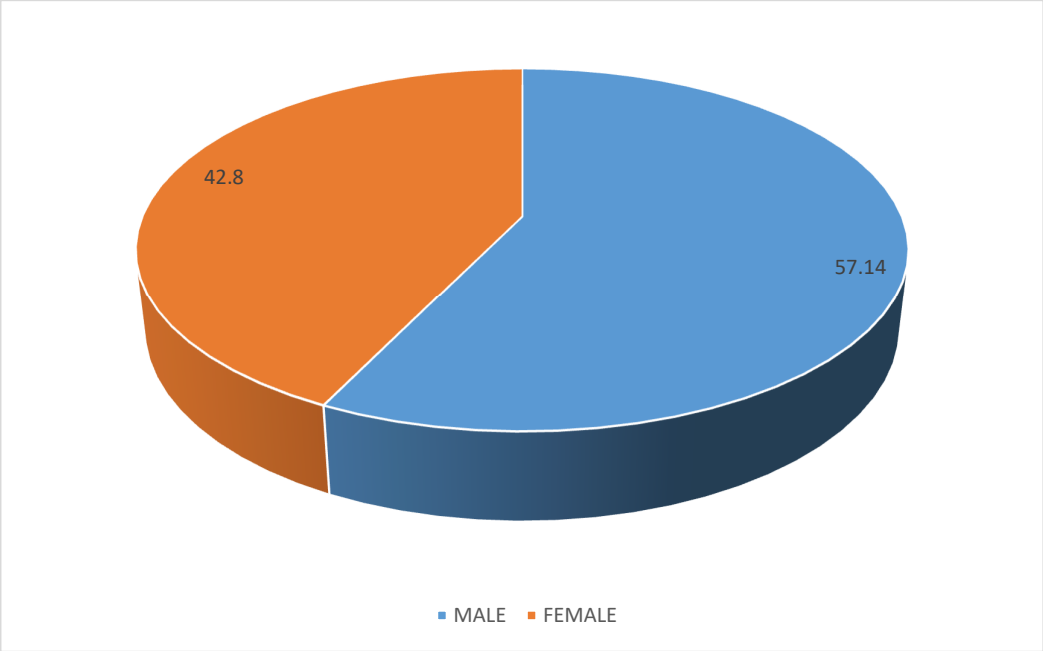

Figure 1: Distribution of subjects according to gender.

2) The following table gives the distribution of subjects according to comorbidities.

Table 2: Distribution of subjects according to comorbidities.

Comorbidities	**Number of subjects (%)**
Diabetes mellitus	1 (2.04%)
Hypertension	23 (46.93%)
Hypertension and diabetes mellitus	14 (28.57%)
None	11 (22.44%)

Among the comorbid conditions identified, hypertension was the most prevalent, affecting 23 (46.93%) subjects. Hypertension combined with diabetes mellitus was present in 14 (28.57%) subjects. Diabetes mellitus alone was observed in only one subject, comprising 2.04% of the sample. Notably, 11 (22.44%) subjects reported having no comorbidities.

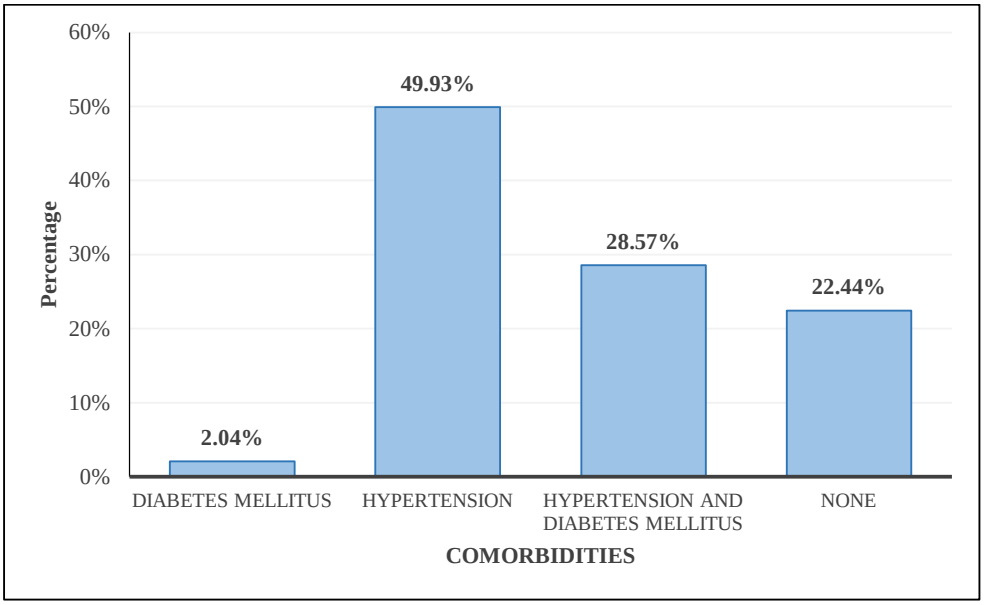

Figure 2: Distribution of subjects according to comorbidities.

3) The following table gives the distribution of subjects according to chief complaints.

Table 3: Distribution of subjects according to chief complaints.

Chief Complaints	Number of subjects (%)
Headache	42 (85.71%)
Vomiting	29 (59.18%)
Dizziness	18 (36.73%)
Seizures	23 (46.93%)
Increased Forgetfulness	1 (2.04%)
Altered Sensorium	1 (2.04%)
Right Sided Mild Weakness	2 (4.08%)

Headache emerges as the most prevalent chief complaint, reported by 42 (85.71%) subjects. Following closely, vomiting was noted in 29 (59.18%) subjects. Other frequently reported complaints include seizures, reported by 23 (46.93%) subjects, and dizziness, noted by 18 (36.73%) subjects. Additionally, there were isolated instances of increased forgetfulness, altered sensorium, and right-sided mild weakness, each reported by one or two subjects.

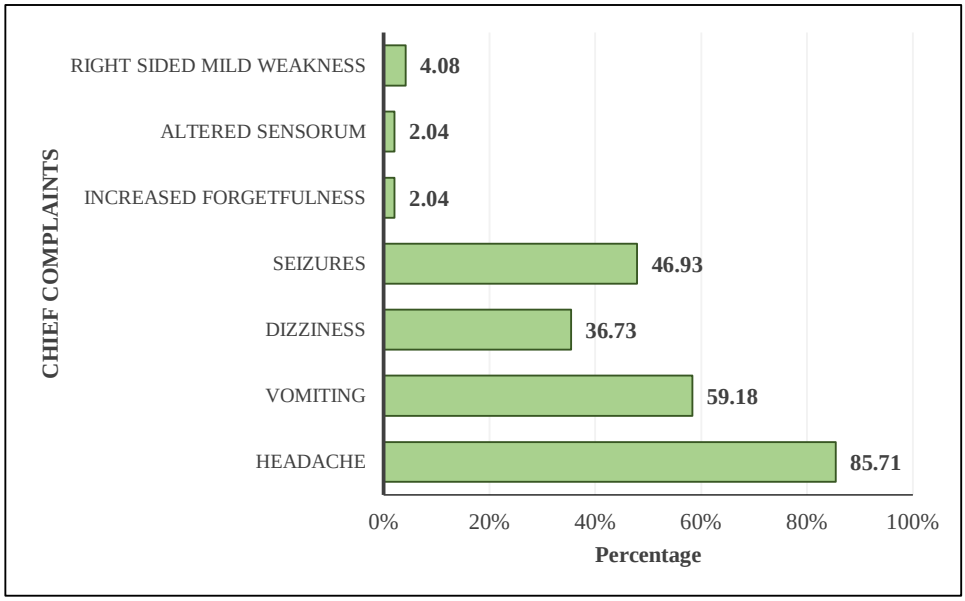

Figure 3: Distribution of subjects according to chief complaints.

4) The following table gives the distribution of subjects according to number of lesions on MRI.

Table 4: Distribution of subjects according to number of lesions on MRI.

Number of Lesions on MRI	**Number of subjects (%)**
Multiple	5 (10.20%)
One	44 (89.79%)

The majority of subjects, comprising 44 (89.79%) subjects had only one lesion detected on their MRI scans while 5 (10.20%) subjects exhibited multiple lesions.

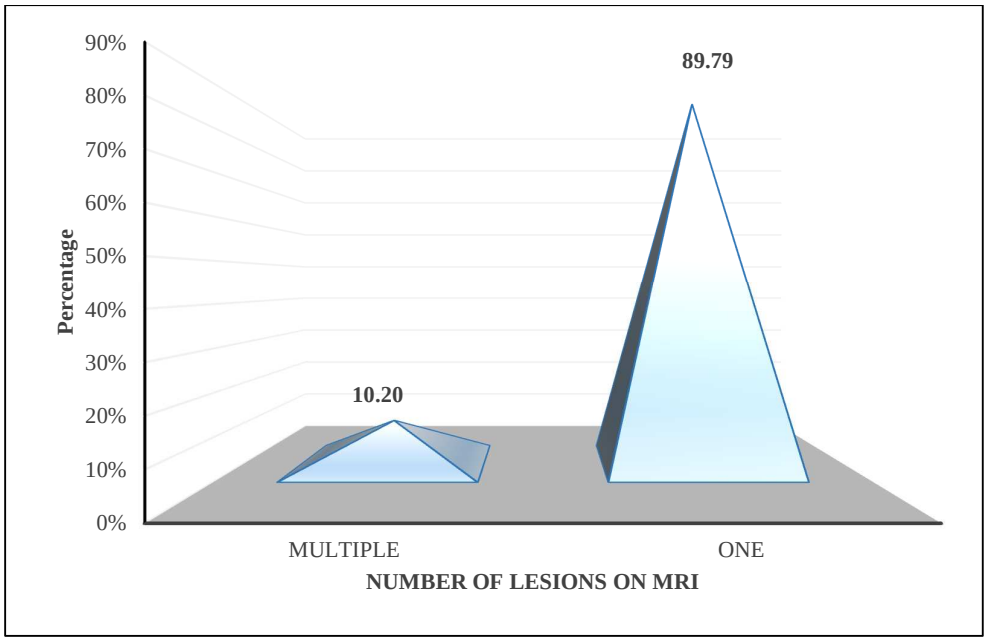

Figure 4: Distribution of subjects according to number of lesions on MRI.

5) The following table gives the distribution of subjects according to location.

Table 5: Distribution of subjects according to location.

Location	**Number of subjects (%)**
Bilateral Parietal Region	2 (4.08%)
Left Anterior Temporal Region	1 (2.04%)
Left Frontal Region	5 (10.20%)
Left Frontoparietal Region	2 (4.08%)
Left High Frontal Region	1 (2.04%)
Left Medial Temporal Region	1 (2.04%)
Left Occipital Region	1 (2.04%)
Left Para-saggital Frontal	4 (8.16%)
Left Parietal Region	4 (8.16%)
Left Parieto-Occipital Region	1 (2.04%)
Left Parieto-Temporal Region	1 (2.04%)
Left Posterior Parietal Region	1 (2.04%)
Left Temporal Region	2 (4.08%)
Midline Hypothalamus	1 (2.04%)
Right Anterior Temporal	1 (2.04%)
Right Frontal Region	8 (16.32%)
Right Medial Temporal Region and Left Posterior Parietal Region	1 (2.04%)
Right Occipital Region	2 (4.08%)
Right Para-sggital Frontal Region	1 (2.04%)
Right Parietal Region	5 (10.20%)
Right Parieto-Occipital Region	1 (2.04%)
Right Parieto-Temporal Region	1 (2.04%)
Right Temporal Region	1 (2.04%)
Bilateral Para-saggital Frontoparietal Region	1 (2.04%)

Among the noted locations, the most frequently affected were the right frontal region and the left frontal region, with 8 (16.32%)subjects and 5 (10.20%) subjects, respectively. Additionally, the right parietal region was affected in 5 (10.20%)

subjects. Other regions, such as the bilateral parasagittal frontoparietal region, left parasagittal frontal, and left parieto-occipital region, had varying percentages of affected subjects, each accounting for 2.04% to 8.16% of the total sample.

6) The following table gives the distribution of subjects according to T1 and T2 signal.

Table 6: Distribution of subjects according to T1 and T2 signal.

Variables	**Sub Category**	**Number of subjects (%)**
T1 Signal	Hyperintense	3 (6.12%)
	Hypointense	23 (46.93%)
	Isointense	17 (34.69%)
	Mixed Intense	6 (12.24%)
T2 Signal	Hyperintense	26 (53.06%)
	Hypointense	5 (10.20%)
	Isointense	3 (6.12%)
	Mixed Intense	15 (30.61%)

For T1 signal intensity, hypointense signals were most prevalent, observed in 23 (46.93%) subjects, followed by isointense signals in 17 (34.69%) subjects. Hyperintense signals were noted in 3 (6.12%) subjects, while a mixed intensity was observed in 6 (12.24%) subjects. Conversely, in terms of T2 signal intensity, hyperintense signals were the most common, found in 26 (53.06%) subjects. Mixed intensity signals were observed in 15 (30.61%) subjects, followed by hypointense signals in 5 (10.20%) subjects and isointense signals in 3 (6.12%) subjects.

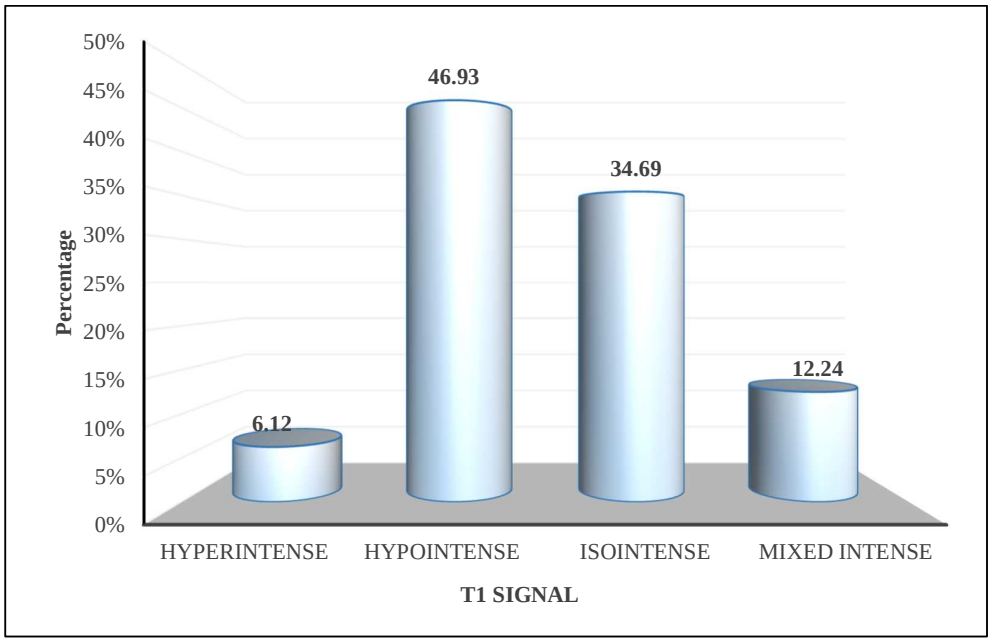

Figure 5: Distribution of subjects according to T1 signal.

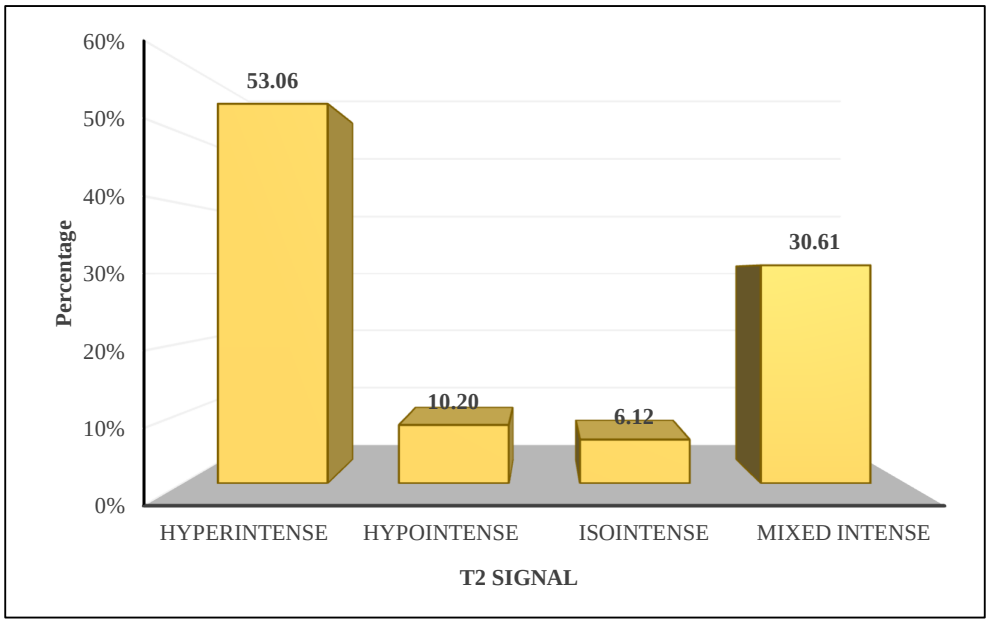

Figure 6: Distribution of subjects according to T2 signal.

7) The following table gives the distribution of subjects according to enhancement pattern.

Table 7: Distribution of subjects according to enhancement pattern.

Enhancement Pattern	**Number of subjects (%)**
Heterogeneous	23 (46.93%)
Homogeneous	8 (16.32 %)
Peripherally Enhancing	16 (32.65%)
N/A	2 (4.08%)

The most prevalent enhancement pattern was heterogeneous enhancement, noted in 23 (47.91%) subjects. Peripherally enhancing patterns were also common, observed in 16 (33%) subjects. Other enhancement patterns included homogeneous enhancement 7 (14.5 %). Notably, two subjects (4.17%) were categorized as "N/A," suggesting the enhancement pattern was not applicable (as they were plain studies without contrast).

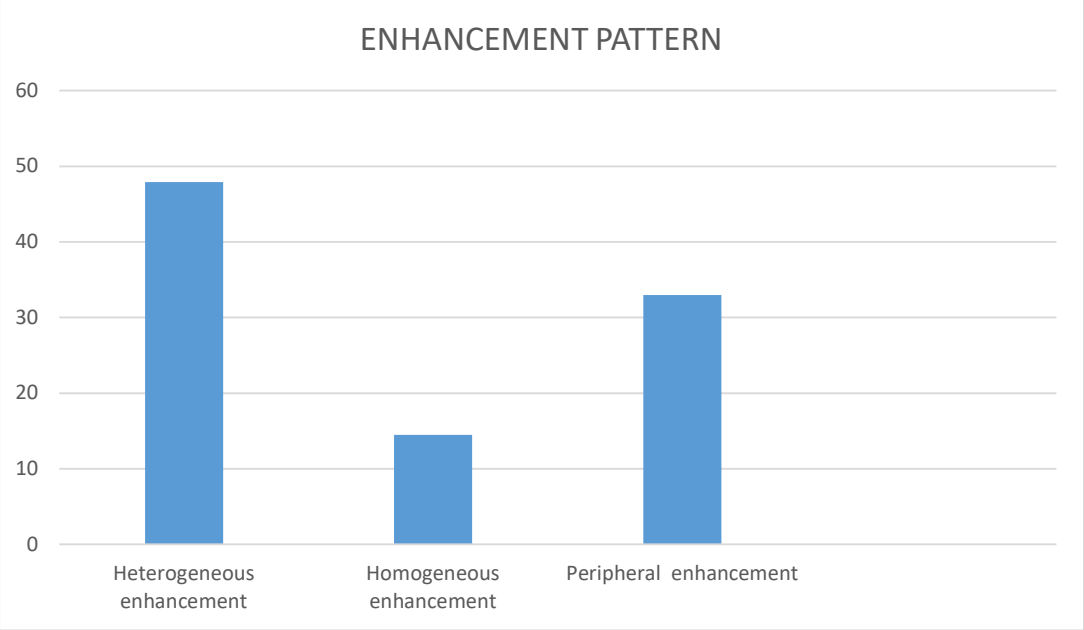

Figure 7: Distribution of lesions according to Enhancement pattern.

8) The following table gives the distribution of subjects according to MRI Spectroscopy findings.

Table 8: Distribution of subjects according to MRI Spectroscopy findings.

MR Spectroscopy findings	**Number of subjects (%)**
Increased Intralesional Choline	49 (100%)
Increased Intralesional Lactate & Lipid	24 (48.97%)
Decreased Intralesional NAA	42 (85.71%)
Increased intralesional Alanine	05 (10.20%)

The findings were the presence of increased intralesional choline (100 %), along with intralesional lactate & lipid elevation (48.97%) and intralesional NAA reduction (85.71%). Additionally, Other notable findings include instances of increased intralesional alanine observed in 5 (10.20%) subjects.

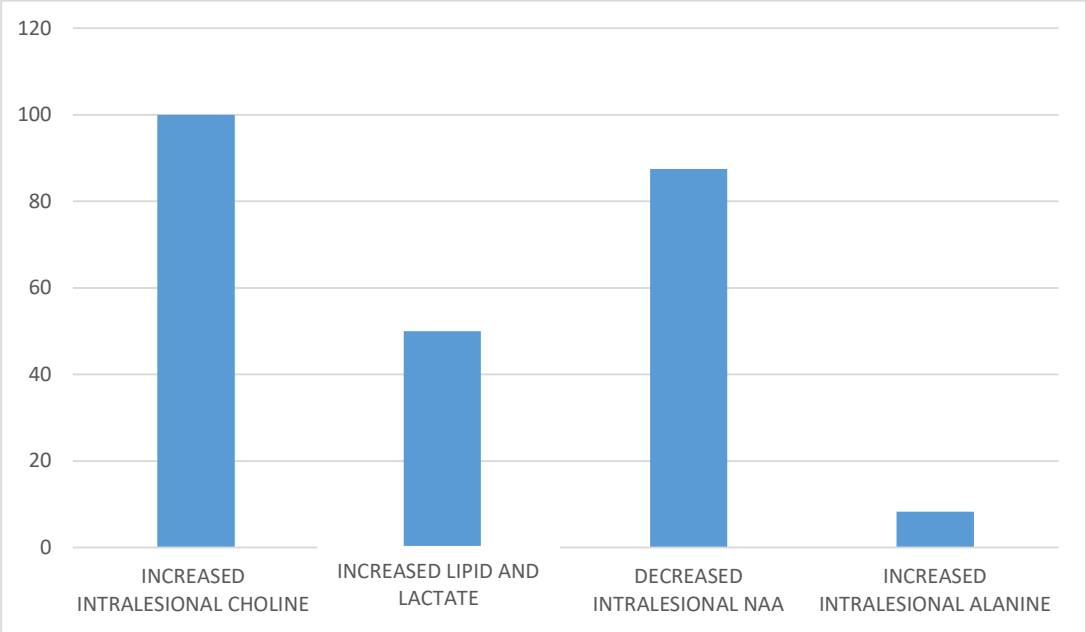

Figure 8: Distribution of lesions according to predominant metabolite.

The data of subjects regarding ratio of Metabolites suggested that there was an increase in choline to creatine ratios. The mean intra CHO/CR ratio is 3.83 ± 1.71, with a median of 3.6 and a range from 1.4 to 7.6. Similarly, the mean peri CHO/CR ratio is 2.25 ± 1.69, with a median of 2.2 and a range from 0.4 to 6.4.

9) The following table gives the distribution of subjects according to diffusion restriction.

Table 9: Distribution of subjects according to diffusion restriction.

Diffusion Restriction	**Number of subjects (%)**
Absent	5 (10.20%)
Present	44 (89.79%)

The majority of subjects, accounting for 44 (89.79%)subjects exhibited diffusion restriction.

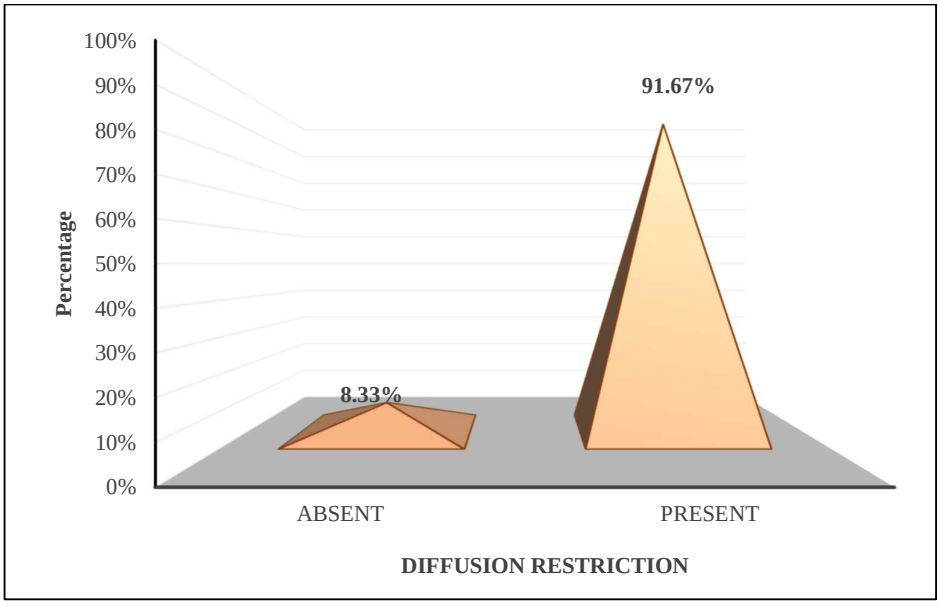

Figure 9: Distribution of subjects according to diffusion restriction.

10) The following table gives the distribution of subjects according to final diagnosis.

Table 10: Distribution of subjects according to final diagnosis.

Final Diagnosis	Number of subjects (%)
Malignant lesions	43 (87.75 %)
Benign lesions	06 (12.24 %)

Final Diagnosis	Number of subjects (%)
High Grade Glioma	23 (46.93%)
Low Grade Glioma	13 (26.53%)
Meningioma	6 (12.24%)
Metastasis	7 (14.28%)

The most prevalent diagnosis among the subjects is malignant lesions 43 (87.75 %) [high-grade glioma, identified in 23 (46.93%) subjects. Low-grade glioma was the second most common diagnosis, observed in 13 (26.53%) subjects. Metastasis was diagnosed in 7 (14.28%) subjects] and benign [meningioma] was diagnosed in 6 (12.24%) subjects.

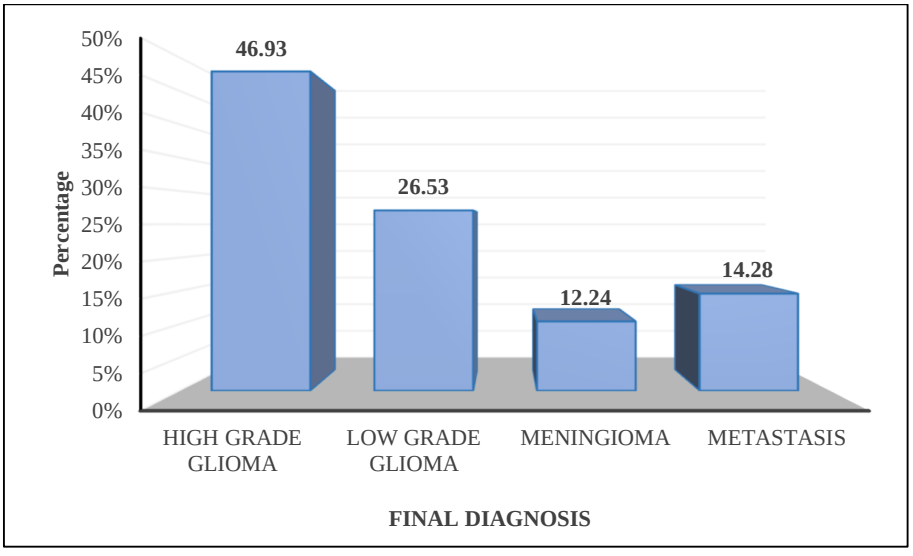

Figure 10: Distribution of subjects according to final diagnosis.

11) The following table gives the comparison of demographic details over diagnosis.

Table 11: Comparison of demographic details over diagnosis.

Variables	**Sub Category**	**High Grade Glioma**	**Low Grade Glioma**	**Meningioma**	**Metastasis**	**p-value**
Age (years)	Mean ± SD Median (Min, Max)	57.61 ± 13.27 58 (30, 78)	42.23 ± 13.27 39 (28, 65)	54.6 ± 9.21 58 (42, 63)	58.86 ± 5.84 57 (52, 68)	**0.0043^{A*}**
Gender	Female	7(30.43%)	6(46.15%)	3(50%)	5(71.43%)	0.2339^{MC}
	Male	16(69.57%)	7(53.85%)	3(50%)	2(28.57%)	

*Abbreviation: A – One-way ANOVA, MC – Chi square test with Monte Carlo simulation, * indicates statistical significance.*

From one way ANOVA, it is observed that, there is significant difference in mean age over final diagnosis. Further from Tukey's HSD, it is observed that, there is a significant difference observed between Metastasis and Low-Grade Glioma (p-value = 0.0278), as well as between Low Grade Glioma and High-Grade Glioma (p-value = 0.0039).

From Chi square test, it is observed that, there is no significant difference in the distribution of gender over final diagnosis.

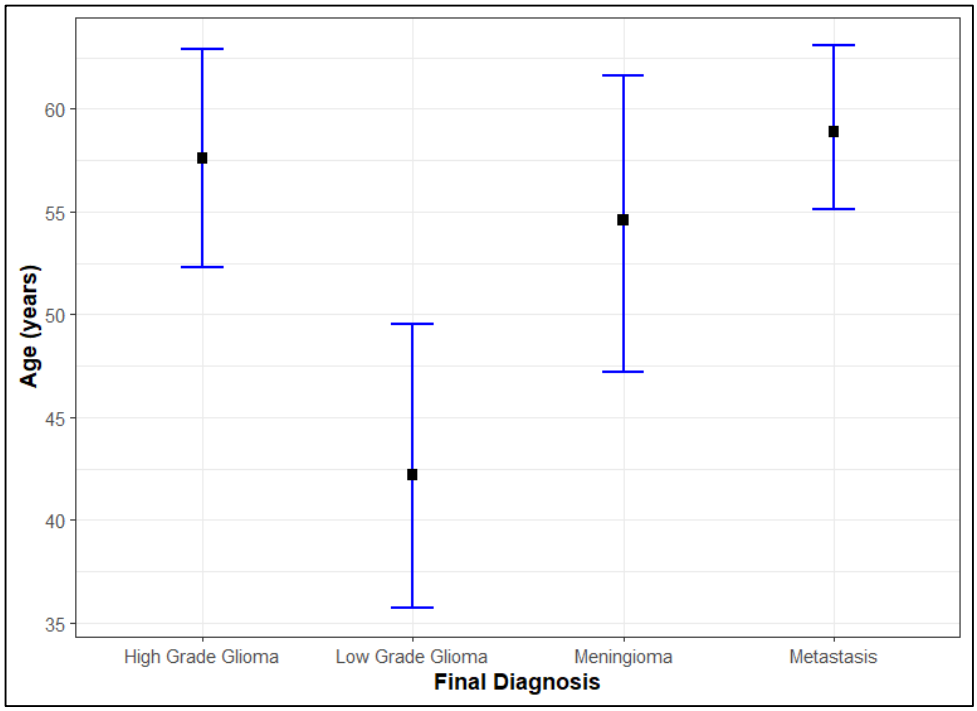

Figure 11: Mean plot of age over final diagnosis.

12) The following table gives the comparison of comorbidities over diagnosis.

Table 12: Comparison of comorbidities over diagnosis.

Comorbidities	**High Grade Glioma**	**Low Grade Glioma**	**Meningioma**	**Metastasis**	**p-value**
Diabetes mellitus	1(4.35%)	0	0	0	0.7711^{MC}
Hypertension	12(52.17%)	6(46.15%)	3(50%)	2(28.57%)	
Hypertension and diabetes mellitus	7(30.43%)	2(15.38%)	2(33.33%)	3(42.86%)	
None	3(13.04%)	5(38.46%)	1(16.66%)	2(28.57%)	

Abbreviation: MC – Chi square test with Monte Carlo simulation.

From Chi square test, it is observed that, there is no significant difference in the distribution of comorbidities over final diagnosis.

13) The following table gives the comparison of number of lesions on MRI over diagnosis.

Table 13: Comparison of number of lesions on MRI over diagnosis.

Number of Lesions on MRI	**High Grade Glioma**	**Low Grade Glioma**	**Meningioma**	**Metastasis**	**p-value**
Multiple	0	0	0	5(71.43%)	< **0.001^{MC}***
One	23(100%)	13(100%)	6(100%)	2(28.57%)	

*Abbreviation: MC – Chi square test with Monte Carlo simulation, * indicates statistical significance.*

For high-grade glioma, low-grade glioma, and meningioma, all subjects had a single lesion detected on their MRI scans, with 23 (100%) subjects, 13 (100%) subjects, and 6 (100%) subjects, respectively. In contrast, among individuals diagnosed with metastasis, the majority had multiple lesions on MRI scans, with 5 (71.43%) subjects. From Chi square test, it is observed that, there is significant difference in the distribution of number of lesions on MRI over final diagnosis.

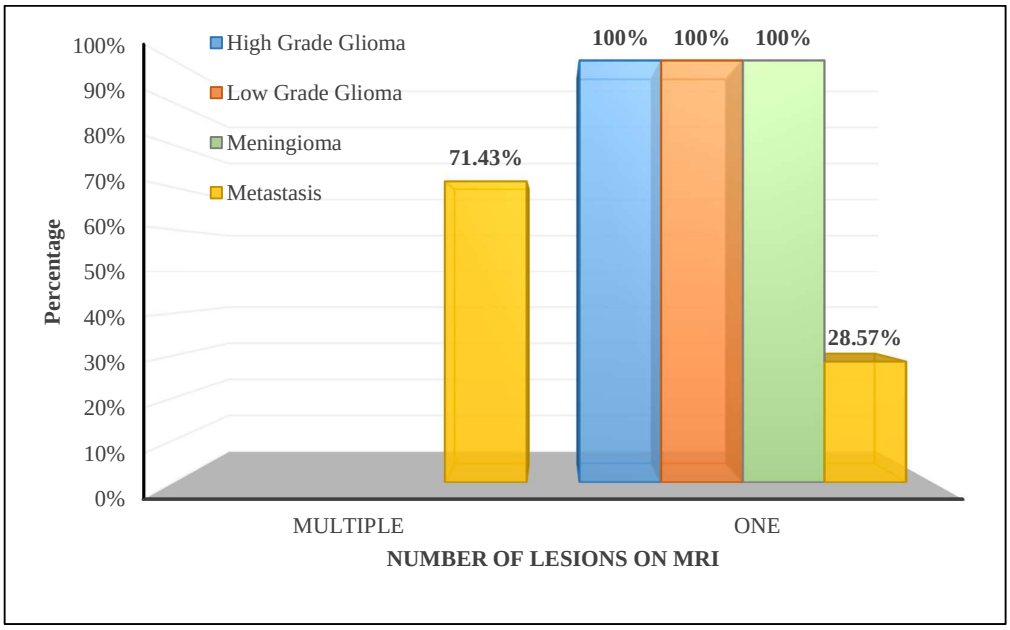

Figure 12: Distribution of number of lesions on MRI over diagnosis.

14) The following table gives the comparison of T1 and T2 signal intensity over diagnosis.

Table 14: Comparison of T1 and T2 signal intensity over diagnosis.

Variables	**Sub Category**	**High Grade Glioma**	**Low Grade Glioma**	**Meningioma**	**Metastasis**	**p-value**
T1 Signal	Hyperintense	1(4.35%)	1(7.69%)	0	1(14.29%)	0.7846^{MC}
	Hypointense	10(43.48%)	6(46.15%)	3(50%)	4(57.14%)	
	Isointense	7(30.43%)	5(38.46%)	3(50%)	2(28.57%)	
	Mixed Intense	5(21.74%)	1(7.69%)	0	0	
T2 Signal	Hyperintense	10(43.48%)	10(76.92%)	3(50%)	3(42.86%)	0.1064^{MC}
	Hypointense	1(4.35%)	2(15.38%)	2(33.33%)	0	
	Isointense	2(8.7%)	0	1(16.66%)	0	
	Mixed Intense	10(43.48%)	1(7.69%)	0	4(57.14%)	

Abbreviation: MC – Chi square test with Monte Carlo simulation.

From Chi square test, it is observed that, there is no significant difference in the distribution of T1 and T2 signal intensities over final diagnosis.

15) The following table gives the comparison of Diffusion Restriction over diagnosis.

Table 15: Comparison of Diffusion Restriction over diagnosis.

Diffusion Restriction	**High Grade Glioma**	**Low Grade Glioma**	**Meningioma**	**Metastasis**	**p-value**
Absent	0	0	5(83.33%)	0	**< 0.001^{MC*}**
Present	23(100%)	13(100%)	1(16.66%)	7(100%)	

*Abbreviation: MC – Chi square test with Monte Carlo simulation, * indicates statistical significance.*

For high-grade glioma and low-grade glioma, all subjects exhibited diffusion restriction, with 23 (100%) subjects and 13 (100%) subjects, respectively. In contrast, among individuals diagnosed with meningioma, the majority had no diffusion restriction observed on their imaging scans, with 5 (83.33%) showing its absence. Similarly, for metastasis, all subjects demonstrated diffusion restriction, with 7 (100%) subjects. From Chi square test, it is observed that, there is significant difference in the distribution of diffusion restriction over final diagnosis.

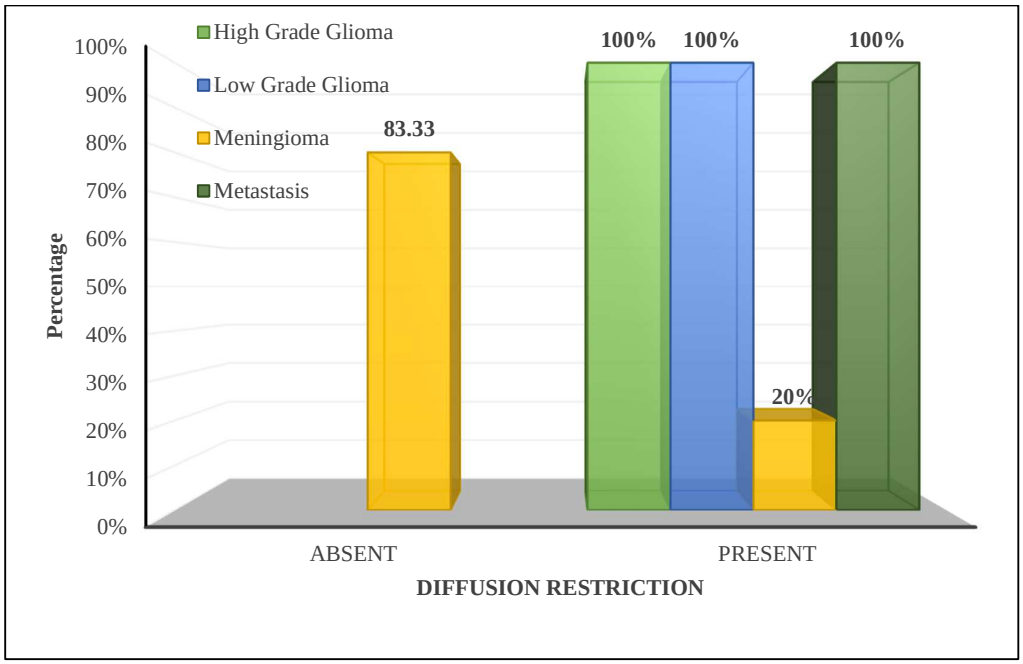

Figure 13: Distribution of diffusion restriction over diagnosis.

16) The following table gives the comparison of Intralesional CHO/CR Ratio over diagnosis.

Table 16: Comparison of Intralesional CHO/CR Ratio over diagnosis.

Final diagnosis	**Intralesional CHO/CR Ratio**		**p-value**
	Mean ± SD	**Median (Min, Max)**	
High Grade Glioma	5.18 ± 1.15	4.9 (3.6, 7.6)	**< 0.001^{K*}**
Low Grade Glioma	2.49 ± 0.3	2.6 (1.9, 2.9)	
Metastasis	1.86 ± 0.3	1.9 (1.4, 2.2)	

*Abbreviation: K – Kruskal Wallis test, * indicates statistical significance.*

From Kruskal Wallis test, it is observed that, there is significant difference in the distribution of Intralesional CHO/CR Ratio over final diagnosis. Further, from Dunn test, it is observed that, there is significant difference in the Intralesional CHO/CR Ratio between Low Grade Glioma and High-Grade Glioma (p-value < 0.001) as well as between Metastasis and High-Grade Glioma (p-value < 0.001).

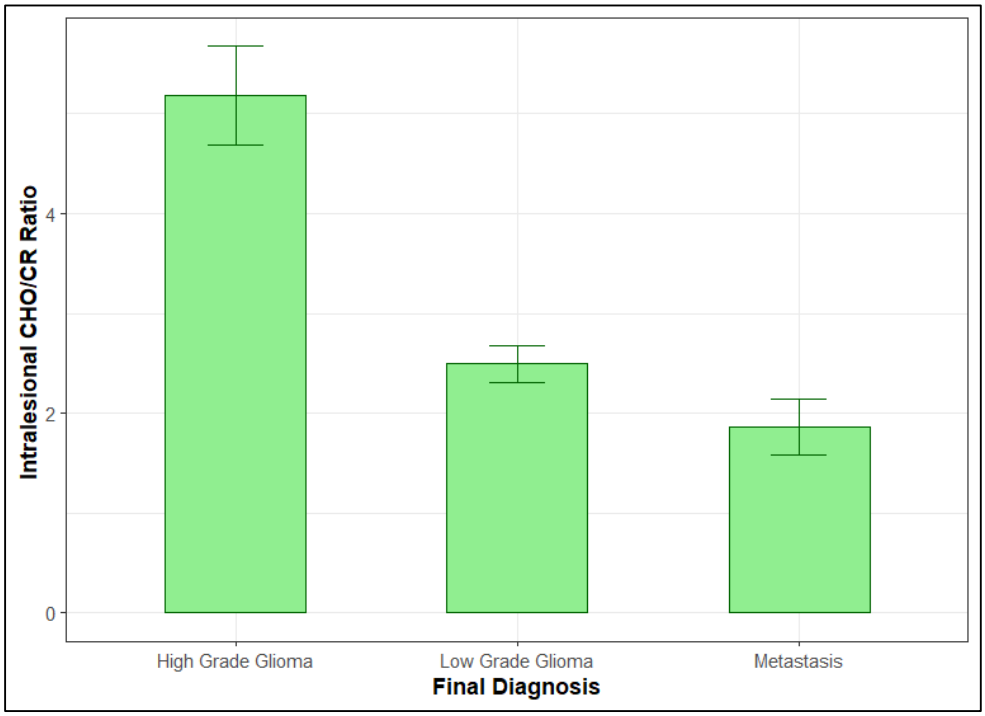

Figure 14: Mean plot of Intralesional CHO/CR Ratio over final diagnosis.

17) The following table gives the comparison of Perilesional CHO/CR Ratio over diagnosis.

Table 17: Comparison of Perilesional CHO/CR Ratio over diagnosis.

Final diagnosis	**Perilesional CHO/CR Ratio**		**p-value**
	Mean ± SD	**Median (Min, Max)**	
High Grade Glioma	3.54 ± 1.26	2.9 (1.9, 6.4)	**< 0.001^{K*}**
Low Grade Glioma	0.8 ± 0.46	0.7 (0.4, 2.2)	
Metastasis	0.71 ± 0.16	0.7 (0.5, 0.9)	

*Abbreviation: K – Kruskal Wallis test, * indicates statistical significance.*

From Kruskal Wallis test, it is observed that, there is significant difference in the distribution of Perilesional CHO/CR Ratio over final diagnosis. Further, from Dunn test, it is observed that, there is significant difference in the Perilesional CHO/CR Ratio between Low Grade Glioma and High-Grade Glioma (p-value < 0.001) as well as between Metastasis and High-Grade Glioma (p-value < 0.001).

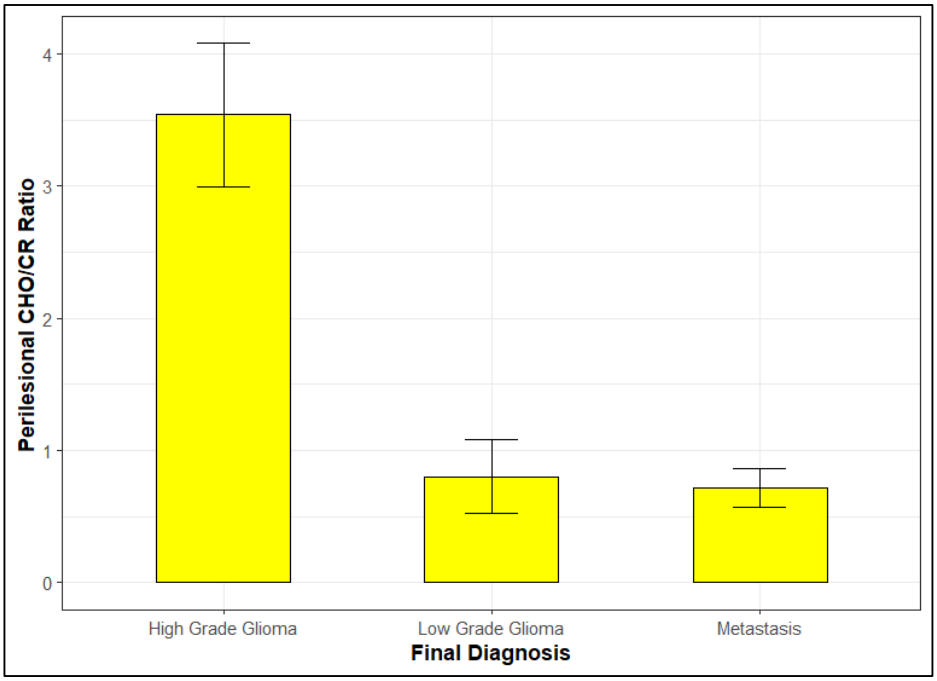

Figure 15: Mean plot of Perilesional CHO/CR Ratio over final diagnosis.

18) The following table gives the comparison of Intralesional ADC Values over diagnosis.

Table 18: Comparison of Intralesional ADC Values over diagnosis.

Final diagnosis	**Intralesional ADC Values**		**p-value**
	Mean ± SD	**Median (Min, Max)**	
High Grade Glioma	0.88 ± 0.31	1.01 (0.11, 1.49)	**< 0.001^{K*}**
Low Grade Glioma	1.45 ± 0.06	1.45 (1.31, 1.53)	
Metastasis	0.85 ± 0.2	0.87 (0.61, 1.1)	

*Abbreviation: K – Kruskal Wallis test, * indicates statistical significance.*

From Kruskal Wallis test, it is observed that, there is significant difference in the distribution of Intralesional ADC Values over final diagnosis. Further, from Dunn test, it is observed that, there is significant difference in the Intralesional ADC Values between Low Grade Glioma and High-Grade Glioma (p-value < 0.001) as well as between Metastasis and Low-Grade Glioma (p-value < 0.001).

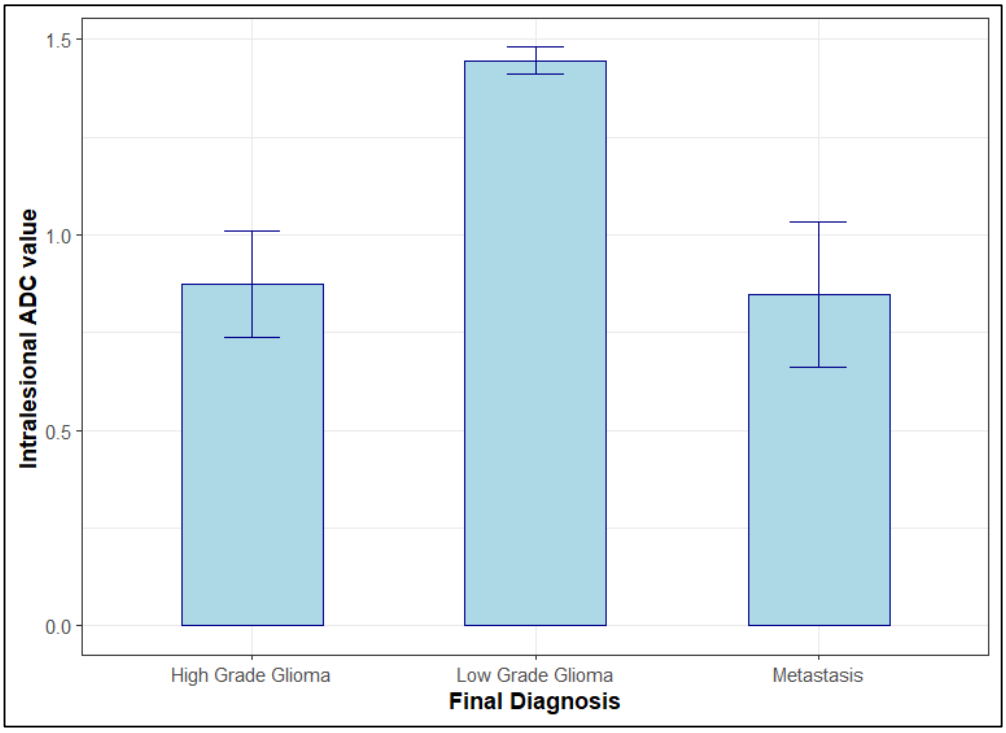

Figure 16: Mean plot of Intralesional ADC Values over final diagnosis.

19) The following table gives the comparison of Perilesional ADC Values over diagnosis.

Table 19: Comparison of Perilesional ADC Values over diagnosis.

Final diagnosis	**Perilesional ADC Values**		**p-value**
	Mean ± SD	**Median (Min, Max)**	
High Grade Glioma	0.87 ± 0.26	0.93 (0.1, 1.13)	**< 0.001^{K*}**
Low Grade Glioma	0.93 ± 0.27	0.99 (0.09, 1.24)	
Metastasis	1.44 ± 0.13	1.43 (1.31, 1.61)	

*Abbreviation: K – Kruskal Wallis test, * indicates statistical significance.*

From Kruskal Wallis test, it is observed that, there is significant difference in the distribution of Perilesional ADC Values over final diagnosis. Further, from Dunn test, it is observed that, there is significant difference in the Perilesional ADC Values between Metastasis and Low-Grade Glioma (p-value < 0.001) as well as between Metastasis and High-Grade Glioma (p-value = 0.0035).

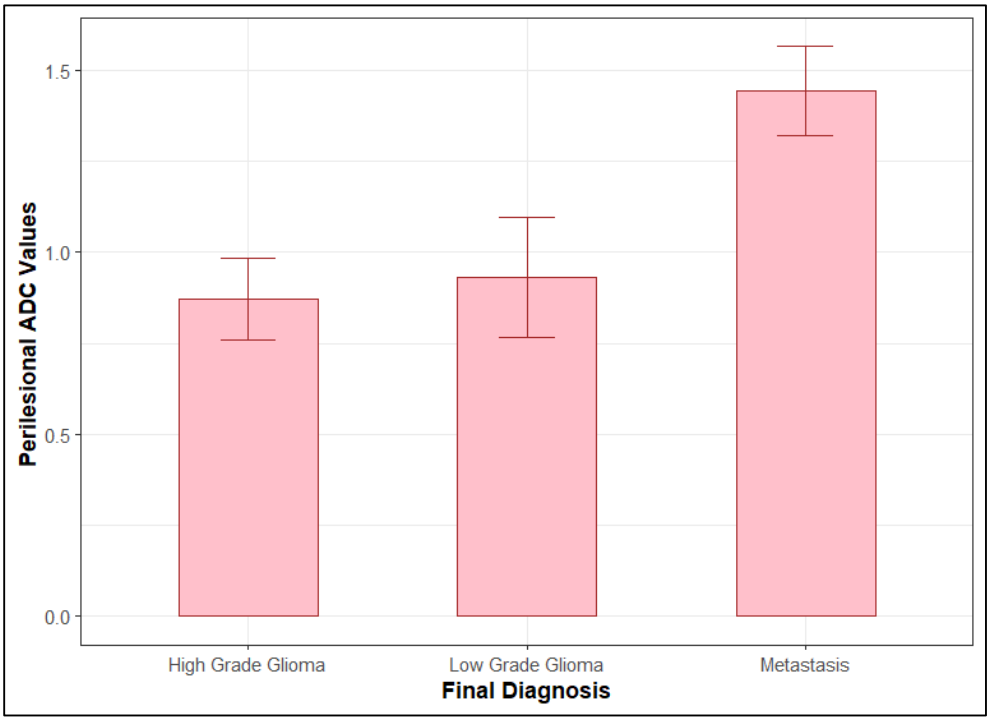

Figure 17: Mean plot of Perilesional ADC Values over final diagnosis.

20) Statistical analysis with regards to comparison between MRI diagnosis and final diagnosis

A) It was observed from the collected data from 48 cases that with respect to the final diagnosis of meningioma there were 6 true positives, zero false positive & negative cases and 36 true negative cases. Following calculations are demonstrated below:

	FINAL DIAGNOSIS OF MENINGIOMA		
TEST RESULT		POSITIVE	NEGATIVE
	POSITIVE	6 (TP)	0 (FP)
	NEGATIVE	0 (FN)	36 (TN)

SENSITIVITY = TP/TP + FN = 100 %

SPECIFICITY = TN/ TN + FP = 100 %

POSITIVE PREDICTIVE VALUE = TP / TP + FP = 100 %

NEGATIVE PREDICTIVE VALUE = TN/ FN + TN = 100 %

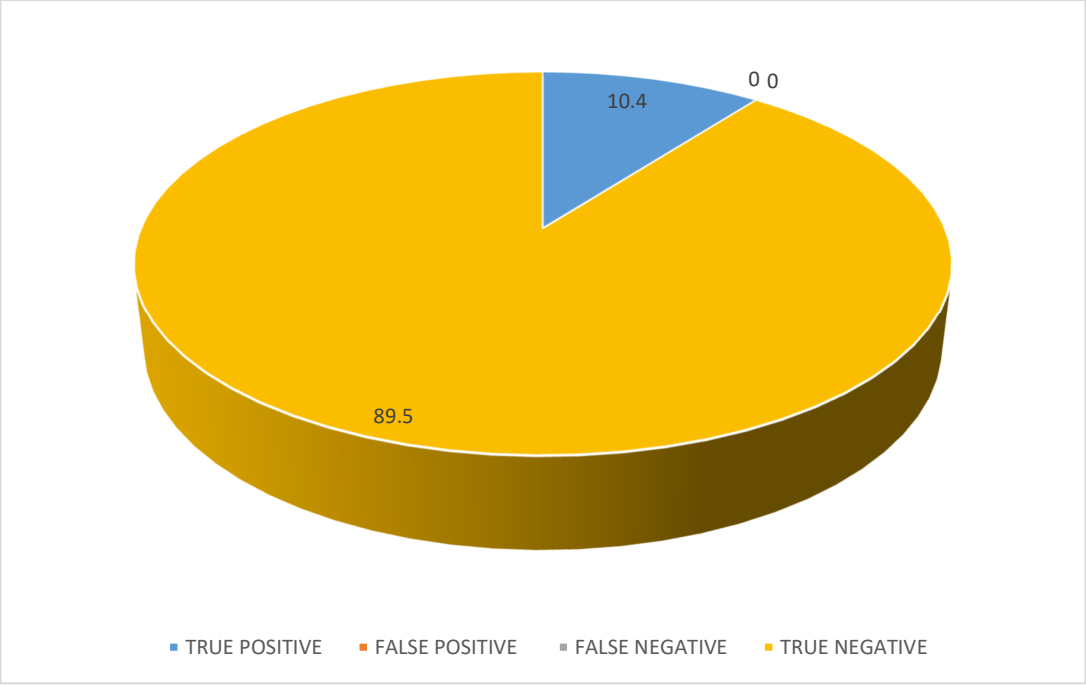

Figure 18: Distribution of meningioma cases over final diagnosis.

B) It was observed from the collected data from 48 cases that with respect to the final diagnosis of high-grade glioma, there were 21 true positives, 02 false positive, 03 false negative cases and 15 true negative cases. Following calculations are demonstrated below:

	FINAL DIAGNOSIS OF HIGH-GRADE GLIOMA		
TEST RESULT		POSITIVE	NEGATIVE
	POSITIVE	21 (TP)	02 (FP)
	NEGATIVE	03 (FN)	16 (TN)

SENSITIVITY = TP/TP + FN = 87.5 %

SPECIFICITY = TN/ TN + FP = 88.8 %

POSITIVE PREDICTIVE VALUE = TP / TP + FP = 91.3 %

NEGATIVE PREDICTIVE VALUE = TN/ FN + TN = 84.21 %

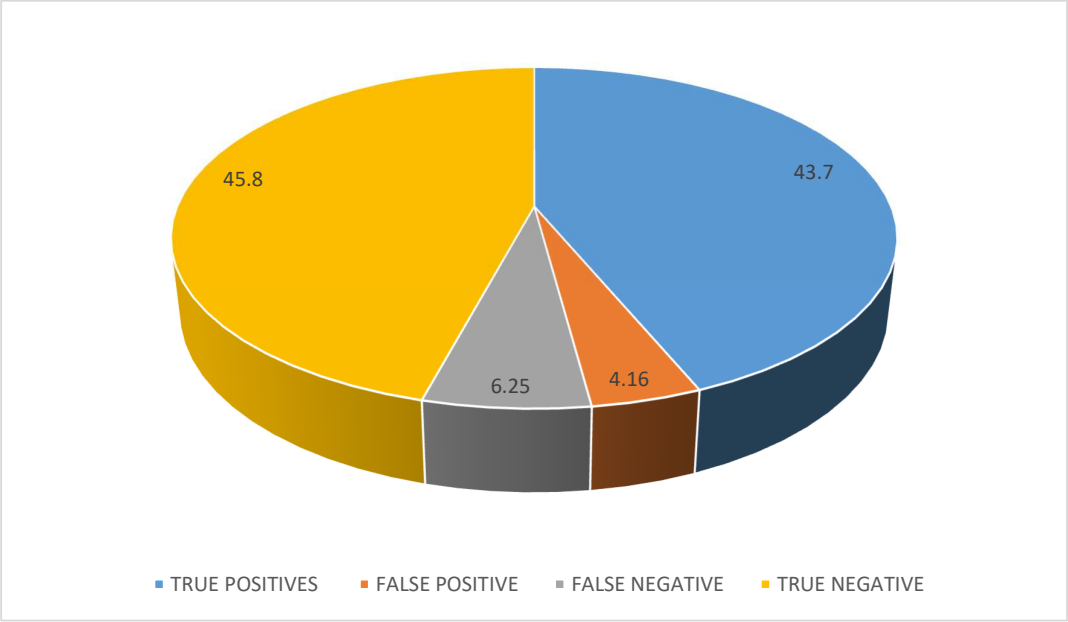

Figure 19: Distribution of high grade glioma cases over final diagnosis.

C) It was observed from the collected data from 48 cases that with respect to the final histopathological diagnosis of meningioma there were 10 true positives, 03 false positive, 02 false negative cases and 27 true negative cases. Following calculations are demonstrated below:

	FINAL DIAGNOSIS OF LOW GRADE GLIOMA		
TEST RESULT		POSITIVE	NEGATIVE
	POSITIVE	10 (TP)	03 (FP)
	NEGATIVE	02 (FN)	27 (TN)

SENSITIVITY = TP/TP + FN = 83.3 %

SPECIFICITY = TN/ TN + FP = 90.0 %

POSITIVE PREDICTIVE VALUE = TP / TP + FP = 76.9 %

NEGATIVE PREDICTIVE VALUE = TN/ FN + TN = 93.1 %

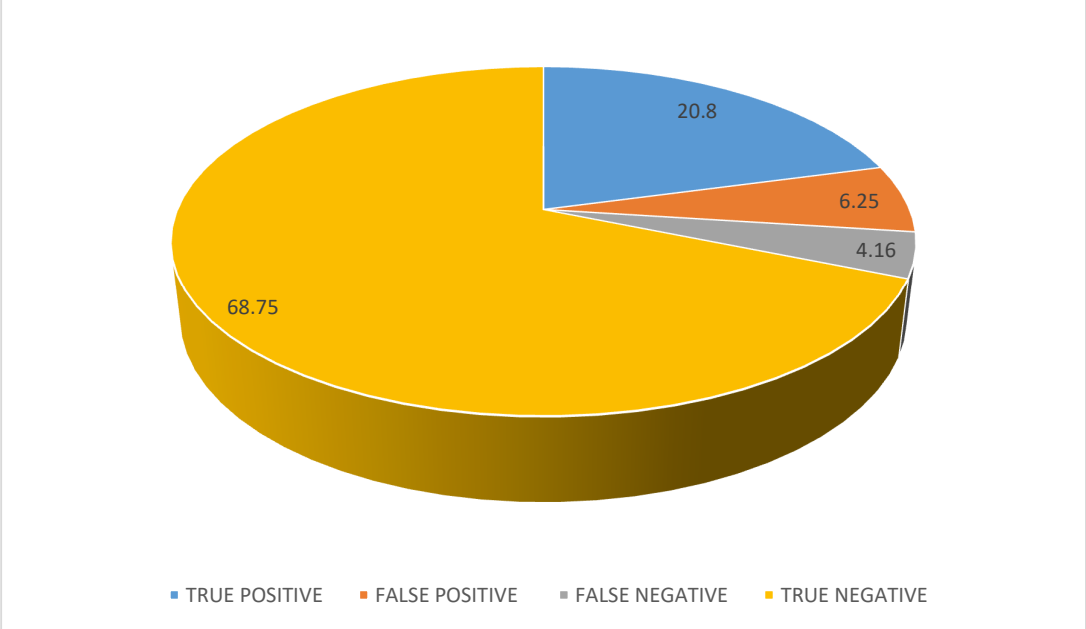

Figure 20: Distribution of low-grade glioma cases over final diagnosis.

21) Comparison between DWI imaging (Intralesional & Perilesional ADC value) Vs MRI Spectroscopy (Intralesional & Perilesional Choline/Creatine ratio)

Following the analysis of the data measurements on 49 subjects, the following pie diagram gives the various observations that were made based on Diffusion Weighted Imaging & magnetic resonance spectroscopic analysis.

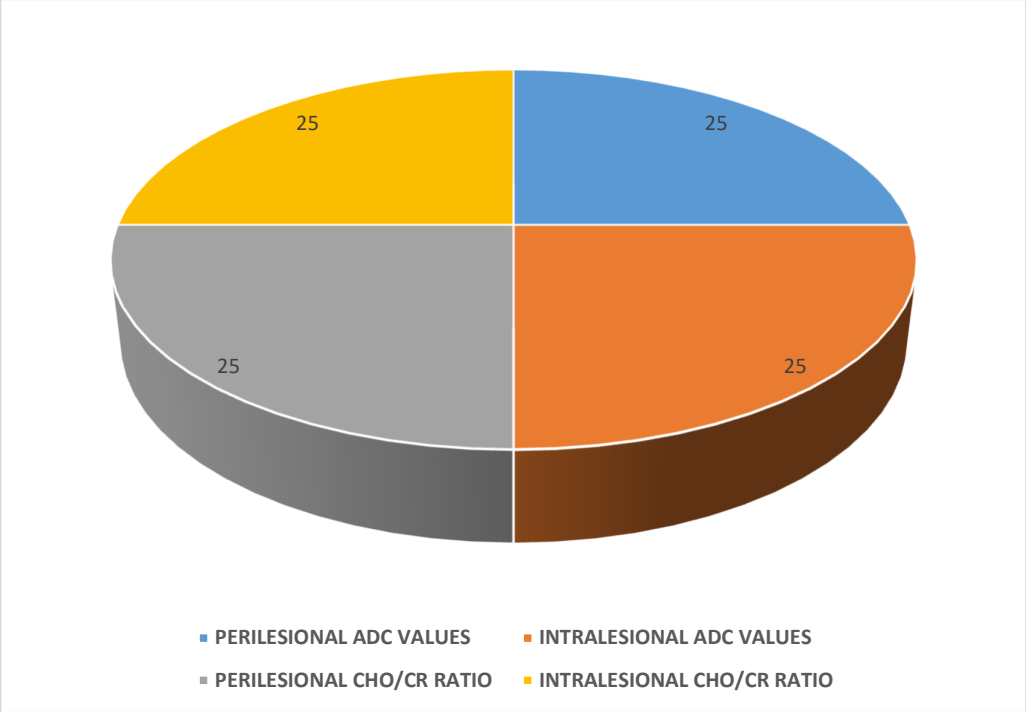

Figure 21: Parameters assessed for comparison between DWI and MRI Spectroscopy

Parameters	Intralesional Cho/Cr ratio	Perilesional Cho/Cr Ratio	Intralesional ADC Values	Perilesional ADC Values
High Grade Glioma Vs Low Grade Glioma	☑	☑	☑	☒
High Grade Glioma Vs Metastasis	☑	☑	☒	☑
Low Grade Glioma Vs Metastasis	☒	☒	☑	☑

Figure 22: Various points of differentiation furnished by ADC values and MRI Spectroscopy

Based on the observations made in the above-mentioned table a consensus can be reached that though both the imaging modalities provide detailed information about the lesions in the study the diffusion weighted imaging and the subsequent ADC value measurement in the intralesional and perilesional regions provides better overall assessment of the brain lesions including the grading of the lesions.

DISCUSSION

Without any uncertainty, the most critical diagnostics technique for assessing intracranial space-occupying lesions involves magnetic resonance imaging, which has previously proven to be more effective to computed tomography. The primary imaging need for evaluating brain tumors is still standard magnetic resonance imaging (MRI). It provides fundamental details regarding the structural features of these tumors, including mass effect, enhancement, edema and inflammation.[97]

MRI is an exceptionally accurate technology for tumor diagnosis and localisation because to its multiplanar sampling and outstanding contrast resolution across various tissues. But increases in specificity have not kept pace with the sensitivity advancements.

We can now see parenchymal architecture and functionality as well as detect processes associated with disease more clearly thanks to recent developments in magnetic resonance imaging (MRI) such as diffusion weighted imaging, perfusion imaging, and MR spectroscopy.

Water molecules' random Brownian motion that occurs within a tissue voxel is measured by diffusion-weighted imaging (DWI), a variant of magnetic resonance imaging. In tissues exhibiting a high density of cells or cellular swelling, diffusion coefficients are often lower. Characterizing tumors and cerebral ischemia are two conditions where diffusion plays a crucial role.

A novel and developing imaging technique called magnetic resonance spectroscopy allows us to examine tissues in tremendous detail and provides a window into the brain's metabolism in vivo. It supplements the data provided by magnetic resonance imaging and aids in determining prognosis and treatment effectiveness. Numerous studies have been done and are still being done to determine the possible applications of MRS in neuroradiology.

In contrast to MRI, which offers detailed structural data, MRS offers a qualitative assessment of the brain's many compounds. These compounds exhibit characteristics of energy / metabolic processes, neural integrity, cell membrane growth or disintegration, and necrotic transformation of brain or tumor tissue.[98]

Since histology is the highest-quality method for diagnosing brain tumors, MRS restricts the use of invasive diagnostic techniques like brain biopsies.[99] We found that supratentorial brain tumors can be effectively diagnosed and characterized with the use of DWI & MR Spectroscopy.

According to our investigation, a standard 3.0 T magnetic resonance imaging equipment can create an excellent spectrum in a fair amount of time without giving the individual any discomfort.

It additionally has the ability to attain a fantastic signal to noise ratio in the brains of humans.

42.8% percent of those cases included in this study were female, and 57.14 % were male.

Most individuals with supratentorial brain tumors who presented were in the age range of 28 to 78.

Headache emerges as the most prevalent chief complaint, reported by 42 (85.71%) subjects. Following closely, vomiting was noted in 29 (59.18%) subjects. Other frequently reported complaints include seizures, reported by 23 (46.93%) subjects, and dizziness, noted by 18 (36.73%) subjects. Additionally, there were isolated instances of increased forgetfulness, altered sensorium, and right-sided mild weakness, each reported by one or two subjects. The findings of Grand S et al. [100] were consistent with these observations.

We found the predominant cause of supratentorial brain tumors to be high grade glioma 23 (46.93%) subjects followed by low-grade glioma observed in 13 (26.53%) subjects.

Additionally, meningioma was diagnosed in 6 (12.24%) subjects. Metastasis was diagnosed in 7 (14.28%) subjects.

The level of choline was higher in every tumor. More cell proliferation and membrane turnover are thought to be the causes of the elevated Cho that has been seen in the majority of brain tumors in prior research[53]. The Cho/Naa ratio was raised since all neoplasms had reduced NAA.

NAA is neuronal marker and its levels are reduced in all neoplasms as they do not contain any neural tissue. Within those neoplasms the level of NAA depends on variations in the degree of necrosis and the makeup of the cells[101]

Spectroscopy revealed that all of them displayed varying degrees of elevated CHO peak and CHO/Cr ratios, with a noteworthy rise from both high-grade and low-grade tumors, and no discernible distinction between brain tumors that were primary and those that had metastasized.

This supported the findings of Martinez-Bisal, Celda[102], and Shokry[97], which showed that a lesion's CHO/NAA ratio could only distinguish between low- and high-grade primary tumors.

While there was no discernible variation in lipid-lactate levels between primary and metastatic brain tumors, there was a substantial difference between low-grade and high-grade tumors.

This also confirmed the findings of Van der Graaf[103], which showed that the presence of lactate peaks was usually indicative of aggressive tumors, supporting increased anaerobic metabolism and cellular necrosis, and that the pathophysiology of primary and metastatic brain tumors is similar.

It is thought that lactate is produced in tumor cells when anaerobic glycolysis occurs and the tricarboxylic acid cycle activity declines[54].

Lactate can be detected in high grade tumors but not in low grade tumors because of the high mitotic activity and necrosis they exhibit. As a result, the degree of malignancy and the presence of lactate seem to be related. Fulham J. et al. [54]. A lactate peak was not observed in low grade tumors in our investigation, but it was present in 75 % of high-grade tumors.

The fact that intralesional voxels in primary tumors showed variable CHO/Cr ratios that increased in proportion to the tumor's grade is an additional noteworthy finding from this study. Consequently, the ability of CHO/Cr ratios to predict tumor grade has been shown to be reliable. Additionally, there was a noticeable difference between the two distinct groups when comparing the CHO/Cr ratios of high-grade and low-grade tumors. A robust correlation has been detected, per Chen et al. [104] and Faria et al. [96], between the raised CHO/Cr ratios in high-grade malignancies relative to low-grade malignancies and the expression of proliferating cells.

In addition, the results indicated a rise in the perilesional CHO/Cr ratio in high-grade primary tumors, which differed significantly from metastatic brain tumors in terms of this ratio. As per Opstad et al. [105] & Faria et al. [96], primary high-grade tumors have been reported to have neoplastic cells infiltrating the tumor microenvironment. This finding is consistent with those findings. Thus, in accordance with Shokry, perilesional edema exhibited spectroscopic malignant alterations in the form of a higher CHO/Cr ratio in primary tumors than in metastatic ones.[97]

Meningiomas are the only neoplasms in which alanine (Ala) resonances are seen.[53, 55] None of the other lesions demonstrated alanine peaks.

The results did not demonstrate a statistically significant difference in intralesional ADC values between high grade primary and metastatic brain tumors, indicating that intralesional ADC values alone were insufficient to distinguish high grade primary tumors from metastatic brain tumors. Although this result disagreed with Chiang et al.[106], which discovered that ADC values in the tumoral regions of metastasis were significantly higher than primary tumors, it matched Pavlisa et al.[93], Ja Lee et al.[94], and Ohba et al.[95], who attributed this result to the increase in cellularity of all these lesions to the point that DWI could not differentiate.

A notable discovery revealed that intralesional apparent diffusion coefficient values of lower-grade primary tumors were higher than those for higher grade tumors. The apparent diffusion coefficient numbers between the two groups differed significantly, with low grade cancers having $1.45 \pm 0.06 \times 10^{-3}$ and high-grade tumors having $0.88 \pm 0.31 mm^{-3}$. Our study's ability to use ADC values to distinguish between low- and high-grade tumors was thus consistent with the findings of Ohba et al.[95], who also observed that ADC values can be used to grade primary tumors.

Additionally, we found that primary higher grades of tumors and metastatic brain tumors differed significantly in their perilesional ADC levels, with the former having higher values.

In metastasis (vasogenic edema), perilesional ADC values around tumor areas were higher (1.44 ± 0.13 x 10-3), indicating no perilesional infiltration, than in high grade primary tumors (0.87 ± 0.26 x 10-3), indicating peri lesion infiltration.

This suggests that the ADC levels will be very sensitive in this regard and that the current study may be capable to differentiate between metastatic lesions and primary brain tumors.

This was in line of findings given by Faria[96] and associates where they linked these to 1^0 higher grade tumors infiltrating the perilesional area and increasing cellularity there. Metastatic cases on the other hand, do not exhibit this infiltration and raise in perilesional edema the ADC values.

The ADC values retrieved from the primary tumoral region possessed the smallest numbers among the research's malignant tumors.

Abdel Monem Nooman Darwiesh Et.Al.[107] conducted a research study which showed that the intra-lesional ADC values are not useful in the differentiation between primary and metastatic tumors while perilesional ADC values can differentiate between primary & metastatic brain tumors which was in part similar to findings in this study.

In the same study they also found that intralesional MRS values (CHO/Cr ratio) were able to grade the tumor and differentiate between high- and low-grade tumors, while Perilesional MRS values (CHO/Cr ratio) could be able to differentiate primary tumors from metastasis which was found to correlate with the findings of this study.

CONCLUSION

Magnetic resonance spectroscopy is a newer non-invasive modality which provides biochemical information about different tissues that cannot be obtained by conventional MRI alone even after contrast administration.

It complements MRI and is particularly useful when the MRI findings are inconclusive. It characterizes lesions based on metabolite patterns and ratios.

Choline, N-acetyl aspartate, creatine, lactate, alanine, amino acids and myoinositol are the major metabolites studied.

In this study magnetic resonance spectroscopy was helpful in characterising the neoplastic lesions.

Among the subjects 43 subjects (87.75%) had malignant lesions and 6 (12.24%) subjects had benign lesions

Choline is considered the most specific marker of intracranial neoplasm.

Increase in Choline levels and Choline/NAA ratios are very suggestive of the malignant nature of the neoplasm, its grading and its follow-up to evaluate the response of the treatment.

Intralesional CHO/CR Ratio can help to differentiate between Low Grade Glioma and High-Grade Glioma as well as between Metastasis and High-Grade Glioma.

Perilesional CHO/CR Ratio can help to differentiate between Low Grade Glioma and High-Grade Glioma as well as between Metastasis and High-Grade Glioma.

Intralesional lipid-lactate levels can help to differentiate between between low grade and high-grade tumors.

Metabolites like amino acids helped to differentiate from similar appearing lesions and alanine was specific for meningiomas.

Hence, it can be concluded that 'H MRS helps in better characterization of different supratentorial lesions.

From the current study it can be understood that the DWI with ADC values calculation could improve the diagnostic efficacy of MR imaging.

Intralesional ADC Values can help to differentiate between Low Grade Glioma and High-Grade Glioma as well as between Metastasis and Low-Grade Glioma while Perilesional ADC Values can help to differentiate between Metastasis and Low-Grade Glioma as well as between Metastasis and High-Grade Glioma.

Intralesional ADC values are not useful in the differentiation between high grade gliomas and metastatic tumors.

Thus, in this study the diffusion weighted imaging and the subsequent ADC value measurement in the intralesional and perilesional regions provides better overall assessment of the brain lesions including the grading of the lesions.

SUMMARY

- A combined total of forty-eight individuals went through DWI and magnetic resonance (MRS) spectroscopy after having supratentorial brain tumors identified by magnetic resonance imaging (MRI) (plain/contrast) examinations.
- Maximum number were between 28 to 78 Yrs.
- Male patients constituted the most of the patients (57.14%).
- Headache, vomiting & seizures were the most frequent presenting complaints.
- The most prevalent diagnosis among the subjects is malignant lesions 43 (87.75%) and benign was diagnosed in 6 (12.24%) subjects.
- Among the patients, 46.93% had diagnosis of high-grade glioma, while 26.53 % exhibited low-grade glioma. Metastasis was noted in 14.28% and meningioma was identified in 12.24% of the patients.
- When comparing gliomas, a larger Cho/Cr proportion was observed.
- As opposed to low grade gliomas high grade gliomas exhibited a substantially greater Cho/Cr ratio.
- As opposed to low grade gliomas, high grade gliomas also contained more lipid-lactate.
- From the current study it can be understood that the DWI with ADC values calculation could improve the diagnostic efficacy
- Alanine peak was found in meningiomas.
- So, the additional information provided by magnetic resonance spectroscopy and DWI imaging was particularly advantageous and added to the data collected via conventional an MRI scan helping in characterization of supratentorial brain tumors.

BIBLIOGRAPHY

1. Jamjom ZAB. Pater of intra-cranial space ocuping lcions: experience at King Khaid University Hiospial. Am Saudi Med. 1989;9(3):93-10.

2. Duncan G, Caird P. Review of 18 years experience of a diagnostic geriatric neurology referral service. Scot-Med-J. 1991;36(139):42.

3. Darrel F, Weinman. Incidence and Behaviour Pattern of intra-cranial Tumors in Ceylon. International Surgery. 1973;58:548-54.

4. Conley FK. Epidermiod and dermiod tumors: Clinical features and surgical management. In: Wilkins RH, Rengachary SS, editors. Neurosurgery. Vol. No. 1, 27 ed. New York: McGraw-Hill; 1996. p. 971-6.

5. Wen-Qing QQ, Shi-Jow, Qing-sheng T, Jian-qing H, Yu-xia L, Qing-zhong X, et al. Statistical analysis of central nervous system tumors in China. J Neurosurg. 1982;56(4):555-64.

6. Lombardi D, Scheithauer BW, Piepgras D, Meyer FB, Forbes GS. Angioglioma and the arteriovenous malformation-glioma association. Journal of Neurosurgery. 1991;75:589-96.

7. Burger PC, Scheithauer BW. Tumors of Central Nervous System. Atlas of tumor Pathology, Third series, Fase 10, Washington DC: AFIP; 1994.

8. Mangombe NJ, Ombachi RB. Brain tumors at Kenyata Naional Hospital, Nairobi. East Afr Med J. 2000;77(8):444-7.

9. Fiaz But M, Khan SA, Chaudhy NA, Queshi OR. Interanal space occupying lesions a morphological analysis. Biomedica. 2005;21:31-5.

10. Majos C, Aguilera C, Alonso J, Julia Sape M, Castener S, Sanchez I. Proton MR spectroscopy improves discrimination between tumor and pseudotumoral lesion in solid brain masses. AJNR Am J Neuroradiol. 2009;30:544-51.

11. Burger PC. Malignant astrocytic neoplasms: classification, pathologic anatomy, and response to treatment. Semin Oncol. 1986;13:16-26.

12. Paley RJ, Persing JA, Doctor A, Westwater JJ, Roberson JP, Edlich RF. Multiple sclerosis and brain tumor: a diagnostic challenge. J Emerg Med. 1989;7:241-4.

13. Cousins JP. Clinical MR spectroscopy: Fundamentals, current applications and future potential. AJR Am J Roengenol. 1995;164:1337-47.

14. Bulakbasi N, Kocaoglu M, Ors F, Taytun C, Ucoz T. Combination of single-voxel proton MR spectroscopy and apparent diffusion coefficient calculation in the evaluation of common brain tumors. AJNR Am J Neuroradiol. 2003;24:225-33.

15. Moller-Hartmann W, Herminghaus S, Krings T, Marquard i, Lanfermann H, Pilatus U, et al. Clinical applications of proton magnetic resonance spectroscopy in the diagnosis of intracranial mass lesions. Neuroradiology. 2002;44:371-81.

16. Butzen J, Prost R, Chetty V, Donahue K, Neppl R, Bowen W, et al. Discrimination between neoplastic and non-neoplastic brain lesions by use of Proton MR spectroscopy: the limits of accuracy with a logistic regression model. AJNR Am J Neuroradiol. 2000;21:1213-9.

17. Nagar VA, Ye J, Xu M, Ng WH, Yeo TT, Ong PL, Lim CC. Multivoxel MR spectroscopic imaging--distinguishing intracranial tumors from non-neoplastic disease. Ann Acad Med Singapore. 2007;36(5):309-13.

18. Cianfoni A, Niku S, Imbesi SG. Metabolite findings in tumefactive demyelinating lesions utilizing short echo time proton magnetic resonance spectroscopy. AJNR Am J Neuroradiol. 2007;28(2):272-7.

19. Mishra AM, Gupta RK, Jaggi RS, Reddy JS, Jha DK, Husain N, et al. Role of diffusion-weighted imaging and in vivo proton magnetic resonance spectroscopy in

the differential diagnosis of ring-enhancing intracranial cystic mass lesions. J Comput Assist Tomogr. 2004;28:540-7.

20. Kumar A, Kaushik S, Tripathi RP, Kaur P, Khushu S. Role of in vivo proton MR spectroscopy in the evaluation of adult brain lesions: our preliminary experience. Neurol India. 2003;51:474-8.

21. Irfan A, Qureshi A. Intracranial space occupying lesions-review of 386 cases. J Pak Med Assoc. 1995;45(12):319-20.

22. Gray HF. The complete Gray's Anatomy. New York: senate, stuttgart; 2003.

23. Adult Brain Tumors Ireatment, Bethesda: National Cancer Institue; 2012. Available from: URL:

ht://www.cancer.gov/cancertopics/pad/treatment/adultbrain/Health/Professional/page/AlPages#Referencel.1. Accessed on: 10.01.2012.

24. Huff SJ, Brenner BE, Brain Neoplasms. Available from: URL: hut:/misc.medscape.com/pi/iphone/medscapeapp/html/A77964-business.html. Access Date: 18.08.2013.

25. Ohgaki H. Epidemiology of brain tumors. Methods Mol Biol. 2009;472:323-42.

26. Yeole BB. Trends in the brain cancer incidence in India. Asian Pac J Cancer Prev. 2008;9(2):267-70.

27. Edge SB, Byrd DR, Compton CC. AJCC Cancer Staging Manual. 7th ed. New York: Springer; 2010.

28. Kleihues P, Burger PC, Scheithauer BW. The new WHO classification of brain tumors. Brain Pathol. 1993;3(3):255-68.

29. Louis DN, Ohgaki H, Wiestler OD, Cavenee WK, Burger PC, Jouvet A, et al. The 2007 WHO classification of tumors of the central nervous system. Acta Neuropathol. 2007;114(2):97-109.

30. Louis, DN, Ohgak H, Wiester, OD, Cavene, WR. World Health Organization Classification of Tumors of the Nervous System. Lyon: IARC; 2007.

31. Meha M, Vogelbaum MA, Chang S. Neoplasms of the central nervous system. In: DeVita VT, Lawrence TS, Rosenberg SA, eds. Cancer: Principles and Practice of Oncology. 9th ed. Philadelphia: Lippincott Williams and Wilkins; 2011. p. 1700-49.

32. Hutter A, Schwetye KE, Bierhals AJ, McKinstry RC. Brain neoplasms: epidemiology, diagnosis, and prospects for cost-effective imaging. Neuroimaging Clin N Am. 2003;13(2):237-50.

33. Drudea A, Papan N. Imaging Modalities in Brain Tumors: Imaging of Brain Tumors with Histological Correlations. In: Drevolegas A, eds. Philadelphia.

34. Chavan GB. MEI Made easy. 29th ed. New Delhi: Jaype Brothers Medical Publishers; 2013.

35. Haga JR. CT and MRI of the whole body. 5th ed. Philadelphia: Mosby, Elsevier; 2009.

36. Bizzi A, De Stefano N, Gullapalli R, Lin DDM. Clinical MR Spectroscopy: Techniques and Applications. London: Cambridge University Press; 2009.

37. Atlas SW. Magnetic Resonance Imaging of the Brain and Spine. 3rd ed. New York: Lippincott Williams & Wilkins; 2002.

38. Bernasconi A, Tasch E, Cendes F, Li LM, Arnold DL. Proton magnetic resonance spectroscopic imaging suggests progressive neuronal damage in human temporal lobe epilepsy. Prog Brain Res. 2002;135:297-304.

39. Cabello JR, Cohen JS. Phospholipid metabolites as indicators of cancer cell function. NMR Biomed. 1992;5:226-33.

40. Moon RB, Richards JH. Determination of intracellular pH by 31P magnetic resonance. J Biol Chem. 1973;248(20):7276-8.

41. Hoult DI, Busby SJW, Gadian DG, Radda GK, Richards RE, Seeley PJ. Observation of tissue metabolites using 31P nuclear magnetic resonance. Nature London. 1974;252:285-7.

42. Branny M, Langer BG, Glick RP, Venkatasubramanian PN, Wilbur AC, Spigos D, et al. In Vivo B.- Spectroscopy in Humans at 1.5 T. Radiology. 1988;167:839-44.

43. Moller-Hartmann W, Herminghaus S, Krings T. Clinical application of proton magnetic resonance spectroscopy in the diagnosis of intracranial mass lesions. Neuroradiology. 2005;44:371-81.

44. Murphy M, Loosemore A, Clifton AG. The contribution of proton magnetic resonance spectroscopy (MRS) to clinical brain tumor diagnosis. Br J Neurosurg. 2002;16:329-34.

45. Shah N, Sattar A, Benanti M, Hollander S, Cheuck L, Mathew W. Magnetic Resonance Spectroscopy as an Imaging Tool for Cancer: A Review of the Literature. JAOA. 2006; 106(L),23-7.

46. Bertholdo D, Watcharakorn A, Castillo M. Brain Proton Magnetic Resonance Spectroscopy. Neuroimaging Clin. 2013;23(3):359-80.

47. Barbarella G, Ricci R. In vivo single voxel 1H MRS of glial brain tumors: correlation with tissue histology and in vitro MRS. Int J Oncol. 1998;12(2):461-8.

48. Law M, Yang S, Wang H. Glioma grading: sensitivity, specificity, and predictive values of perfusion MR imaging and proton MR spectroscopic imaging compared with conventional MR imaging. AJNR. 2003;24:1989-98.

49. Knop EA, Danders T, in L. Advanced MR imaging of tumors using spectroscopy and perfusion. Presented at the 39th annual meeting of the American Society of Neuroradiology, Boston, April 2001.

50. Herminghaus S, Platis V, Marquard M, Moller-Hartmann W, Schuierer G, Lanfermann H, et al. Differentiation of low from high grade gliomas: American Society of Neuroradiology, Boston. April 2006.

51. Hall WA, Liu H, Maxwell RE. Influence of 1.5-Tesla intraoperative MR imaging on surgical decision making. Acta Neurochir Suppl. 2007;85:29-37.

52. Harting I, Jost G, Hacke N. Role of Magnetic resonance spectroscopy of brain tumors. Nervenarzt. 2005;76(4):403-17.

53. Bruhn H, Frahm J, Gyngell ML, Merboldt KD, Hanicke W, Sauter R, et al. Noninvasive differentiation of tumors with use of localized H-1 MR spectroscopy in vivo: initial experience in patients with cerebral tumors. Radiology. 1989;172:541-8.

54. Fulham MJ, Bizzi A, Dietz MJ, Shih HH, Raman R, Sobering GS, et al. Mapping of brain tumor metabolites with proton MR spectroscopic imaging: clinical relevance. Radiology. 1992;185(3):675-86.

55. Taylor-Robinson SD, Thomas EL, Sargentoni J, Marcus CD, Davison BR, Bell JD. Cirrhosis of the human liver: an in vitro 31P nuclear magnetic resonance study. Biochim Biophys Acta. 1995; 1272:113-8.

56. Tzika AA, Zarifi MK, Goumnerova L, Astrakas LG, Zurakowski D, Young-Poussaint T, et al. Neuroimaging in pediatric brain tumors: Gd-DTPA-enhanced, hemodynamic, and diffusion MR imaging compared with MR spectroscopic imaging. AJNR. 2002;23:322-33.

57. Sutton LN, Wang ZJ, Wehrli SL, Marwaha S, Molloy P, Phillips PC, Zimmerman RA. Proton Spectroscopy of Suprasellar Tumors in Pediatric Patients. Neurosurgery. 2007;41(2):388-95.

58. Miller BL. A review of chemical issues in 1H NMR spectroscopy: N-acetyl-L-aspartate, creatine and choline. NMR Biomed. 1991;4:47-52.

59. Castillo, Kwock L, Mukherji SK, Swann T, Saldhana F, Braganza G. Clinical applications of proton MR spectroscopy. AJNR. 1995;4:17-5.

60. Go KG, Kamman RL, Mooyaart EL. Localized proton spectroscopy and spectroscopic imaging in cerebral gliomas, with comparison to positron emission tomography. Neuroradiology. 2007;37:198-206.

61. Shimizu H, Kumabe T, Tominaga T, Kayama T, Hara K, Ono Y, et al. Noninvasive evaluation of malignancy with proton magnetic resonance spectroscopy in human brain tumors. AJNR Am J Neuroradiol. 1996 May;17(5):737-47.

62. Sijens PE, van Dijk P, Oudkerk M. Correlation between choline level and Gd-DTPA enhancement in patients with brain metastases of mammary carcinomas. Magn Reson Med. 1994 Nov;32(5):549-55.

63. Howe FA, Barton SJ, Cudlip SA, Stubbs M, Saunders DE, Murphy M, et al. Metabolic profiles of human brain tumors using quantitative in vivo 1H Magnetic resonance spectroscopy. Magn Reson Med. 2003 Feb;49(2):223-32.

64. Warren KE. NMR Spectroscopy and Pediatric Brain Tumors. The Oncologist. 2004 Jun;9(3):312-8.

65. Astrakas LG, Zurakowski D, Tzika AA, Zarifi MK, Anthony DC, De Girolami U, et al. Noninvasive magnetic resonance spectroscopic imaging biomarkers to predict the clinical grade of pediatric brain tumors. Clin Cancer Res. 2006 Dec 1;10(24):8220-8.

66. Castillo M, Smith JK, Kwoch L. Correlation of myoinositol levels and grading of cerebral astrocytomas. AJNR Am J Neuroradiol. 2000 Nov-Dec;21(10):1645-9.

67. Preul MC, Caramanos Z, Collins DL, Villemure JG, Leblanc R, Olivier A. Accurate, noninvasive diagnosis of human brain tumors by using proton magnetic resonance spectroscopy. Nat Med. 1996 Mar;2(3):323-5.

68. Dowling C, Bollen AW, Stanley L, Hawk U. Preoperative proton MR spectroscopic imaging of brain tumors: Correlation with histopathologic analysis of resection specimens. AJNR Am J Neuroradiol. 2001 Apr;22(4):604-12.

69. Arnold DL, Emrich JF, Shoubridge EA, Villemure JG, Feindel W. Characterization of astrocytomas, meningiomas, and pituitary adenomas by phosphorus magnetic resonance spectroscopy. J Neurosurg. 1991 Mar;74(3):447-53.

70. Majós C, Cucurella G, Aguilera C, Coll S, Pons ILC. Pons Intraventricular Meningiomas: MR Imaging and MR Spectroscopic Findings in Two Cases. Am J Neuroradiol. 1999 May;20(5):882-5.

71. Zacharia TT, Law M, Naidich TP, Leeds NE. Central Nervous System Lymphoma Characterization by Diffusion-Weighted Imaging and MR Spectroscopy. AJR Am J Roentgenol. 2008 Feb;190(2):W194-200.

72. Chawla S, Zhang Y, Wang S, Chaudhary S, Chou C, O'Rourke DM, et al. Proton magnetic resonance spectroscopy in differentiating glioblastomas from primary cerebral lymphomas and brain metastases. J Comput Assist Tomogr. 2010 Nov-Dec;34(6):836-41.

73. Castillo M, Kwock L, Scatliff JH, Gudeman S, Greenwood R. Proton MR spectroscopic characteristics of a presumed giant subcortical heterotopia. AJNR Am J Neuroradiol. 1993 Mar;14(2):426-9.

74. Server A, Josefsen R, Kulle B, Maehlen J, Schellhorn T, Gadmar O, et al. Proton magnetic resonance spectroscopy in the distinction of high-grade cerebral gliomas from single metastatic brain tumors. Acta Radiol. 2010 Apr 1;51(3):316-25.

75. Poptani H, Gupta RK, Roy R, Samuel S, Angelliko G, Casillas G. Characterization of intracranial mass lesions with in vivo proton MR spectroscopy. AJNR Am J Neuroradiol. 1995 Sep;16(8):1593-603.

76. Cho YD, Choi GH, Lee SP, Kim JK. ^{1}H-MRS metabolic patterns for distinguishing between meningiomas and other brain tumors. Magn Reson Imaging. 2003 Jul;21(6):663-72.

77. Mukherji SK, Schiro S, Castillo M, Kwock L, Soper R, Blackstock W, et al. Proton MR Spectroscopy of Squamous Cell Carcinoma of the Upper Aerodigestive Tract: In Vitro Characteristics. AJNR Am J Neuroradiol. 1996 Sep;17(8):1485-90.

78. Son BC, Kim MC, Choi BG, Kim EN, Baik HM, Choe BY, et al. Proton magnetic resonance chemical shift imaging (^{1}H CSI)-directed stereotactic biopsy. Acta Neurochir (Wien). 2001;143(1):45-9.

79. Bhujwalla ZM, Artemov D, Natarajan K, Solaiyappan M, Kollars P, Kristjansen PE. Reduction of vascular and permeable regions in solid tumors detected by macromolecular contrast magnetic resonance imaging. Clin Cancer Res. 2003 Jan 15;9(1):355-62.

80. Kim SH, Chang KH, Song IC, Han MH, Kim HC, Kang HS, et al. Brain abscess and brain tumor: discrimination with in vivo H1 MR spectroscopy. Radiology. 1997 Jan;204(1):239-45.

81. Grand S, Passaro G, Ziegler A, Estève F, Boujet C, Hoffmann D, et al. Necrotic Tumor versus Brain Abscess: Importance of Amino Acids Detected at ^{1}H MR Spectroscopy-Initial Results. Radiology. 1999 Dec;213(3):785-93.

82. Krouwer HG, Kim TA, Rand SD, Prost RW, Haughton VM, Ho KC, Jaradeh SS, Meyer GA, Blindauer KA, Cusick JF, Morris GL, Walsh PR. Single-voxel proton MR spectroscopy of nonneoplastic brain lesions suggestive of a neoplasm. AJNR Am J Neuroradiol. 1998 Oct;19(9):1695-703.

83. Garg M, Gupta RK, Husain M, et al. Brain Abscesses: Etiologic Categorization with in Vivo Proton MR Spectroscopy. Radiology. 2004 Feb;230(2):519-27.

84. Hagmann P, Jonasson L, Maeder P, et al. Understanding diffusion MR imaging techniques: from scalar diffusion-weighted imaging to diffusion tensor imaging and beyond. Radiographics. 2006;26 Suppl 1:S205-23. doi:10.1148/rg.26si065510.

85. Qayyum A. Diffusion-weighted imaging in the abdomen and pelvis: concepts and applications. Radiographics. 2009;29(6):1797-810. doi:10.1148/rg.296095521.

86. Moritani T, Ekholm S, Westesson PL. Diffusion-Weighted MR Imaging of the Brain. Springer; 2009. ISBN:3540787852.

87. Greenberg MS. Handbook of Neurosurgery. Thieme; 2010. ISBN:1604063262.

88. UK. PP. Diffusion MRI: Theory, Methods, and Applications. Oxford University Press, USA; 2010. ISBN:0199708703.

89. Moritani T, Ekholm S, Westesson PA. Diffusion-Weighted MR Imaging of the Brain. Springer; 2009. ISBN:3540787852.

90. Harris AD, Pereira RS, Mitchell JR, Hill MD, Sevick RJ, Frayne R. A comparison of images generated from diffusion-weighted and diffusion-tensor imaging data in hyper-acute stroke. J Magn Reson Imaging. 2004;20(2):193-200. doi:10.1002/jmri.20116.

91. De Foer B, Vercruysse JP, Pilet B, et al. Single-Shot, Turbo Spin-Echo, Diffusion-Weighted Imaging versus Spin-Echo-Planar, Diffusion-Weighted Imaging in the

Detection of Acquired Middle Ear Cholesteatoma. AJNR Am J Neuroradiol. 2006;27(7):1480.

92. Geneidi EAS, Hanaa SRR, Kamal AMM. Role of DWI in differentiation between cholesteatoma and recurrent otitis media. QJM. 2020. doi:10.1093/qjmed/hcaa068.

93. Pavlisa G, Rodos M, Gordana P. The differences of water diffusion between brain tissue infiltrated by tumor and peritumoral vasogenic edema. Clin Imaging. 2009;33:96–101.

94. Lee EJ, TerBrugge K, Choi DS. Diagnostic value of peritumoral minimum apparent diffusion coefficient for differentiation between glioblastoma multiforme from solitary metastatic lesions. AJR Am J Roentgenol. 2011;196:71–6.

95. Ohba S, Ushioda T, Nakagawa T. Diffusion magnetic resonance imaging for enhanced visualization of malignant cerebral tumors and abscesses. Neurol India. 2011;59:674–8.

96. Faria AV, Macedo FC, Marsaioli AJ. Classification of brain tumor extracts by high resolution 1H MRS using partial least squares discriminate analysis. Braz J Med Biol.

97. Shokry A. MRS of brain tumors: diagrammatic representations and diagnostic approach. Egypt J Radiol Nucl Med. 2012;43(4):603–12.

98. Sibtain NA, Howe FA, Saunders DE. The clinical value of proton magnetic resonance spectroscopy in adult brain tumors. Clin Radiol. 2007;62:109–19.

99. Burger PC, Scheithauer BW, Paulus W. Pilocytic astrocytoma. In: Kleihues P, Cavenee WK, editors. Pathology and genetics of tumors of the nervous system. Lyon, France: International Agency for Research on Cancer; 2000. p. 45–51.

100. Grand S, Laï ES, Estève F, Rubin C, Hoffmann D, Rémy C, et al. In vivo 1H MRS of brain abscesses versus necrotic brain tumors. Neurology. 1996;47:846-8.

101. Kugel H, Heindel W, Ernestus RI, Bunke J, du Mesnil R, Friedmann G. Human brain tumors: spectral patterns detected with localized H-1 MR spectroscopy. Radiology. 1992;183(3):701-9.

102. Martinez MC, Celda B. Proton MR spectroscopy imaging in the study of human cancer. J Nucl Med Mol Imaging. 2009;53:618–30.

103. Van Der Graaf M. In vivo magnetic resonance spectroscopy: basic methodology and clinical applications. Eur Biophys J. 2010;39(4):527–40.

104. Chen J, Huang SL, Li T. In vivo research in astrocytoma cell proliferation with proton magnetic resonance spectroscopy: correlation with histopathology and immunohistochemistry. Neuroradiology. 2006;48(5):312–8.

105. Opstad KS, Murphy MM, Wilkins PR. Differentiation of metastases from high-grade gliomas using short echo time 1H spectroscopy. J Magn Reson Imaging. 2004;20:187–92.

106. Chiang IC, Kuo YT, Lu CY, Yeung KW, Lin WC, Sheu FO, et al. Distinction between high-grade gliomas and solitary metastases using peritumoral 3-T magnetic resonance spectroscopy, diffusion, and perfusion imaging. Neuroradiology. 2004;46:619–27.

107. Researchgate.net. [cited 2024 Jun 25]. Available from: https://www.researchgate.net/publication/303816083_Role_of_magnetic_resonance_spectroscopy_diffusion_weighted_imaging_in_differentiation_of_supratentorial_brain_tumors/fulltext/57dc67e708aeea195935ca45/Role-of-magnetic-resonance-spectroscopy-diffusion-weighted-imaging-in-differentiation-of-supratentorial-brain-tumors.pdf

LIMITATIONS

- MRI brain is an expensive investigation as compared to CT scan
- MRI brain is a time-consuming investigation in case of emergencies
- Limited sample size has a limited external applicability
- Future multi-centric studies involving a large sample size and the use of randomized sampling techniques could increase the validity of the results and can further help in generating clinical and radiological evidence for making recommendations in the day-to-day practice.

ANNEXURES – I

INFORMED CONSENT FORM

"MAGNETIC RESONANCE SPECTROSCOPY AND DIFFUSION WEIGHTED IMAGING CHARACTERIZATION OF SUPRATENTORIAL BRAIN TUMORS: A ONE YEAR HOSPITAL BASED CROSS SECTIONAL STUDY"

Name of Student/Principal Investigator: REG. NO. BS0121003

Name of Guide/Co Investigators: Dr _____

Objective: To characterize supratentorial tumors into benign and malignant using magnetic resonance spectroscopy & diffusion weighted imaging (DWI) imaging sequences of magnetic resonance imaging in addition to conventional magnetic resonance sequences.

Introduction: Intracranial tumors are a significant health problem. Brain tumors are subdivided into supra-tentorial & infra-tentorial brain tumors. Differentiation of low grade from high grade glioma, neoplastic from non-neoplastic brain masses by using conventional MRI is frequently difficult, and many cases require biopsy or follow-up imaging. Gadolinium enhancement is useful in evaluation of brain tumors. Recent MR imaging techniques, such as MR spectroscopy, can further improve the diagnostic accuracy of MR imaging in the diagnosis of such tumors. Magnetic resonance spectroscopy is a technique that allows the study of some metabolites in the brain or neoplasms that point to the nature of these lesions, grading of brain tumors, and follow-up and to evaluate the response of these lesions to treatment. Magnetic resonance spectroscopy is an analytical method used to identify molecules and to determine their biophysical characteristics. Thus, this technique is a multi-parametrical molecular

imaging method that can complete MRI study enabling the detection of biochemical patterns of different features and aspects of brain tumor. Diffusion-weighted imaging (DWI) helps us to obtain additional information about the brain from the microscopic movement of water molecules. DWI has been used to detect the nature of brain tumors according to their cellularity and to differentiate between high cellular and low cellular brain tumors.

Explanation of procedure:

I request you to kindly participate in the study titled study **''MAGNETIC RESONANCE SPECTROSCOPY AND DIFFUSION WEIGHTED IMAGING CHARACTERIZATION OF SUPRATENTORIAL BRAIN TUMORS: A ONE YEAR HOSPITAL BASED CROSS SECTIONAL STUDY''** at Dr. Prabhakar Kore Charitable Hospital and Medical Research Centre, Belgaum" is being conducted by REG. NO. BS0121003, Post Graduate in Radio- Diagnosis at J. N. Medical College Belgaum, Karnataka, under the guidance of Dr _____, Department of Radio-Diagnosis, J. N. Medical College, Belgaum.

We request you to participate in this study as you are eligible to be included. During the study you will be asked questions regarding your present and past medical history and you will be required to answer to the best of your knowledge. You will also be crucially examined as per the protocol drawn as and when required. Study will be conducted over a period of one year. Once the patient signs the informed consent history and examination will be recorded as per proforma.

Magnetic resonance imaging (MRI) uses a large magnet and radio waves to look at structures inside your body. You will have to undertake an MRI scan which is done in a closed environment. During the scan, you lie on a table that slides inside a tunnel-shaped

machine. Doing the scan can take a long time, and you must stay still. The scan is painless. The MRI machine makes a lot of noise.

If you agree to participate in the study, please furnish the details pertaining to the study.

Benefits:

Results will help to get extra details of supra-tentorial tumors with the use of MR spectroscopy and DWI sequences when done in addition to conventional MRI sequences and will also help in differentiation of these tumors into benign and malignant.

Withdrawal from participation in the study: Participation in this study is voluntary. You will be free to decide whether to participate in this study or continue participation once enrolled. In case you decide to withdraw your participation, you are free to do so. However, please convey the decision to the principal investigator.

Possible benefits from participating in the study: You will/will not have nor get any benefits by participating in this study. The data gathered will help the population at large.

Possible risks from participating in the study: There are no risks involved in participating in this study.

Privacy and confidentiality: The information collected from you will be coded, to prevent any person from identifying you. Your identity will never be revealed. The data collected from you will be kept confidential and only processed or aggregated data will be used for publication.

Financial incentives: You will not receive any payment for participating in this study.

Authorization for publication of aggregated data: Results obtained after processing of the aggregated data will be published for scientific purposes and or presented to scientific groups. However, your identity will never be revealed.

QUESTION:

any enquiries in the future or in case of research-related injury illness, you may contact the following persons.

REG. NO. BS0121003	**Dr _____**	**Dr. Harsha Hegade**
Post-Graduate, Department of Radio-Diagnosis. J.N.Medical College, Belagavi	Guide, Professor, Department of Radio-Diagnosis J.N.Medical College, Belagavi	Professor Chairman, J.N. Medical College Institutional Ethical Committee For Human Subjects Research, Belagavi

Legal rights: By signing this consent form, we are not waving any of your legal rights.

CONSENT STATEMENT

I am making a voluntary decision to participate in the study **''Magnetic Resonance Spectroscopy & Diffusion Weighted Imaging Characterization Of Supra-tentorial Brain Tumors: A One Year Hospital Based Cross Sectional Study''.** My signature below indicates that I have decided to participate and I have read the information provided above or the information provided above has been read to me in the language that I understand best. I was given the opportunity to ask questions and that they have been answered to my satisfaction.

Name of the participant:

Signature or left thumb impression of the participant:

Name of the witness:

Signature or left thumb impression of the witness:

Name of the investigator:

Signature of the investigator:

PARENTAL CONSENT TO PARTICIPATE IN RESEARCH STUDY:

1. "I understand that my child is participating in the study, which includes MRI BRAIN".
2. I confirm that I have read and understood the information in the patient information sheet. Procedure is explained to me in detail along with information about the advantages and disadvantages of taking part in the study. I have been given the opportunity to discuss all aspects of the trial, to ask questions and hereby consent my child's participation in the study outlined above.
3. I understand that the decision to take part in this study is completely voluntary and I am aware that I can choose to withdraw from the study at any point of time.
4. I consent to the photographing or recording of the procedure to be performed including appropriate portions of my child's body, for medical, scientific or educational purposes provided my child's identity is not revealed in the pictures or by the descriptive texts accompanying them.
5. I understand that there is no significant risk involved in the test that would be done in this study.
6. No guarantee or assurance has given by anyone as to the results that may be obtained.
7. My signature on this form signifies that I have willingly decided to participate my child after understanding the above information".

Participant's Name _____

Parent's Name _____

Signature _____

Name and signature of witness _____

Name and signature of interviewer _____

Date: _____

Place_____

ANNEXURES – II

PROFORMA FOR DATA COLLECTION

TITLE: MAGNETIC RESONANCE SPECTROSCOPY AND DIFFUSION WEIGHTED IMAGING CHARACTERIZATION OF SUPRATENTORIAL BRAIN TUMORS: A ONE YEAR HOSPITAL BASED CROSS SECTIONAL STUDY''

HISTORY:

NAME: **AGE:**

GENDER

REFFERING DOCTOR:

PRESENTING COMPLAINTS:

SYMPTOM	PRESENT	ABSENT	IF PRESNT THEN DURATION	NUMBER OF EPISODES IF APPLICABLE
a) HEADACHE				
b) DIZZINESS				
c) SEIZURES				
d) VOMITING				
e) NECK STIFFNESS				
f) NEUROLOGICAL DEFICITS				
g) OTHERS				

PAST HISTORY:

a) **HYPERTENSION**

b) **DIABETES MELLITUS**

c) **TUBERCULOSIS**

FAMILY HISTORY:

BRIEF PHYSICAL EXAMNIATION:

WAS ANY PREVIOUS IMAGING:

FINDINGS OF PREVIOUS SCAN:

PRESENT MRI FINDINGS:

NO OF LESIONS:

SITE	**SIDE (RIGHT/LEFT/MIDLINE/BILATERAL)**	**REGION INVOLVED (FRONTAL, PARIETAL, TEMPORAL & OCCIPITAL)**

SIGNAL INTENSITY:

SEQUENCE	**HYPOINTENSE**	**HYPERINTENSE**	**ISOINTENSE**	**MIXED INTENSE**
T1				
T2				

ENHANCEMENT:

ENHANCEMENT	**INTENSITY**	**PATTERN**

MRI SPECTROSCOPY FINDINGS:

METABOLITE DETECTED: **a. CHOLINE** **b. CREATINE** **c. LIPID** **d. LACTATE** **e. NAA** **f. ALANINE**	
METABOLITE RATIO:	

DIFFUSION WEIGHTED IMAGING:

DIFFUSION RESTRICTION	PRESENT	ABSENT

MRI DIAGNOSIS:

LOCATION	ADC VALUES
INTRALESIONAL	
PERILESIONAL	

ANNEXURE III: IMAGES / FIGURES

PHOTOGRAPHS OF CASES

Case A

A CASE OF A 57YRS OLD FEMALE WITH T2 WEIGHTED, T1 WEIGHTED IMAGES REPRESENTING A LESION IN THE RIGHT PARASAGGITAL FRONTAL REGION WITH EVIDENCE OF DIFFUSION RESTRICTION ON b 1000 DWI SEQUENCE AND ADC MAPS WITH POST CONTRAST ENHANCEMENT

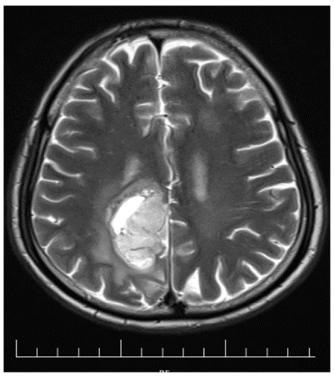

T2 WEIGHTED IMAGE

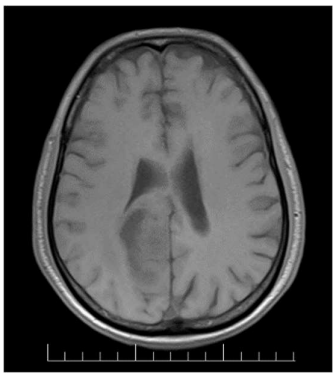

T1 WEIGHTED IMAGE

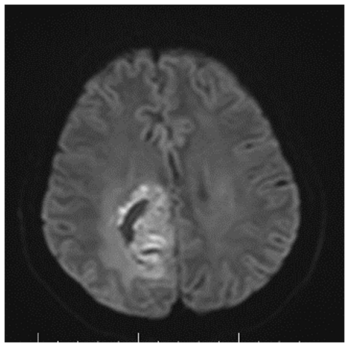

B 1000 DWI

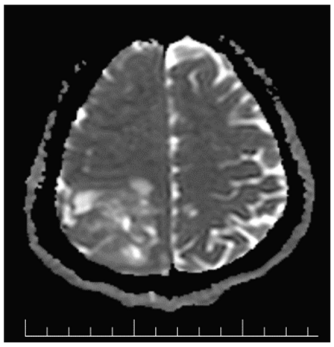

ADC MAPS

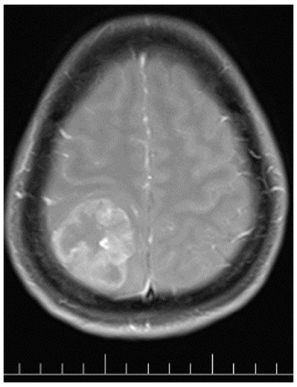

T1FS PC

Case B

A CASE OF A 39 YRS OLD MALE WITH T2 AND T1 WEIGHTED IMAGES SHOWING A LESION IN THE LESION LEFT FRONTAL REGION WITH EVIDENCE OF DIFFUSION RESTRICTION ON b1000 DWI SEQUENCE AND ADC MAPS WITH POST CONTRAST ENHANCEMENT

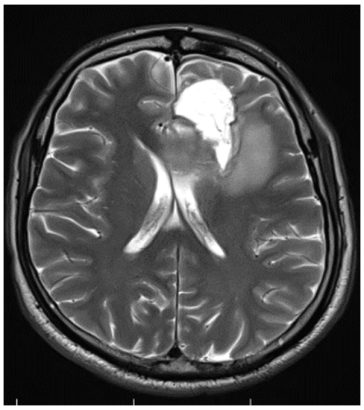

T2 WEIGHTED IMAGE

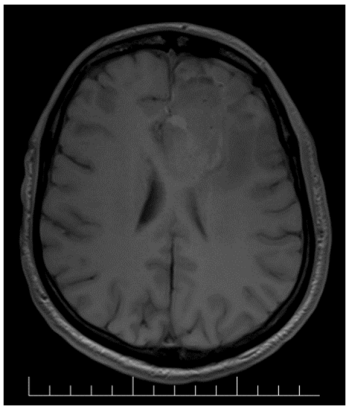

T1 WEIGHTED IMAGE

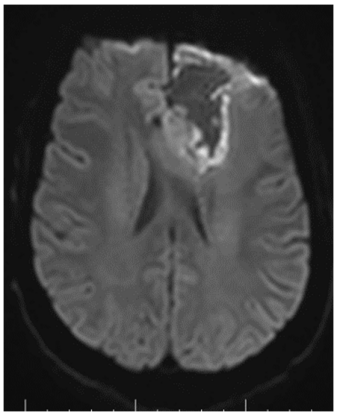

b 1000 DWI

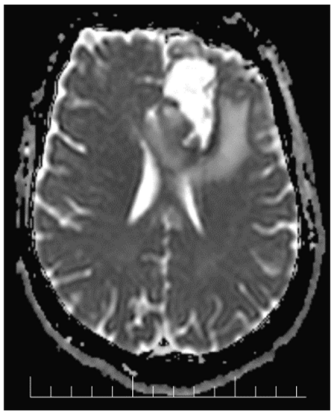

ADC MAPS

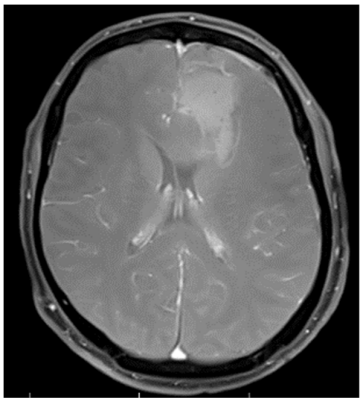

T1 FS PC

CASE C

A CASE OF A 54 YRS OLD FEMALE COMPLANING OF HEADCAHE, DIZZINESS, SEIZURES AND VOMITING WITH T2 AND T1 WEIGHTED IMAGES SHOWING A LESION IN THE RIGHT FRONTO-PARIETAL REGION WITH EVIDENCE OF DIFFUSION RESTRICTION ON b1000 DWI SEQUENCE AND ADC MAPS WITH POST CONTRAST ENHANCEMENT

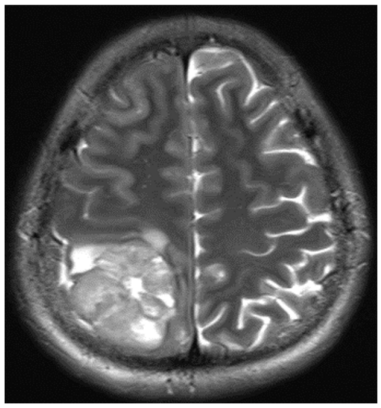

T2 WEIGHTED IMAGE

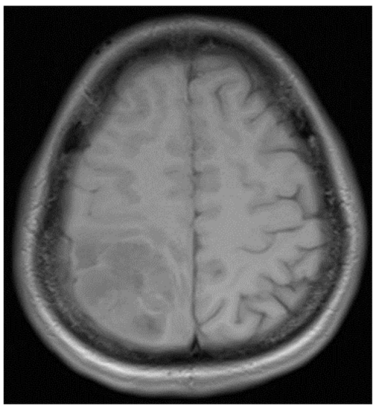

T1 WEIGHTED IMAGE

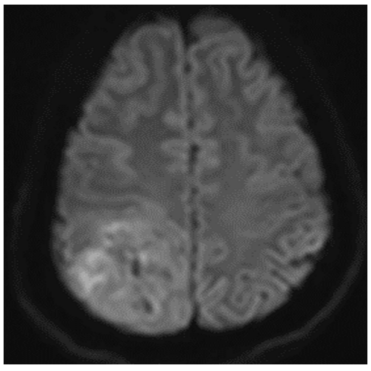

b 1000 DWI

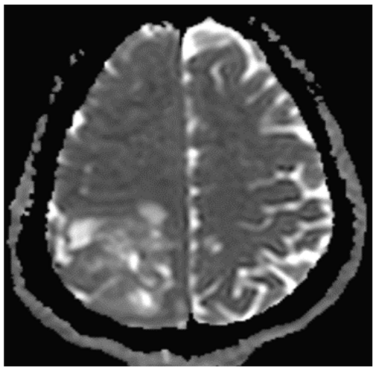

ADC MAPS

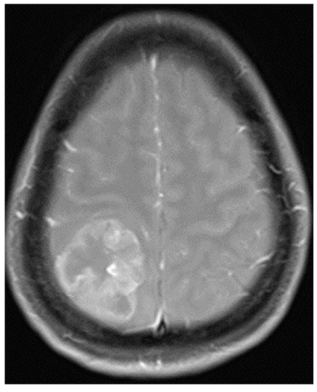

T1 FS PC

SPECTROSCOPY IMAGE PLATES

CASE IMAGES-1

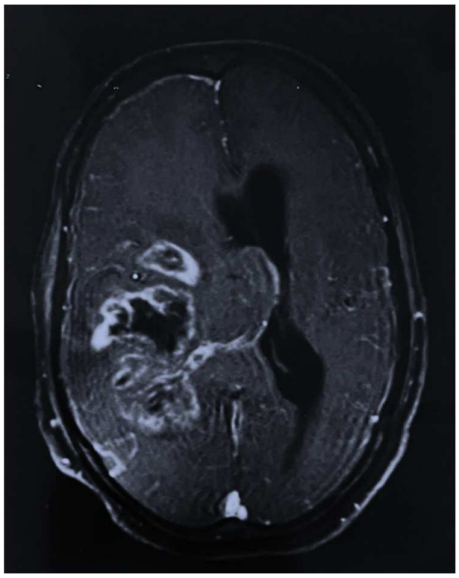

IMAGE 1: MRI AXIAL CONTRAST ENHANCED T1 WEIGHTED IMAGE SHOWS A WELL DEFINED INTRA-AXIAL PERIPHERALLY ENHANCING LESION IN THE RIGHT FRONTOPARIETAL REGION WITH ADJACENT EDEMA AND MASS EFFECT ON THE IPSILATERAL LATERAL VENTRICLE

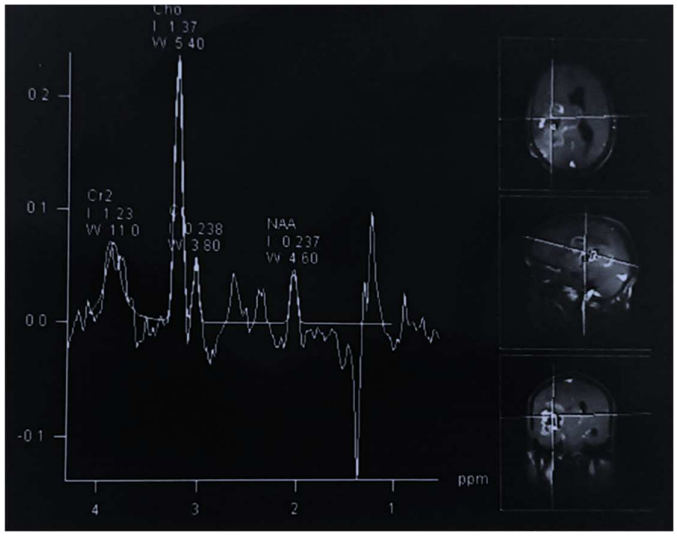

IMAGE 2: MRS SHOWING LESION IN THE RIGHT FRONTOPARIETAL REGION SHOWING HIGHLY ELEVATED CHOLINE WITH PROMINENT LIPID AND LACTATE PEAK CHARACTERISTIC OF HIGH GRADE NEOPLASM

CASE IMAGES-2

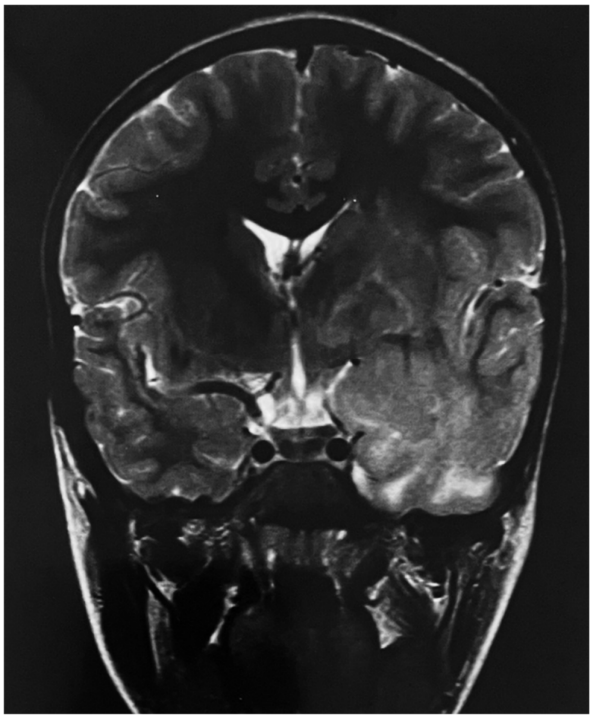

IMAGE 3: MRI SHOWING LOW GRADE GLIOMA – CORONAL T2 WEIGHTED IMAGE SHOWING AN ILL DEFINED T2 HYPERINTENSITY

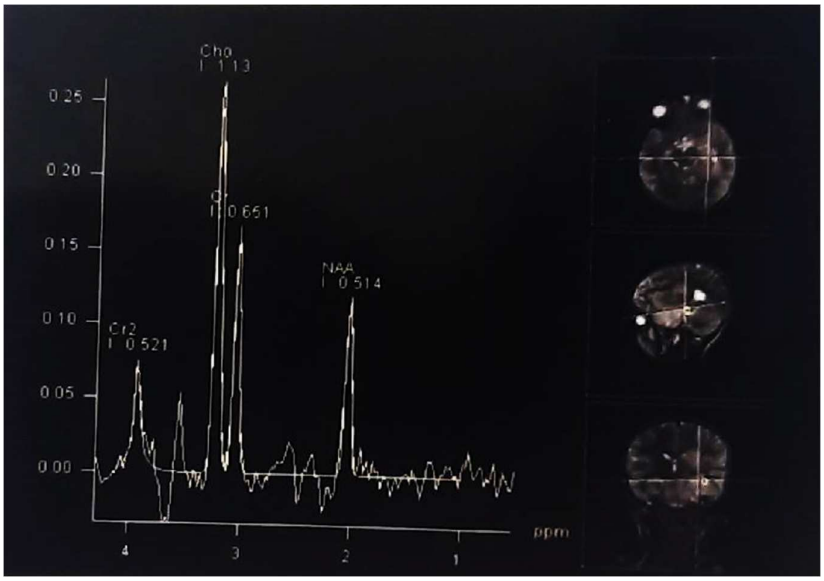

IMAGE 4: MRS SHOWING LOW GRADE GLIOMA – MR SPECTROSCOPY OF THE LESION IN THE LEFT TEMPORAL REGION SHOWED ELEVATED CHOLINE WITH REDUCED NAA PEAK

CASE IMAGES-3

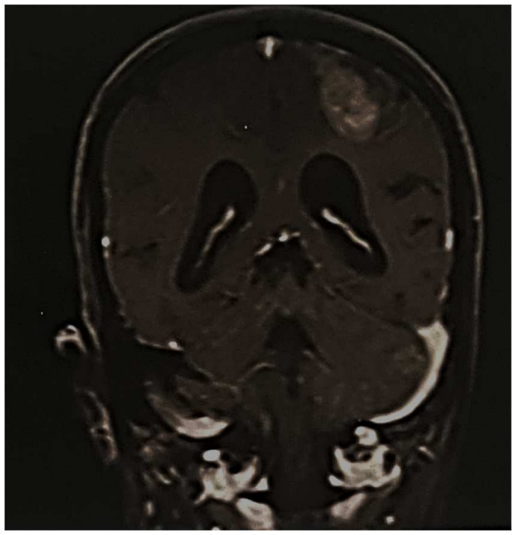

IMAGE 5: MRI SHOWING METASTASIS – CORONAL CONTRAST ENHANCED T1 WEIGHTED IMAGES SHOW MULTIPLE WELL DEFINED INTRA – AXIAL HETEROGEENOUSLY ENHANCING MASS LESIONS

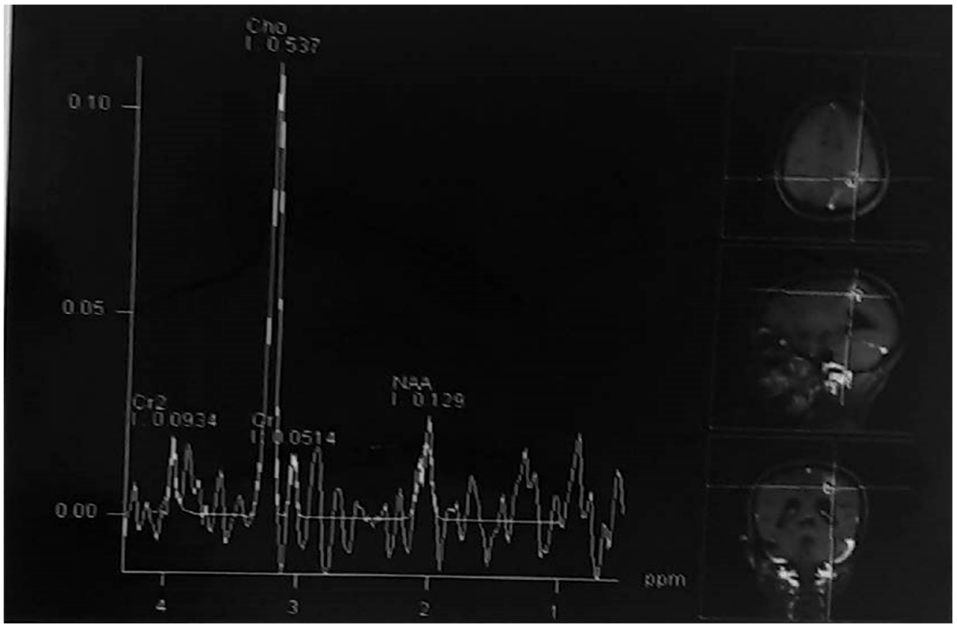

IMAGE 6: MRS SHOWING METASTASIS – MR SPECTROSCOPY OF THE LESION IN THE LEFT PARIETAL REGION SHOWS HIGHLY ELEVATED CHOLINE WITH SUPRESSION OF NAA

ANNEXURE – IV

KEY TO MASTER CHART

DESCRIPTION	ABBREVATION
MALE	M
FEMALE	F
HYPERTENSION	HTN
DIABETES MELLITUS	DM
HEADACHE	HA
VOMITING	VO
DIZZINESS	DZ
SEIZURES	SZ
ALTERED SENSORIUM	ALS
MILD RIGHT SIDED WEAKNESS	MRSW
INCREASED FORGETFULNESS	IF
MULTIPLE	ML
RIGHT ANTERIOR TEMPORAL	RAT
RIGHT FRONTAL REGION	RFR
LEFT TEMPORAL REGION	LTR
BILATERAL PARIETAL REGION	BPR
LEFT PARIETAL REGION	LPR
LEFT POSTERIOR PARIETAL REGION	LPPR
RIGHT PARIETO-TEMPORAL REGION	RPTR
LEFT PARIETO-OCCIPITAL REGION	LPOR
RIGHT PARIETAL REGION	RPR
LEFT PARASAGGITAL FRONTAL	LPF
LEFT FRONTAL REGION	LFR
LEFT FRONTOPARIETAL REGION	LFPR
RIGHT PARASGGITAL FRONTAL REGION	RPFR
LEFT PARIETO-TEMPORAL REGION	LPTR
LEFT MEDIAL TEMPORAL REGION	LMTR
RIGHT OCCIPITAL REGION	ROR

BILATERAL PARASAGGITAL FRONTOPARIETAL REGION	BPFPR
LEFT HIGH FRONTAL REGION	LHFR
RIGHT PARIETO-OCCIPITAL REGION	RPOR
LEFT OCCIPITAL REGION	LOR
MIDLINE HYPOTHALAMUS	MH
LEFT ANTERIOR TEMPORAL REGION	LATR
RIGHT TEMPORAL REGION	RTR
RIGHT MEDIAL TEMPORAL REGION	RMTR
HYPOINTENSE	HYPO
HYPERINTENSE	HYPER
MIXED INTENSITY	MXI
PERIPHERALLY ENHANCING	PER
HOMOGENEOUSLY ENHANCING	HO
HETEROGENEOUSLY ENHANCING	HET
INTRALESIONAL	INT
PERILESIONAL	PRL
DECREASED	REDU
INCREASED	ICR
CHOLINE	CHOL
LIPID-LACTATE	LC
NAA	N ACETYL ASPARTATE
ALANINE	ALN
CREATINE	CR
HIGH GRADE GLIOMA	HGG
LOW GRADE GLIOMA	LGG
MENINGIOMA	MENIN
METASTASIS	MTS
PRESENT	PRE
ABSENT	ABS

Master chart

SL No	AGE	GENDER	COMORBIDITIES	CHIEF COMPLANITS	NUMBER OF LESIONS ON MRI	LOCATION	T1 SIGNAL	T2 SIGNAL	ENHANCEMENT PATTERN	MR SPECTROSCOPY FINDINGS	RATIO OF METABOLITES	DIFFUSION RESTRICTION	INTREALESIONAL ADC VALUES	PRL ADC VALUES	FINAL DIAGNOSIS	HISTOPATHOLOGY DIAGNOSIS
1	48	F	NONE	HA & VO	ONE	RAT	ISO	HYPER	HO	INT CHOL & ALN IS ICR	INTRA ICR CHOL / CR RATIOS	ABS	N/A	N/A	MENIN	MENIN
2	57	F	NONE	HA, SZ & VO	ONE	RFR	HYPER	MXI	HET	INT CHOL & INT LC IS ICR & INT NAA IS REDU	INTRA ICR CHOL / NAA & CHOL / CR RATIOS, INTRA CHO/CR RATIO 1.4 & PERI CHO/CR RATIO 0.6	PRE	1.10 X 10^{-3}	1.31 X 10^{-3}	MTS	N/A
3	35	M	HTN	SZ	ONE	RFR	HYPO	HYPER	PER	INT & PRL CHOL IS ICR & INT NAA IS REDU	INTRA ICR CHOL / NAA & CHOL / CR RATIOS,INTRA CHO/CR RATIO 1.9 & PERI CHO/CR RATIO 0.8	PRE	1.31 X 10-3	0.98 X 10^{-3}	LGL	LGL
4	46	M	NONE	SZ & MRSW	ONE	LTR	ISO	HYPER	HO	INT & PRL CHOL IS ICR & INT NAA IS REDU	INTRA ICR CHOL / NAA & CHOL / CR RATIOS, INTRA CHO/CR RATIO 2.2 & PERI CHO/CR RATIO 0.6	PRE	1.42 X 10-3	0.91 X 10^{-4}	LGL	LGL
5	52	F	NONE	VO & ALS	ML	BPR	HYPO	HYPER	HO	INT CHOL IS ICR & INT NAA IS REDU	INTRA ICR CHOL / NAA & CHOL / CR RATIOS, INTRA CHO/CR RATIO 1.6 & PERI CHO/CR RATIO 0.5	PRE	1.02 X 10^{-3}	1.59 X 10^{-3}	MTS	N/A
6	65	F	HTN	HA & SZ	ONE	LPR	ISO	HYPO	PER	INT & PRL CHOL IS ICR & INT NAA IS REDU	INTRA ICR CHOL / NAA & CHOL / CR RATIOS, INTRA CHO/CR RATIO 2.6 & PERI CHO/CR RATIO 0.5	PRE	1.53 X 10-3	0.93 X 10^{-3}	LGL	LGL
7	57	F	HTN & DM	HA & IF	ONE	RFR	HYPO	MXI	PER	INT & PRL CHOL & INT LC IS ICR & INT NAA IS REDU	INTRA ICR CHOL / NAA & CHOL / CR RATIOS , INTRA CHO/CR RATIO 4.1 & PERI CHO/CR RATIO 2.8	PRE	0.81 X 10^{-3}	0.93 X 10^{-3}	HGL	HGL
8	65	F	HTN & DM	SZ	ML	LPPR	ISO	MXI	HET	INT CHOL & LC IS ICR & INT NAA IS REDU	INTRA ICR CHOL / NAA & CHOL / CR RATIOS, INTRA CHO/CR RATIO 2.0 & PERI CHO/CR RATIO 0.8	PRE	1.00X 10^{-3}	1.61 X 10^{-3}	MTS	N/A
9	68	M	HTN	SZ	ONE	RPTR	ISO	HYPO	HET	INT & PRL CHOL & INT LC IS ICR & INT NAA IS REDU	INTRA ICR CHOL / NAA & CHOL / CR RATIOS, INTRA CHO/CR RATIO 4.9 & PERI CHO/CR RATIO 2.8	PRE	1.01 X 10^{-3}	0.95 X 10^{-3}	HGL	HGL
10	58	M	HTN	HA SZ & MRSW	ONE	LPOR	HYPO	MXI	PER	INT & PRL CHOL & INT LC IS ICR & INT NAA IS REDU	INTRA ICR CHOL / NAA & CHOL / CR RATIOS, INTRA CHO/CR RATIO 5.3 & PERI CHO/CR RATIO 5.4	PRE	1.10 X 10-3	1.01 x 10^{-3}	HGL	HGL
11	49	M	HYPERTENSIVE	HA & SZ	ONE	RPR	ISO	MXI	PER	INT & PRL CHOL & INT LC IS ICR & INT NAA IS REDU	INTRA ICR CHOL / NAA & CHOL / CR RATIOS, INTRA CHO/CR RATIO 5.8 & PERI CHO/CR RATIO 2.9	PRE	0.92 X 10^{-3}	1.13 X 10^{-3}	HGL	LGL
12	58	M	HTN	HA & VO	ONE	RFR	HYPER	HYPER	HO	INT & PRL CHOL & INT LC IS ICR & INT NAA IS REDU	INTRA ICR CHOL / NAA & CHOL / CR RATIOS, INTRA CHO/CR RATIO 6.1 & PERI CHO/CR RATIO 2.5	PRE	1.08 X 10^{-4}	0.99 X 10^{-4}	HGL	HGL
13	34	F	HTN	HA & DZ	ONE	LPF	HYPO	HYPER	HET	INT & PRL CHOL IS ICR & INT NAA IS REDU	INTRA ICR CHOL / NAA & CHOL / CR RATIOS, INTRA CHO/CR RATIO 2.3 & PERI CHO/CR RATIO 0.9	PRE	1.43 X 10^{-3}	0.90 X 10^{-3}	LGL	LGL
14	34	M	NONE	HA, SZ & VO	ONE	RFR	ISO	ISOINTENSE	N/A	INT & PRL CHOL & INT LC IS ICR & INT NAA IS REDU	INTRA ICR CHOL / NAA & CHOL / CR RATIOS, INTRA CHO/CR RATIO 4.2 & PERI CHO/CR RATIO 3.6	PRE	1.06 X 10^{-3}	0.99 X 10^{-3}	HGL	HGL
15	30	F	NONE	VO & SZ	ONE	LFR	HYPO	HYPER	HET	INT & PRL CHOL IS ICR & INT NAA IS REDU	INTRA ICR CHOL / NAA & CHOL / CR RATIOS, INTRA CHO/CR RATIO 2.8 & PERI CHO/CR RATIO 0.7	PRE	1.46 X 10^{-3}	1.02 X 10^{-3}	LGL	LGL
16	70	F	DM	HA, SZ & VO	ONE	LFPR	HYPO	HYPER	PER	INT & PRL CHOL & INT LC IS ICR & INT NAA IS REDU	INTRA ICR CHOL / NAA & CHOL / CR RATIOS, INTRA CHO/CR RATIO 6.3 & PERI CHO/CR RATIO 2.2	PRE	1.02 X 10^{-3}	0.81 X 10^{-3}	HGL	HGL
17	62	F	HTN	HA, DZ & VO	ONE	LPR	ISO	MXI	PER	INT & PRL CHOL & INT LC IS ICR & INT NAA IS REDU	INTRA ICR CHOL / NAA & CHOL / CR RATIOS, INTRA CHO/CR RATIO 5.4 & PERI CHO/CR RATIO 2.8	PRE	1.02 X 10^{-3}	0.91 X 10^{-3}	HGL	HGL
18	65	F	HTN	HA & DZ	ONE	LFR	HYPO	HYPER	PER	INT & PRL CHOL & INT LC IS ICR & INT NAA IS REDU	INTRA ICR CHOL / NAA & CHOL / CR RATIOS, INTRA CHO/CR RATIO 7.3 & PERI CHO/CR RATIO 6.4	PRE	1.0 X 10^{-3}	0.81 X 10^{-3}	HGL	HGL
19	30	M	NONE	HA	ONE	RFR	ISO	HYPER	HET	INT & PRL CHOL IS ICR & INT NAA IS REDU	INTRA ICR CHOL / NAA & CHOL / CR RATIOS, INTRA CHO/CR RATIO 2.7 & PERI CHO/CR RATIO 2.2	PRE	1.39X 10^{-3}	0.80 X 10^{-3}	LGL	HGL
20	74	M	HTN	VO & SZ	ONE	RPFR	HYPO	HYPER	PER	INT & PRL CHOL & INT LC IS ICR & INT NAA IS REDU	INTRA ICR CHOL / NAA & CHOL / CR RATIOS, INTRA CHO/CR RATIO 4.6 & PERI CHO/CR RATIO 4.9	PRE	1.01 X 10^{-3}	0.97 X 10^{-3}	HGL	HGL
21	46	M	HTN & DM	HA & SZ	ONE	LPR	HYPO	HYPER	PER	INT & PRL CHOL & INT LC IS ICR & INT NAA IS REDU	INTRA ICR CHOL / NAA & CHOL / CR RATIOS, INTRA CHO/CR RATIO 3.9 & PERI CHO/CR RATIO 3.4	PRE	1.06 X 10^{-4}	0.99X 10^{-4}	HGL	HGL
22	39	M	NONE	HA & VO	ONE	LFR	MXI	MXI	HET	INT & PRL CHOL IS ICR & INT NAA IS REDU	INTRA ICR CHOL / NAA & CHOL / CR RATIOS, INTRA CHO/CR RATIO 2.9 & PERI CHO/CR RATIO 0.9	PRE	1.47 X 10^{-3}	1.06 X 10^{-3}	LGL	LGL
23	54	M	HTN	HA & VO	ONE	LPF	HYPO	HYPER	HET	INT & PRL CHOL & INT LC IS ICR & INT NAA IS REDU	INTRA ICR CHOL / NAA & CHOL / CR RATIOS, INTRA CHO/CR RATIO 6.0 & PERI CHO/CR RATIO 2.8	PRE	1.11 X 10^{-3}	0.82 X 10^{-3}	HGL	HGL
24	55	M	HTN & DM	HA & DZ	ONE	LPTR	MXI	MXI	HET	INT & PRL CHOL & INT LC IS ICR & INT NAA IS REDU	INTRA ICR CHOL / NAA & CHOL / CR RATIOS, INTRA CHO/CR RATIO 3.6 & PERI CHO/CR RATIO 3.7	PRE	1.03X 10^{-3}	1.02 X 10^{-3}	HGL	HGL
25	47	M	NONE	HA & VO	ONE	LPR	HYPO	HYPER	HET	INT & PRL CHOL & INT LC IS ICR & INT NAA IS REDU	INTRA ICR CHOL / NAA & CHOL / CR RATIOS, INTRA CHO/CR RATIO 4.5 & PERI CHO/CR RATIO 4.6	PRE	1.05 X 10^{-3}	0.94 X 10^{-3}	HGL	HGL
26	49	M	HTN & DM	HA, DZ, SZ & VO	ONE	RPR	MXI	MXI	HET	INT & PRL CHOL & INT LC IS ICR & INT NAA IS REDU	INTRA ICR CHOL / NAA & CHOL / CR RATIOS, INTRA CHO/CR RATIO 6.3 & PERI CHO/CR RATIO 2.3	PRE	0.7 X 10^{-3}	0.81 X 10^{-3}	HGL	HGL
27	28	M	NONE	HA & VO	ONE	RPR	HYPER	HYPO	HET	INT & PRL CHOL IS ICR & INT NAA IS REDU	INTRA ICR CHOL / NAA & CHOL / CR RATIOS, INTRA CHO/CR RATIO 2.6 & PERI CHO/CR RATIO 0.4	PRE	1.45 X 10^{-3}	1.03 X 10^{-3}	LGL	HGL
28	78	M	HTN & DM	HA, SZ & VO	ONE	LMTR	ISO	MXI	HET	INT & PRL CHOL & INT LC IS ICR & INT NAA IS REDU	INTRA ICR CHOL / NAA & CHOL / CR RATIOS, INTRA CHO/CR RATIO 6.5 & PERI CHO/CR RATIO 3.9	PRE	0.66 X 10^{-3}	0.90 X 10^{-3}	HGL	HGL
29	41	M	HTN	HA, DZ & VO	ONE	LFPR	MXI	MXI	PER	INT & PRL CHOL & INT LC IS ICR & INT NAA IS REDU	INTRA ICR CHOL / NAA & CHOL / CR RATIOS, INTRA CHO/CR RATIO 4.4 & PERI CHO/CR RATIO 2.7	PRE	0.74 X 10^{-3}	1.01 X 10^{-3}	HGL	HGL
30	65	F	HTN & DM	HA & SZ	ONE	LPF	HYPO	HYPER	HET	INT & PRL CHOL & INT LC IS ICR & INT NAA IS REDU	INTRA ICR CHOL / NAA & CHOL / CR RATIOS, INTRA CHO/CR RATIO 3.6 & PERI CHO/CR RATIO 5.5	PRE	0.64 X 10^{-3}	1.03 X 10^{-3}	HGL	HGL

31	62	F	HTN & DM	HA & VO	ONE	RFR	ISO	HYPER	HET	INT CHOL & ALN IS ICR	INTRA ICR CHOL / NAA & CHOL / CR RATIOS	ABS	N/A	N/A	MENIN	MENIN
32	28	M	HTN	HA & DZ	ONE	RFR	HYPO	HYPER	HET	INT & PRL CHOL IS ICR & INT NAA IS REDU	INTRA ICR CHOL / NAA & CHOL / CR RATIOS, INTRA CHO/CR RATIO 2.6 & PERI CHO/CR RATIO 0.4	PRE	1.51 X 10^{-3}	1.01 X 10-3	LGL	LGL
33	54	F	HTN & DM	HA, DZ, SZ & VO	ONE	RPR	ISO	MXI	HO	INT & PRL CHOL IS ICR & INT NAA IS REDU	INTRA ICR CHOL / NAA & CHOL / CR RATIOS, INTRA CHO/CR RATIO 2.2 & PERI CHO/CR RATIO 0.9	PRE	0.71 X 10^{-3}	1.53 X 10^{-3}	MTS	N/A
34	42	M	HTN	HA & DZ	ONE	RPR	HYPO	HYPER	HET	INT CHOL & LC IS ICR	INTRA ICR CHOL / NAA & CHOL / CR RATIOS	PRE	0.95 X 10^{-3}	0.97 X 10^{-3}	MENIN	MENIN
35	58	F	HTN & DM	HA, DZ & VO	ONE	ROR	ISO	ISO	HET	INT CHOL & ALN IS ICR	INTRA ICR CHOL / NAA & CHOL / CR RATIOS	ABS	N/A	N/A	MENIN	MENIN
36	56	F	HTN	HA, SZ & VO	ML	BPR	HYPO	MXI	N/A	INT CHOL & LC IS ICR	ICR CHOL / NAA & CHOL / CR RATIOS, INTRA CHO/CR RATIO 1.9 & PERI CHO/CR RATIO 0.7	PRE	0.62 X 10^{-3}	1.43 X 10^{-3}	MTS	N/A
37	60	M	HTN	HA & VO	ML	BPFPR	HYPO	HYPER	PER	INT CHOL IS ICR & INT NAA IS REDU	ICR CHOL / NAA & CHOL / CR RATIOS, INTRA CHO/CR RATIO 1.7 & PERI CHO/CR RATIO 0.6	PRE	0.61 X 10^{-3}	1.33 X 10^{-3}	MTS	N/A
38	63	M	HTN	HA & DZ	ONE	LHFR	HYPO	HYPO	HO	INT CHOL & ALN IS ICR	INTRA ICR CHOL / NAA & CHOL / CR RATIOS	ABS	N/A	N/A	MENIN	MENIN
39	65	F	HTN & DM	HA, DZ & VO	ONE	LPF	HYPO	HYPER	PER	INT & PRL CHOL IS ICR & INT NAA IS REDU	INTRA ICR CHOL / NAA & CHOL / CR RATIOS, INTRA CHO/CR RATIO 2.3 & PERI CHO/CR RATIO 0.7	PRE	1.48 X 10^{-3}	1.09 X 10^{-3}	LGL	LGL
40	76	F	HTN & DM	HA, DZ & VO	ONE	LFR	MXI	MXI	PER	INT & PRL CHOL & INT LC IS ICR & INT NAA IS REDU	INTRA ICR CHOL / NAA & CHOL / CR RATIOS, INTRA CHO/CR RATIO 3.8 & PERI CHO/CR RATIO 2.6	PRE	1.49 X 10^{-3}	0.91 X 10^{-3}	HGL	HGL
41	52	M	NONE	HA, SZ & VO	ONE	RPOR	ISO	MXI	HET	INT & PRL CHOL & INT LC IS ICR & INT NAA IS REDU	INTRA ICR CHOL / NAA & CHOL / CR RATIOS, INTRA CHO/CR RATIO 4.7 & PERI CHO/CR RATIO 3.7	PRE	1.09 X 10^{-3}	0.93 X 10^{-3}	HGL	HGL
42	44	M	HTN	HA, SZ & VO	ONE	LTR	HYPO	HYPER	PER	INT & PRL CHOL IS ICR & INT NAA IS REDU	INTRA ICR CHOL / NAA & CHOL / CR RATIOS, INTRA CHO/CR RATIO 2.8 & PERI CHO/CR RATIO 0.9	PRE	1.40 X 10^{-3}	0.99X 10^{-3}	LGL	LGL
43	78	M	HTN	HA & VO	ONE	LFR	HYPO	HYPER	HET	INT & PRL CHOL & INT LC IS ICR & INT NAA IS REDU	INTRA ICR CHOL / NAA & CHOL / CR RATIOS, INTRA CHO/CR RATIO 5.4 & PERI CHO/CR RATIO 2.5	PRE	0.69 X 10^{-3}	0.93 X 10^{-3}	HGL	HGL
44	55	F	HTN	HA, SZ & VO	ONE	LOR	ISO	HYPER	HET	INT & PRL CHOL IS ICR & INT NAA IS REDU	INTRA ICR CHOL / NAA & CHOL / CR RATIOS, INTRA CHO/CR RATIO 2.1 & PERI CHO/CR RATIO 0.5	PRE	1.51 X 10^{-3}	1.24 X 10^{-3}	LGL	LGL
45	50	F	HTN & DM	HA, DZ & SZ	ONE	MH	ISO	HYPER	HO	INT & PRL CHOL IS ICR & INT NAA IS REDU	INTRA ICR CHOL / NAA & CHOL / CR RATIOS, INTRA CHO/CR RATIO 2.6 & PERI CHO/CR RATIO 0.9	PRE	1.44 X 10^{-3}	0.97 X 10^{-3}	LGL	HGL
46	30	M	HTN	HA & DZ	ONE	LATR	MXI	HYPER	HET	INT & PRL CHOL & INT LC IS ICR & INT NAA IS REDU	INTRA ICR CHOL / NAA & CHOL / CR RATIOS, INTRA CHO/CR RATIO 7.6 & PERI CHO/CR RATIO 5.5	PRE	1.10 X 10^{-3}	0.97 X 10^{-3}	HGL	HGL
47	59	F	HTN	HA & DZ	ONE	RTR	ISO	ISOINTENSE	HET	INT & PRL CHOL & INT LC IS ICR & INT NAA IS REDU	INTRA ICR CHOL / NAA & CHOL / CR RATIOS, INTRA CHO/CR RATIO 4.9 & PERI CHO/CR RATIO 1.9	PRE	0.67 X 10^{-3}	1.09 X 10^{-3}	HGL	LGL
48	68	M	HTN & DM	HA, DZ, SZ & VO	ML	RMTR & LPPR	HYPO	HYPER	PER	INT & PRL CHOL IS ICR & INT NAA IS REDU	INTRA ICR CHOL / NAA & CHOL / CR RATIOS, INTRA CHO/CR RATIO 2.2 & PERI CHO/CR RATIO 0.9	PRE	0.87 X 10^{-3}	1.31 X 10^{-3}	MTS	N/A
49	50	M	HTN	HA, DZ & VO	ONE	ROR	HYPO	HYPO	HO	INT CHOL & ALN IS ICR	INTRA ICR CHOL / NAA & CHOL / CR RATIOS	ABS	N/A	N/A	MENIN	MENIN